OLD DOMINION UNIVERSITY RESEARCH FOUNDATION

DEPARTMENT OF MECHANICAL ENGINEERING AND MECHANICS
SCHOOL OF ENGINEERING
OLD DOMINION UNIVERSITY
NORFOLK, VIRGINIA

ANALYSIS OF LONGWAVE RADIATION FOR THE EARTH-ATMOSPHERE SYSTEM

By

S. N. Tiwari, Principal Investigator

C. S. Vemuru

and

S. V. Subramanian

Final Report
For the period ending July 31, 1983

Prepared for the
National Aeronautics and Space Administration
Langley Research Center
Hampton, Virginia

Under
Research Grant NAG-1-21
John T. Suttles, Technical Monitor
Atmospheric Environmental Sciences Division

(NASA-CR-173155) ANALYSIS OF LONGWAVE RADIATION FOR THE EARTH-ATMOSPHERE SYSTEM Final Report, period ending 31 Jul. 1983 (Old Dominion Univ., Norfolk, Va.) 155 p HC A08/MF A01 CSCL 20N G3/32

N84-17437

Unclas
18322

November 1983

DEPARTMENT OF MECHANICAL ENGINEERING AND MECHANICS
SCHOOL OF ENGINEERING
OLD DOMINION UNIVERSITY
NORFOLK, VIRGINIA

ANALYSIS OF LONGWAVE RADIATION FOR THE EARTH-ATMOSPHERE SYSTEM

By

S. N. Tiwari, Principal Investigator

C. S. Vemuru

and

S. V. Subramanian

Final Report
For the period ending July 31, 1983

Prepared for the
National Aeronautics and Space Administration
Langley Research Center
Hampton, Virginia

Under
Research Grant NAG-1-21
John T. Suttles, Technical Monitor
Atmospheric Environmental Sciences Division

Submitted by the
Old Dominion University Research Foundation
P. O. Box 6369
Norfolk, Virginia 23508

November 1983

FOREWORD

This report summarizes the work completed on the research project "Radiative Transfer Models for the Earth Radiation Budget Studies." The work was supported by the NASA/Langley Research Center (Experiment Analysis Branch of the Atmospheric Environmental Sciences Division) through research grant NAG-1-21. The grant was monitored by Dr. John T. Suttles of the Atmospheric Environmental Sciences Division. The authors are grateful to Dr. S. K. Gupta for providing various help during the course of this study.

TABLE OF CONTENTS

LIST OF TABLES

LIST OF FIGURES

LIST OF FIGURES (continued)

LIST OF FIGURES (concluded)

LIST OF SYMBOLS

$B(\omega, T)$	Planck function, W cm^{-2} sr^{-1}
$E(\mu_o)$	Upward radiance at the cloud base due to surface reflectance, W cm^{-2} sr^{-1}
$E(\omega)$	Total radiant energy, W cm^{-2} sr^{-1}
$E_G(\omega)$	Thermal radiation emitted by the underlying surface and atmosphere
$E_{GR}(\omega)$	Reflected atmospheric radiation from the surface
$E_R(\omega)$	Incident solar radiation reflected by the surface
$E_\phi(\omega)$	Radiation scattered by single or multiple scattering processes in the atmosphere without having been reflected from the surface
$E\phi_R(\omega)$	Scattered energy which has undergone a reflection from the surface.
$\bar{F}(\omega, T)$	Downward atmospheric radiation
h	Top of the atmosphere
$J_\omega[T(z)]$	Nonequilibrium source function
$T(z)$	Atmosphere temperature, K
T_s	Surface temperature, K
$\varepsilon(\omega)$ or ε_s	Surface emittance
$\rho(\omega)$	Diffuse surface reflectance
η	Nonequilibrium parameter, η_c/η_r
η_c	Molecular collisional relaxation time
η_r	Radiative lifetime of the excited state
$\tau(\omega, z)$ or $\tau_\omega(z)$	Transmittance of the medium
$\tau^c_\omega(\Delta z)$	Cloud-layer transmittance
ω	Wave number, cm^{-1}

ANALYSIS OF LONGWAVE RADIATION FOR THE EARTH-ATMOSPHERE SYSTEM

By

S. N. Tiwari,[1] C. S. Vemuru,[2] and S. V. Subramanian[3]

SUMMARY

Accurate radiative transfer models are used to determine the upwelling atmospheric radiance and net radiative flux in the entire longwave spectral range. The validity of the quasi-random band model is established by comparing the results of this model with the results of line-by-line formulations and with available theoretical and experimental results. Existing radiative transfer models and computer codes are modified to include various surface and atmospheric effects (such as surface reflection, nonequilibrium radiation, and cloud effects). The program is used to evaluate the radiative flux in clear atmosphere, provide sensitivity analysis of upwelling radiance in presence of clouds, and determine the effects of various climatological parameters on the upwelling radiation and anisotropic function. The program is used also to evaluate homogeneous and nonhomogeneous gas emissivities under different conditions and the results are presented in a supplement to this report entitled "Accurate Evaluation of Homogeneous and Nonhomogeneous Gas Emissivities."

[1] Eminent Professor, Department of Mechanical Engineering and Mechanics, Old Dominion University, Norfolk, Virginia 23508.

[2] Graduate Research Assistant, Department of Mechanical Engineering and Mechanics, Old Dominion University, Norfolk, Virginia 23508.

[3] Research Assistant Professor, Department of Mechanical Engineering and Mechanics, Old Dominion University, Norfolk, Virginia 23508. Present affiliation: Development Engineer, AVCO-LYCOMING, Stratford, Connecticut 06497.

1. INTRODUCTION

Extensive study of the radiative transfer phenomena in the Earth's atmospheric system has been carried out in the last two decades (refs. 1 to 4). This is important for the understanding of the meteorological process on all scales and the spatial variation in surface temperature in the Earth atmosphere. Techniques for measuring the Earth's surface temperature include airborne instruments and satellite-mounted radiometers. In order to understand and interpret the instrument performance and readings, it is desirable to develop radiation models and numerical techniques that account for the absorption and attenuation of actual atmospheric radiation. Development of accurate models for radiative transfer in the atmosphere is extremely important for Earth radiation budget studies and climate modeling (refs. 4 to 6). These models have to be used for simulation and interpretation of Earth radiation budget measurements as well as for retrieval of various surface and atmospheric parameters from satellite-measured radiances (ref. 7). Since the radiation budget of the planet has been identified as an important element of the climate system, its measurements are being attempted with increasing accuracy (refs. 8 and 9). As a result, considerable improvement is warranted in the accuracy of the theoretical models dealing with atmospheric radiation transfer.

Many models for radiation absorption by molecular gases are available in the literature. The simplest one is the gray gas model (or the emissivity approximation) and the most sophisticated and accurate one is the line-by-line (LBL) model (or the direct integration procedure). Between the emissivity approximation and direct integration method lie several narrow-and wide-band models and band model correlations which vary greatly in complex-

ity and accuracy. A comprehensive review of various line and band models is available in reference 4. Use of either a LBL model or a narrow-band model is suggested for most atmospheric applications. The narrow-band models usually recommended for atmospheric studies are the Elsässer (or regular model, statistical (Meyer-Goody or Goody) model, and quasi-random band (QRB) model. The QRB is probably the best band model to represent accurately the absorption of a vibration-rotation band and is suitable for calculating the atmospheric transmittance and upwelling radiance. The fundamental features of the QRB are discussed, in detail, in references 10 to 12, and the procedure for calculating the atmospheric transmittance and upwelling radiance is given in reference 12. In spectral ranges where both line absorption and scattering are important, a widely used approximation for calculating spectrally integrated radiative flux is the exponential-sum fitting of transmissions (ESFT) method. The basis for this method is that the transmission function for a given spectral interval is fit by a sum of exponentials. The method is described in reference 13.

Radiative transfer models used in earlier climatic investigations employed radiation charts, generalilzed absorption coefficients, and emissivity approximations (refs. 5, 14-16). Rodgers (ref. 17) has indicated that the use of multi-interval narrow-band radiative transfer schemes in climate modeling studies will constitute a significant step forward and result in improved accuracy of the model output. Fels and Kaplan (ref. 18) have investigated the effects of using different radiative transfer schemes on the thermal structure of the atmosphere and its consequences to atmospheric dynamics. They employed two different radiative absorption models, the emissivity approximation and Goody's statistical band formulation, and performed

numerical experiments with the NCAR general circulation model. They observed a significant difference in the cooling rates in the two experiments which resulted in significantly different mean temperature fields and meridional circulation.

Very high accuracy can be achieved in the radiation computation by using the LBL integration procedure in the radiative transfer models (ref. 19). However, the procedure is too cumbersome and makes excessive demands on computer time. Tiwari and Gupta (ref. 20) have shown that the QRB model can be used for computing atmospheric transmittances with accuracy comparable to that of the LBL method and with computer usage more than an order of magnitude smaller. Kunde (ref. 11) has also used this model to compute outgoing infrared radiances from planetary atmospheres. However, before use of the QRB model can be recommended for Earth radiation budget and climate modeling studies, further work needs to be done to validate the model on a sound basis. This model should be used for absorption bands of different species in different spectral ranges. It is quite possible that the model is not justified at shorter wavelengths and smaller pressure path lengths. Furthermore, under realistic atmospheric conditions, the model may give good results in certain spectral ranges, but is poor in other ranges.

For critical applications, it is essential to validate the quasi-random band model under as many different but realistic conditions as possible by comparing the results of this model with available experimental and theoretical results. For several molecular species, experimental results for spectral transmittance and total band absorpance are given by Burch et al. (ref. 21) under different pressure and path length conditions. Thus it is highly desirable to compare the results of the QRB model with these experi-

mental results. For cases where experimental results are not available, it is important to compare the QRB results with LBL results. For certain spectral ranges and atmospheric conditions, results of atmospheric transmittances are available in the literature which have been obtained by using a sophisticated program called LOWTRAN (ref. 22). It is therefore desirable to obtain the QRB results exactly for these conditions for comparison with the LOWTRAN results. Another model used frequently in atmospheric studies is the K-distribution approximation (refs. 23-27). It has been applied successfully only to water vapor bands (refs. 24 and 25), but there are indications that it could be used with reasonable accuracy for other bands also (refs. 26 and 27). It is therefore important to compare the results of the QRB model with the K-distribution formulation for different bands under varying conditions. Recently (refs. 28 and 29), another model and computer code called FASCODE (Fast Atmospheric Signature Code) has been developed f the line-by-line calculation of radiance and transmittance with particular applicability to the Earth's atmosphere. In this model, an algorithm for the accelerated convolution of line shape functions (Lorentz, Voigt and Doppler) with spectral line data is used. The contribution from continuum absorption is also included in the model. The program is applicable to spectral regions from the microwave to the visible. It may, therefore, be desirable to compare the results of this model with the results of QRB formulation.

The objective of this study is to validate the QRB model for a few realistic conditions by comparing the results of this model with the LBL, experimental, and LOWTRAN results. Detailed verification of the QRB model results with the results of other formulations is beyond the scope of this

study. After the model validations, the aim of this study is to use the QRB model for evaluating the gas emissivities in several important spectral ranges and also in the entire longwave range. The QRB formulation is especially useful for this when a mixture of several molecullar species are involved. This study could provide benchmark solutions for gas emissivity under different pressure and temperature conditions. Such information are useful not only in atmospheric studies, but also in the fields of infrared signature work, combustion processes, and fire research. Another important aim of this study is to use the QRB model for evaluating the upwelling atmospheric radiance under different realistic surface and atmospheric conditions. Such formulations (and relevant information) are very useful in developing an accurate data reduction scheme for the measurement of atmospheric pollutants by remote sensing (refs. 4 and 30), and for Earth radiation budget and climate modeling studies (refs. 5-9, 31-33).

A major factor influencing the radiation balance and the general circulation of the Earth's atmosphere is the presence of clouds which occupy about 50 percent of the planet Earth on a global basis. Clouds absorb and scatter the incoming solar radiation and absorb and emit terrestrial radiation. Although clouds have been included in the study of transfer of solar radiation through the Earth's atmosphere for many years, there have been very few studies which include the effects of clouds on the longwave radiation (refs. 32-40). Clouds vary greatly in thickness, height, liquid water/ice content, and geometrical shape and size; and all these factors contribute in a complicated manner to the large variability of the cloud radiative properties. Some of these effects are being considered in recent studies (refs. 41-47). Most of the treatments given to clouds in the long-wave

radiation transfer models have been very simplistic. It is therefore essential to modify the existing radiative transfer models appropriately and investigate the effects of large variability in the radiative and geometrical properties of the clouds on the thermal radiances and fluxes.

The basic formulation of the radiative transfer equations and the expressions for the upwelling radiance and flux are presented in the next chapter, "Basic Theoretical Formulation." The spectral models used in this study are discussed briefly in chapter 3 entitled "Absorption Models." The computational procedure and data source for calculating the transmittance, upwelling radiance, and radiative flux are given in chapter 4. The results of the entire study pertaining to atmospheric applications are presented in three separate chapters entitled, "Accurate Evaluation of Longwave Radiation in Clear Atmosphere," "Sensitivity Analysis of Upwelling Radiance in Presence of Clouds," and "Evaluation of Anisotropic Functions in the Longwave Region." The results of emissivity calculations are given in a supplement to this report entitled, "Accurate Evaluation of Homogeneous and Nonhomogeneous Gas Emissivities.

2. BASIC THEORETICAL FORMULATIONS

Basic governing equations for radiative transfer in the atmosphere are available in the literature. However, many of these equations need to be modified for specific applications. For some applications, entirely new relations are needed to express a particular phenomena.

The radiation emergent from the atmosphere may be given by the expression (refs. 4, 30):

$$E(\omega) = E_G(\omega) + E_R(\omega) + E_{GR}(\omega) + E_\phi(\omega) + E_{\phi R}(\omega) \qquad (2.1)$$

The various components of the upwelling radiation are pictori lly shown in figure 2.1 and are defined in the list of symbols. In genei al, these are functions of surface and atmospheric temperatures, surface emittance and reflectance, sun zenith angle, scattering characteristics of particles, and transmittance of the atmosphere.

In the spectral region of infrared measurements, the effect of scattering and solar-reflected radiation is usually omitted. Hence, the expression for thermal radiation emerging from a plane-parallel atmosphere can be written as

$$E(\omega) = E_G(\omega) + E_{GR}(\omega) = \varepsilon(\omega)\, B(\omega,T_s)\, \tau(\omega,0)$$
$$+ \int_0^h B[\omega,T(z)][d\tau(\omega,z)/dz]dz + \rho(\omega)F\text{-}(\omega,T)\, \tau(\omega,0) \qquad (2.2)$$

The first term on the right-hand side of equation (2.2) represents the radiation from the surface; the second term is the radiation from the atmos-

phere, and the third term represents the reflected component of the downward radiation. The contribution of the reflected atmospheric radiation from the surface is usually neglected for surfaces with relatively high values of surface emittance and for the spectral regions where the downward atmospheric emission is small.

The contribution of the sunlight reflected from the surface from the surface is important at shorter wavelengths and is given by the component $E_R(\omega)$ as

$$E_R(\omega) = \frac{1}{\pi} [1 - \varepsilon(\omega)] \cos\theta \, H_S(\omega) \, [\tau(\omega)]^{\alpha} \tag{2.3}$$

where θ is the sun's zenith angle, $[1 - \varepsilon(\omega)]$ is the ground reflectance of the surface, $H_S(\omega)$ is the sun irradiance on the top of the atmosphere, $\alpha = 1 + f(\theta)$ where $f(\theta) = \sec\theta$ for $0 < \theta < 60°$ and $Ch\ \theta$ for $\theta < 60°$ with $Ch\ \theta$ denoting Chapman's function, and $\tau(\omega) = \tau(\omega,0)$ is the transmission vertically through the atmosphere.

For radiation budget and cooling rate calculations, however, the required quantity is the flux density. Upward flux density can be obtained precisely by integrating the upwelling radiance over the zenith angle θ and the azimuth ϕ, such that

$$F(\omega,h) = \int_0^{2\pi} d\phi \int_0^{\pi/2} E(\omega,h) \sin\theta \cos\theta \, d\theta \tag{2.4}$$

Integration of equation (2.4) by using detailed angular distribution of radiation is a tedious problem. However, it is simplified considerably for

a plane-parallel atmosphere and assuming that the source function in equation (2.2) is isotropic. It is possible with the above assumption to adopt the two-stream approximation whereby the equations of transfer are reduced to only two.

For the purpose of analysis (i.e., radiation modeling) and measurement of outgoing flux, it has been suggested to divide the entire longwave spectral range into the following subregions (ref. 31): (a) 0.7 to 4 μ; (b) 4 to 8 μ; (c) 8 to 12 μ; (d) 9 to 10 μ; (e) 12 to 18 μ; and (f) 18 to 50 μ. Specific reasons for suggesting this spectral subdivision are given in reference 33. The Earth radiation budget experiment (ERBE) proposed by NASA (ref. 50) consists of two packages designed to provide three spatial resolution options with three broad spectral bands as: (a) short wave, 0.2 to 5 μ; (b) long wave, 5 to 50 μ; and (c) total, 0.2 to 50 μ. However, for parametric studies, it is desirable also to extend the long wave range to 200 μ (i.e., 5 to 200 μ).

As discussed in the introduction, it is essential to incorporate an appropriate model for the cloudy atmosphere in the general radiative transfer model. For this, information on physical characteristics of clouds is essential. Some of the basic information required is: cloud amount, cloud height, cloud-top texture, height-width ratios, microphysical properties, total water content, liquid/ice water content, and cloud base altitude. All these factors contribute to the variability of the cloud radiative properties. As such, a simplistic description of clouds, where they are considered as opaque/black surfaces, is grossly inadequate. It is essential, therefore, to incorporate into the general radiative transfer schemes appropriate cloud models which take into account as many physical variables as possible.

Basic governing equations for radiative transfer through clouds are available in the literature (refs. 37-40). The upwelling radiance in the presence of a cloud layer of thickness Δz can be expressed as (ref. 44):

$$E(\omega),h) = [\tau_\omega^c \ (\Delta z/\tau_\omega(\Delta z)]\{\varepsilon_s B(\omega,T_s)\tau_\omega(h,0)$$

$$+ \int_0^{z_b} B[\omega,T(z)]d\tau_\omega(h,z)]\}$$

$$+ \int_{z_b+\Delta z}^{h} B[\omega,T(z)]d\tau_\omega(h,z) \tag{2.5}$$

Detailed discussions of the above equation and the dependence of cloud transmittance $\tau\omega^c(\Delta z)$ on its liquid-water content and droplet size distribution is given in reference 44 (a copy of this is attached as Appendix A1). In addition, radiation models of finite clouds of different geometrical shapes and sizes are becoming increasingly available in the literature (refs. 45-49). The existing radiative transfer models should be modified to incorporate other cloud parameters in order to investigate the effects of their variability on upwelling radiances and fluxes.

During the International Radiation Symposium held at Colorado State University in August 1980, it was emphasized that the effect of non-local thermodynamic equilibrium (NLTE) should be considered in the radiative transfer formulations for a better interpretation of the Earth radiation budget experiment (ERBE) data. Inclusion of this effect was emphasized, especially for the fundamental bands of CO_2, O_3, and N_2O.

The monochromatic upwelling radiance under the NLTE condition, in the presence of a cloud layer of thickness Δ, may be expressed as (ref. 51):

$$E(\omega,h) = [\tau_\omega^c(\Delta z)/\tau_\omega(\Delta z)]\{\varepsilon_s B(\omega,T_s)\tau_\omega(h,0) + E(\mu_o)$$

$$+ \int_0^{z_b} J_\omega[T(z)d\tau_\omega(h,z)\}$$

$$+ \int_{z_b+\Delta z}^{h} J_\omega[T(z)]d\tau_\omega(h,z) \tag{2.6}$$

where $J_\omega[T(z)$ represents the nonequilibrium source function and is given in terms of the Planck function as

$$J_\omega[T(z) = \{E\Delta\omega[T(z)] + n\ B[T(z)\}/(1 + n) \tag{2.7}$$

where $n = n_c/n_r$. Equation 2.6 can be ulsed as a diagnostic equation to investigate the influence of NLTE on upwelling atmospheric radiation.

By following the nomenclature adopted by the International Radition Commission for the Earth Radiation Budget Experiments (ERBE) the expression for the upwelling radiance reaching the cloud base z_b from the underlying surface and atmosphere is given by (refs. 44 and 52)

$$L_\nu(z_b) = \varepsilon_s B_\nu(T_s)\tau_\nu(z_b,0) + \int_0^{z_b} B_\nu[T(z)d\tau_\nu(z_b,z) \tag{2.8}$$

where $\tau_\nu(z_b,0)$ is the clear column transmittance with reference to the cloud base z_b. The radiance reaching the top of the cloud layer at $z_b + \Delta z$ is given by

$$L_\nu(z_b+\Delta z) = L_\nu(z_b)\tau_\nu^T(\Delta z) + [1-\tau_\nu^T(\Delta z)]B_\nu(T_c) \tag{2.9}$$

where $\tau_\nu^T(\Delta z)$ represents the total transmittance through the cloud (i.e., it is the product of the transmittance due to cloud and the transmittance of the atmosphere in the cloud) and $B_\nu(T_c)$ is the Planck function evaluated at the cloud average temperature $\bar{T}_c$. The first term on the right hand side of equation (2.9) represents the radiance reaching the cloud top from the underlying surface and atmosphere, and the second term is the radiance due to the cloud emission. A combination of equations (2.8) and (2.9) results in

$$L_\nu(z_b+\Delta z) = \tau_\nu^T(\Delta z)\ \varepsilon_s B_\nu(T_s)\ \tau_\nu(z_b,\ 0)$$

$$+\ \tau^T(\Delta z)\ \int_0^{z_b} B\nu[T(z)]d_\tau\ (z_b,\ z)$$

$$+\ [1-\tau_\nu^T(\Delta z)]B_\nu(T_c) \qquad (2.10)$$

The upwelling radiance reaching the top of the atmosphere (denoted by h in this study) is expressed as

$$L_\nu(h) = L_\nu(z_b+\Delta z)\tau_\nu(h,\ z_b+\Delta z) + \int_{z_b}^{h} B_\nu[T(z)]d\tau_\nu(h,z) \qquad (2.11)$$

A combination of equations (2.10) and (2.11) results in

$$L_\nu(h) = \tau_\nu^C(\Delta z)\tau_\nu(h,0)\varepsilon_s B_\nu(T_s)$$

$$+ \tau_\nu^c(\Delta z)\int_0^{z_b} B_\nu[T(z)]\,d\tau_\nu(h,z)$$

$$+ \tau_\nu(h,z_b+\Delta z)[1-\tau_\nu^T(\Delta z)]B_\nu(T_c)$$

$$+ \int_{z_b}^{h} B_\nu[T(z)]\,d\tau_\nu(h,z) \qquad (2.12)$$

where τ_ν^c is the cloud transmittance. It should be noted that equation (2.12) is a modified form of equation (2.5).

As Δz approaches zero, $\tau_\nu^c\ (\Delta z)$ and $\tau_\nu^T\ (\Delta z)$ approach unity, and equation (2.12) reduces to

$$L_\nu(h) = \varepsilon_s B_\nu(T_s)\ \tau_\nu(h,o) + \int_0^h B_\nu[T(z)]\ d\tau_\nu(h,z) \qquad (2.13)$$

This is an expression for the upwellilng radiance for a plane-parallel clear atmosphere and can be expresed also in a direction θ relative to nadir as

$$L_\nu(\theta) = \varepsilon_s B_\nu(T_s)\tau_{\nu s}(\theta) + \int_{\tau_{\nu h}}^{1} B_\nu(T_z)\ d\tau_{\nu z}(\theta) \qquad (2.14)$$

In a simplified study, the radiance for an overcast atmosphere is obtained from equation (2.14) by treating the cloud top as the underlying surface and considering only that part of the atmosphere which lies above the cloud. For partly cloudy conditions, the radiance is obtained as the cloud fraction weighted sum of the overcast and clear radiances.

The total outgoing radiance is obtained by integrating the spectral radiances

$$L(\theta) = \int_{\Delta\nu} L_\nu(\theta) d\nu \qquad (2.15)$$

By assuming azimuthal symmetry, the spectral outgoing flux can be obtained, in principle, by integrating equation (2.15) over the nadir angle θ from 0 to $\pi/2$ as

$$M_\nu = 2\pi \int_0^{\pi/2} L_\nu(\theta) \sin\theta \cos\theta \, d\theta \qquad (2.16)$$

In practice, however, lengthy numerical integration is avoided by using the diffusivity approximation (ref. 17). The total outgoing flux M can be obtained by integrating M_ν over the frequency range $\Delta\nu$ as

$$M = \int_{\Delta\nu} M_\nu \, M\nu \, d\nu \qquad (2.17)$$

The anisotropic function is defined as

$$R(\theta) = \pi L(\theta)/M \qquad (2.18)$$

The difference between the largest and smallest values of $R(\theta)$ is a good indicator of the extent of limb darkening for most atmosphere models. This is defined as

$$G = R(\theta_{min}) - R(\theta_{max}) \qquad (2.19)$$

where the largest value of $R(\theta)$ corresponds to the minimum value of θ and vice versa.

ORIGINAL PAGE IS
OF POOR QUALITY

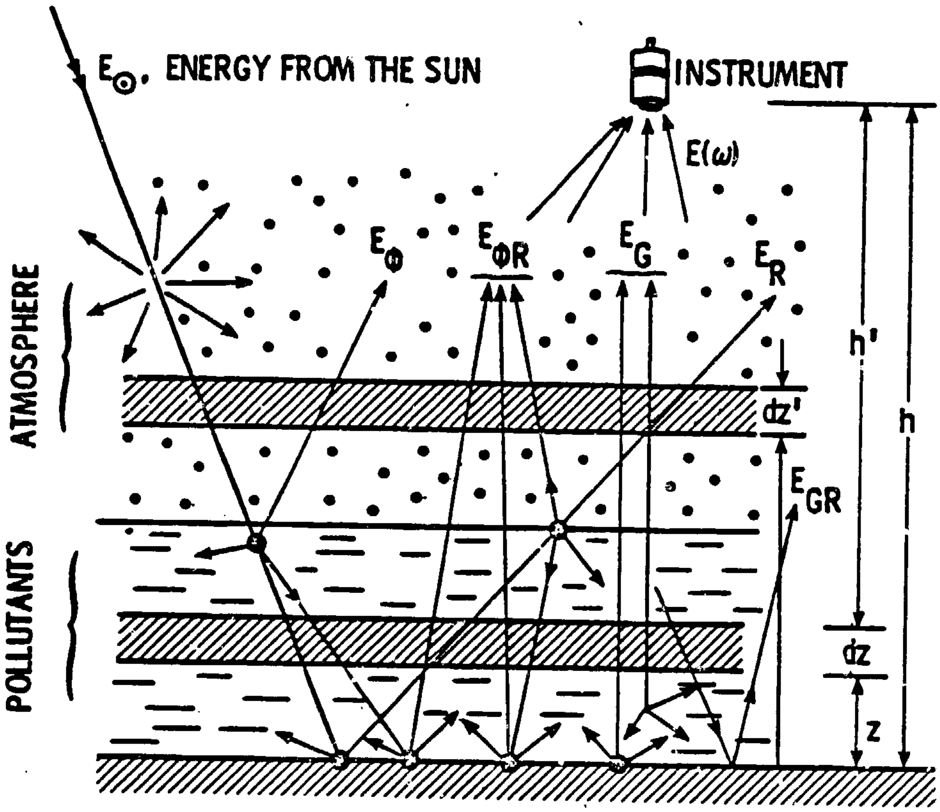

Figure 2.1. Various components of upwelling atmospheric radiation.

3. ABSORPTION MODELS

The greatest problem in computing radiances and fluxes is the integration of spectral relations over the frequency range of interest. The absorption coefficient (and, hence, the transmittance) is a highly variable function of the frequency, and for accurate work it should be evaluated at small frequency intervals. Furthermore, within a band which usually consists of thousands of rotational lines, the absorption coefficient at any frequency is made up of contributions from many lines. In principle, therefore, it is possible to calculate the absorption coefficient with very high accuracy by summing the contributions of all intervening lines. In practice, however, it is a very tedious and time-consuming process. For a wide frequency range with several bands, each with a large number of lines, large amounts of computer resources are required. As such, use of simplified models for spectral absorption is highly desirable.

As mentioned in the introduction, considerable efforts have been spent in the past in devising simplified models to overcome the problem of numerical integration over the complicated line structure of the atmospheric spectrum. A complete review on different absorption models is available in reference 4. The absorption models proposed for the present study are discussed in references 20, 53 and 54. In these references, the validity of the QRB model has been investigated by comparing the results of this model with the LBL, experimental, and other accurate-model results available in the literature. These comparisons show that the QRB formulation offers an accurate and efficient method for calculating the transmittances and radiances in nonhomogeneous nonisothermal systems. Further work, however, is needed to establish the validity of this model. It would be desirable to compare the results of LBL, QRB, LOWTRAN, K-distribution, and FOSCODE models

for selected conditions to establish the validity of the QRB formulation. However, because of high computational costs, this is beyond the scope of the present study.

4. COMPUTATIONAL PROCEDURE AND DATA SOURCE

The numerical procedure for evaluating the spectral atmospheric transmittance and the upwelling radiance and the data source used for the calculations are described briefly in this section.

In calculating the atmospheric transmittance, the atmosphere is divided into a number of layers of equal thickness (in the present case, 1 km). For the present study, the top of the atmosphere was considered first to be 10 km, which is approximately the top of the troposphere. Selected results were also obtained by considering the top of the atmosphere at 20 and 30 kilometers. The pressure path length is given by the expression

$$du_{ij} = Q_{ij}(P_j/P_{NTP})(T_{NTP}/T_j)dz_j \tag{4.1}$$

where Q_{ij} is the volume mixing ratio of the ith constituent in the jth layer, dz_j is the thickness of the jth layer, and P_j and T_j are the pressure and temperature at the center of the jth layer, respectively. The transmittance at location z in the atmosphere is given by

$$\tau(\omega, z) = \exp\left[-\int_0^u \sum_j \sum_i k_{ij}(\omega)du_{ij}\right] \tag{4.2}$$

Following the procedure for evaluating the atmospheric transmittance, upwelling radiance is calculated by dividing the nonhomogeneous atmosphere into a number of homogeneous sublayers. The complete numerical procedure and computer programs are available in references 53 and 54.

The line parameters needed for this study (position, strength, line, width, etc.) were obtained from McClatchey et al. (refs. 55 and 56). The "McClatchey Tape" is available at the NASA/Langley Research Center. The at-

mospheric temperature and pressure profiles were taken from the U.S. Standard Atmosphere 1962 (ref. 57). The information on global annual average model atmosphere is given in table 4.1. The concentration distributions in the atmosphere for H_2O, CO_2, N_2O and O_3 were taken from McClatchey et al. (ref. 55). The CO_2 and N_2O are assumed to be uniformly mixed in the atmosphere. Rotational and vibrational partition functions, required to account for the temperature dependence of the line strengths, were taken from McClatchey et al. (ref. 56).

The categories of other model atmospheres, as obtained from reference 58, are listed in table 4.2. The information on cloud cover and location is given in pertinent chapters.

Table 4.1 Global annual average model atmosphere.

Alt (km)	Press (atm)	Temp (Kel)	Water Vap (PPMV)	Ozone (PPMV)
.5	954.61	284.90	.6957E+04	.2790E-01
1.5	845.59	278.40	.5395E+04	.3078E-01
2.5	746.91	271.91	.3949E+04	.3277E-01
3.5	657.80	265.41	.2701E+04	.3353E-01
4.5	577.52	258.92	.1801E+04	.3531E-01
5.5	505.39	252.43	.1176E+04	.3891E-01
6.5	440.75	245.94	.8887E+03	.4492E-01
7.5	382.99	239.46	.4762E+03	.5412E-01
8.5	331.54	232.97	.2692E+03	.7418E-01
9.5	285.84	226.49	.1170E+03	.1104E+00
10.5	245.40	220.01	.5422E+02	.1707E+00
11.5	209.84	216.65	.2836E+02	.2592E+00
12.5	179.34	216.65	.1534E+02	.3451E+00
13.5	153.27	216.65	.8613E+01	.4404E+00
14.5	131.00	216.65	.5955E+01	.5726E+00
15.5	111.97	216.65	.5940E+01	.7369E+00
16.5	95.72	216.65	.5903E+01	.9991E+00
17.5	81.82	216.65	.5867E+01	.1375E+01
18.5	69.95	216.65	.6291E+01	.1796E+01
19.5	59.80	216.65	.7358E+01	.2289E+01
20.5	51.13	217.08	.9016E+01	.2793E+01
21.5	43.75	218.08	.1151E+02	.3323E+01
22.5	37.46	219.07	.1471E+02	.3898E+01
23.5	32.09	220.06	.1867E+02	.4391E+01
24.5	27.52	221.06	.2355E+02	.4867E+01
25.5	23.62	222.05	.2734E+02	.5371E+01
26.5	20.28	223.04	.2893E+02	.5901E+01
27.5	17.43	224.03	.3026E+02	.6342E+01
28.5	14.99	225.02	.3154E+02	.6628E+01
29.5	12.90	226.01	.3276E+02	.6673E+01

Volume Mixing Ratios (PPMV)

N_2O	CH_4	CO_2
.28	1.6	330.

Table 4.2 Categories of 106 model atmospheres (ref.58).

1. Cloudiness	Clearsky cases	58
	Undercast	48
2. Diurnal Coverage (Local Time)	Daytime cases (0700 - 1859)	52
	Nighttime cases (1900 - 0656)	54
3. Climate Type	Maritime	66
	Continental	40
4. Latitudinal Distribution	Tropical (0° - 30°)	20
	Mid-lat (30° - 60°)	62
	Sub-arctic polar (60° - 90°)	24
5. Seasonal Coverage	Spring (3/16 - 6/15)	16
	Summer (6/16 - 9/15)	33
	Autumn/Fall (9/16 - 12/15)	27
	Winter (12/16 - 3/15)	30

5. ACCURATE EVALUATION OF LONGWAVE RADIATION IN CLEAR ATMOSPHERE

In recent studies (refs. 20, 44, 51, and 54), accurate theoretical models were developed for evaluating the upwelling atmospheric radiance and radiative flux. The existing computer codes were refined to include detailed information on the LBL and QRB absorption and various surface and atmospheric parameters. The feasibility of the QRB model for atmospheric studies were made to investigate the influence of various surface and atmospheric parameters on the upwelling radiances. Some of the important results of recent investigations are discussed here very briefly, and the details are available in the cited references.

5.1 Evaluation of Atmospheric Transmittance

In the longwave range, atmospheric transmittances were calculated by employing the LBL and QRB formulations in selected spectral intervals. The calculations were made for clear sky conditions, and contributions of all important species were considered in each spectral interval. The results were compared with available theoretical and experimental results (ref. 54). Specific transmittance results for the spectral range from 2,500 to 2,800 cm^{-1} are shown in figures 5.1 and 5.2. The results calculatred by the LBL and QRB Models and LOWTRAN program (by considering only the 3.17-μ water vapor band) are shown in figure 5.1. The results are found to be in good agreement. The results presented in figure 5.2 are also for the same spectral range, but, in this case, contributions of other bands (3.57-μ O_3, 3.85-μ CH_4, and 4.5-μ N_2O) have been included in calculating the atmospheric transmittance. From a comparison of results presented in these figures it may be concluded that the QRB results are in good agreement with the LBL and

LOWTRAN results and that the transmittance (in this spectral range) is mainly due to the 3.17-μ H_2O band. Results for other spectral ranges are available in reference 54.

For further study, it is suggested to calculate the atmospheric transmittance, in different spectral ranges, by employing the QRB, K-distribution, LOWTRAN, and FASCODE models and compare the results with the results of LBL formulation.

5.2 Evaluation of Upwelling Radiance and Radiative Flux

For the standard atmospheric conditions (table 4.1), the results for upwelling radiance and radiative flux were obtained for selected spectral ranges by employing the QRB formulation. In each spectral range, contributions of all important species were considered. For preliminary study, the top of the atmosphere was taken to be at 10 km; but, later results were obtained also by considering the top of the atmosphere at 20 and 30 km. The contribution of the reflected component of solar radiation was included in the calculation of the upwelling radiance for an illustrative case, but the contribution of atmospheric radiation reflected from the surface was neglected.

Specific results for the spectral range from 2,500 to 2,800 cm^{-1} are presented in figure 5.3 for the case in which the contribution of reflected solar radiation was included. For a fixed surface emittance, the upwelling radiance is seen to increase with increasing surface temperature. This is because the surface and atmospheric emissions are relatively higher at higher surface temperatures. For a fixed surface temperature, the radiance is seen to increase with decreasing surface emittance. This is because, for lower surface emittance, the reflected component of the solar radiation is

larger, and this makes the total upwelling radiance relatively higher. Similar conclusions were drawn also from the results presented in references 28 and 54. The results presented in the rest of this section were obtained by neglecting the contributions of the reflected solar radiation.

For standard atmospheric conditions, the variation in upwelling radiance and radiative flux at different altitudes is illustrated in figure 5.4 for the spectral range of 5-50 μ where most of the longwave radiative processes occur. The results clearly show that the upwelling radiance and flux increase with increasing surface temperature and decrease with increasing altitude. As pointed out earlier, this is because the surface and atmospheric emissions will be relatively higher for higher surface temperatures; and the radiative energy will attenuate with increasing atmospheric thickness. It is further noted that the attenuation above 20 km is relatively small, and the top of the atmosphere can be taken as 30 km for most applications.

For different longwave spectral ranges, the variations in upwelling radiance and radiative flux with surface temperature are shown in figures 5.5 and 5.6, respectively. The solid curves represent the results for the atmospheric top at 10 km and the broken curves for the atmospheric top at 30 km. It is seen that the radiative contributions from different spectral regions add up to give the highest values for the spectral range 5-50 μ; the values for other spectral ranges are relatively lower. As noted earlier, the results for 30 km are relatively lower than for 10 km. The results for the atmospheric window (10.5 - 12.5 μ) are the lowest and are identical for 10 and 30 kilometers. This is because there are only a few weakly absorbing species in this range and they do not contribute to the radiative proc-

ess beyond certain height.

The variation of upwelling radiance and radiative flux with surface emittance is shown in figures 5.7-5.9. The results presented in figures 5.7 and 5.8 are for the spectral range 5-50 μ, and the results in figure 5.9 are for the window region. The results show that for a given surface temperature the radiance and flux increase with increasing surface emittance. This is true, in general, for all nonreflecting radiating surfaces. For the earth-atmosphere system, however, the trend exhibited in figures 5.7 - 5.9 is true only if the contribution of reflected solar radiation is neglected.

From the results presented in this section, it may be concluded that the QRB formulation is quite suitable for most atmospheric applications. The procedure for calculating the upwelling radiance and radiative flux has been developed by using the QRB model and illustrative results have been obtained for the standard atmospheric conditions. The results demonstrate that for a fixed surface emittance the upwelling radiance and flux increase with increasing surface temperature and decrease with increasing height. The radiative attenuation above 20 km is small and the top of the atmosphere can be considered as 30 km for most applications. The radiative contributions from different spectral ranges add up to give the total upwelling radiance. The contribution from the window region is quite small and the spectral region 5-20 contributes considerably to the entire longwave radiation.

ORIGINAL PAGE IS
OF POOR QUALITY

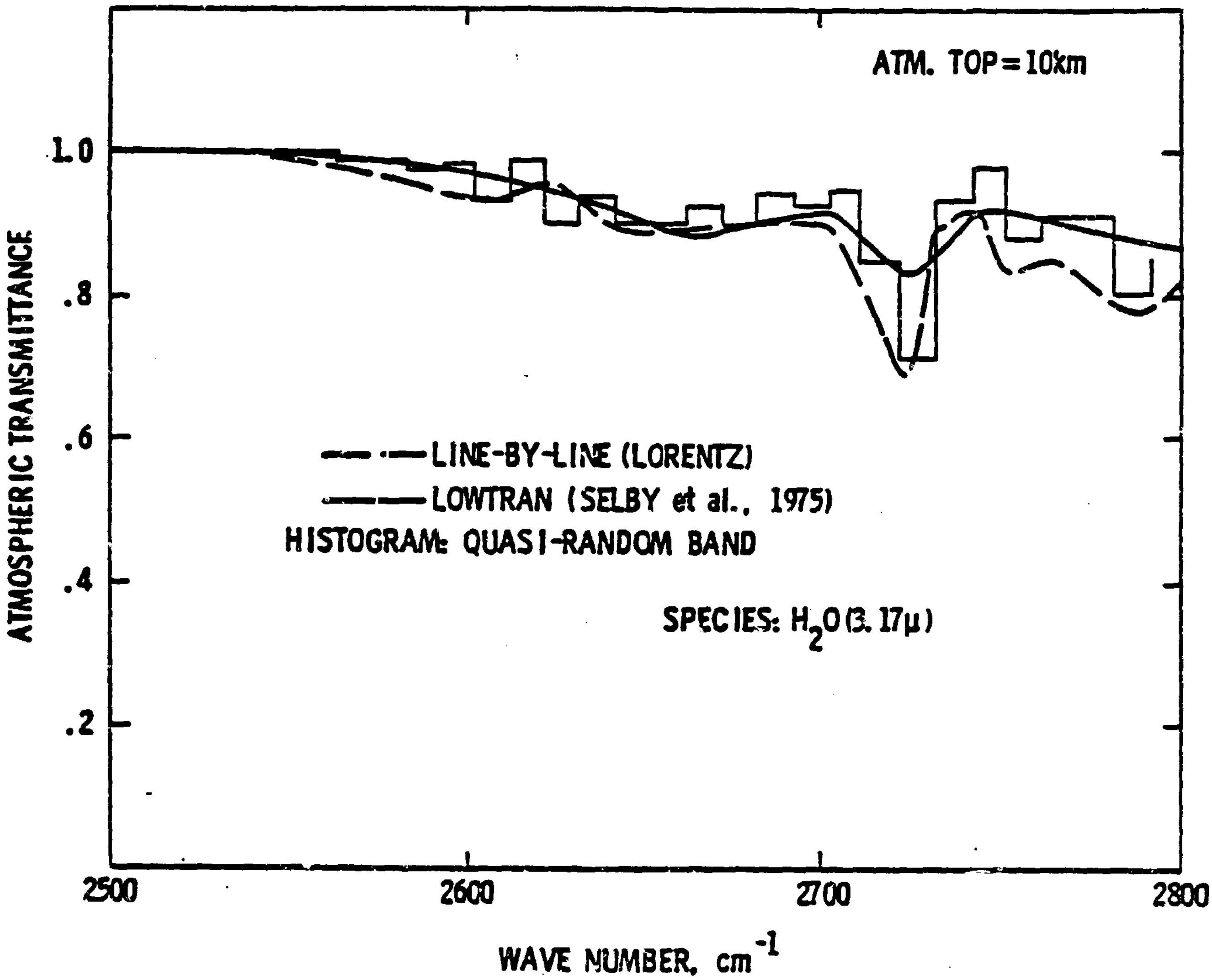

Figure 5.1 Comparison of atmospheric transmittance in the spectral range from 2500 to 2800 cm^{-1} considering water vapor only.

ORIGINAL PAGE IS
OF POOR QUALITY

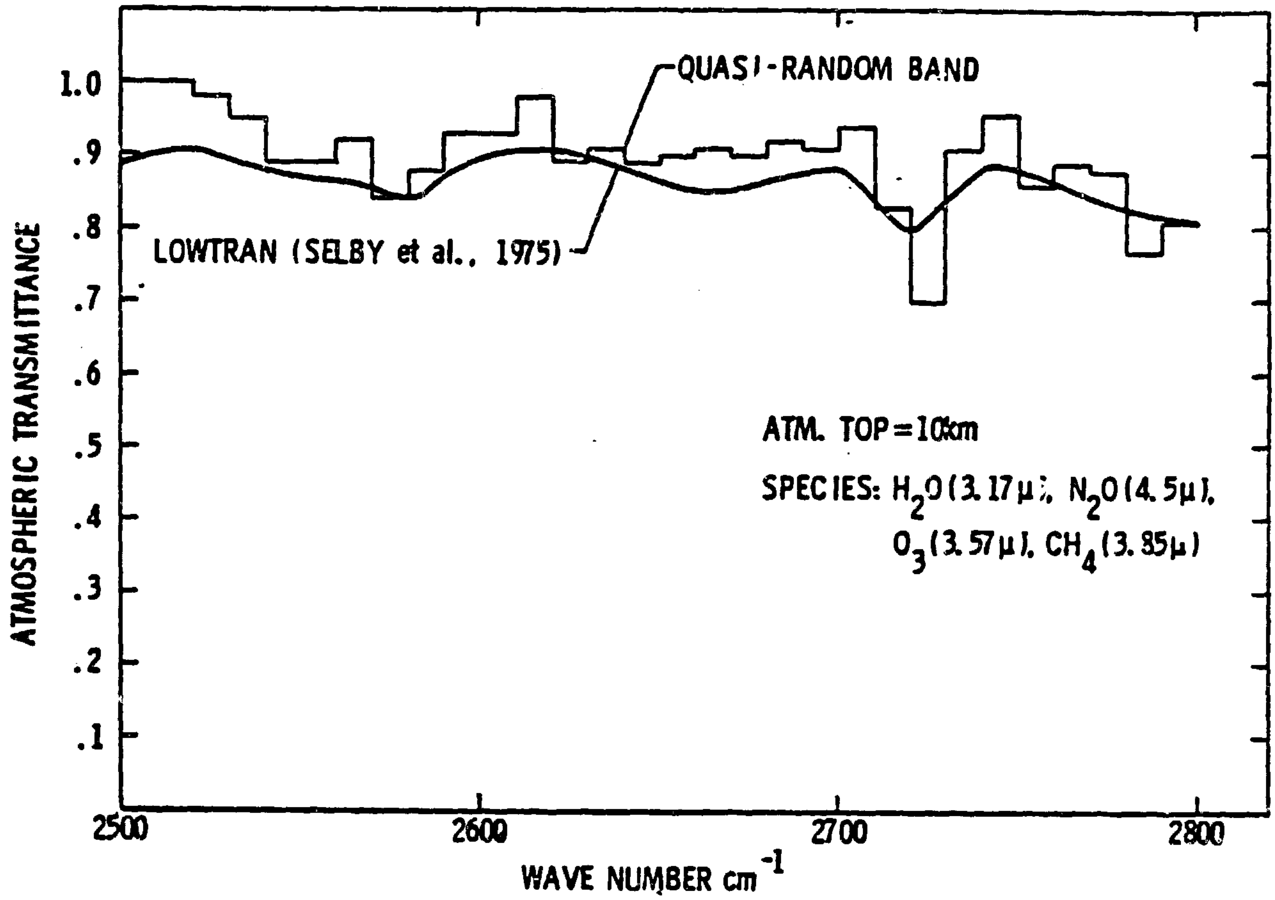

Figure 5.2 Comparison of atmospheric transmittance in the spectral range from 2500 to 2800 cm^{-1}.

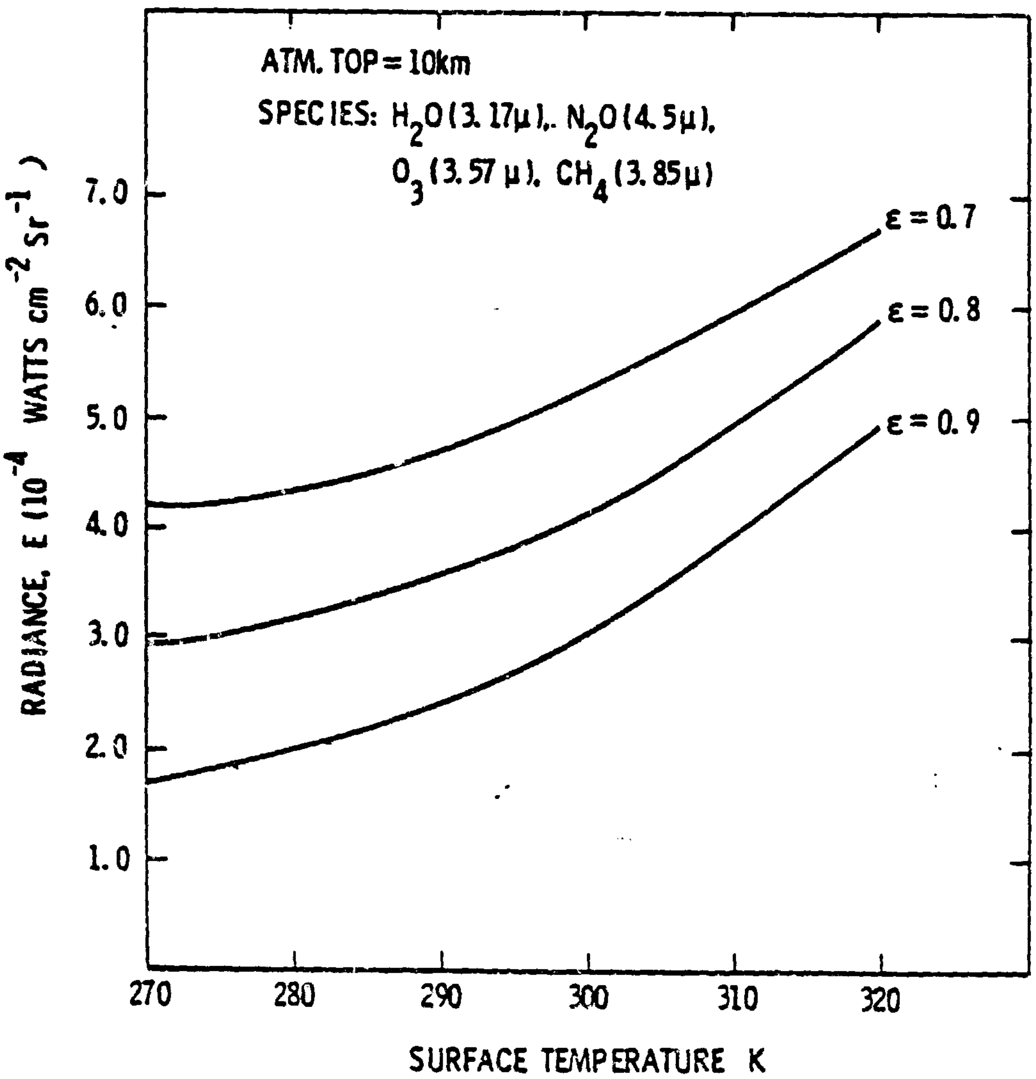

Figure 5.3 Upwelling radiance as a function of surface temperature (spectral range from 2500 to 2800 cm^{-1}).

ORIGINAL PAGE IS
OF POOR QUALITY

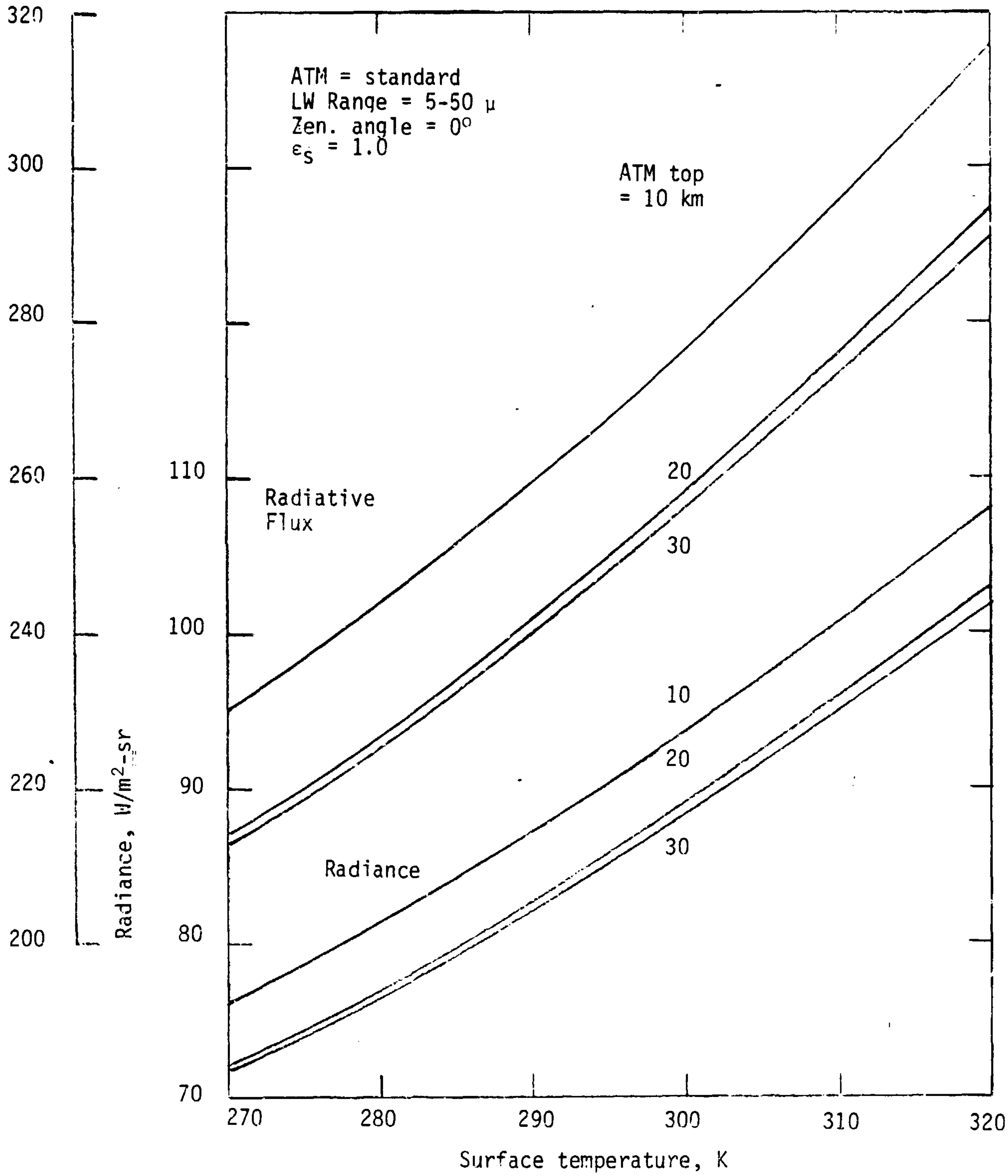

Figure 5.4 Variation in upwelling radiance and radiative flux with surface temperature for different altitudes LW Range = 5-50 μ.

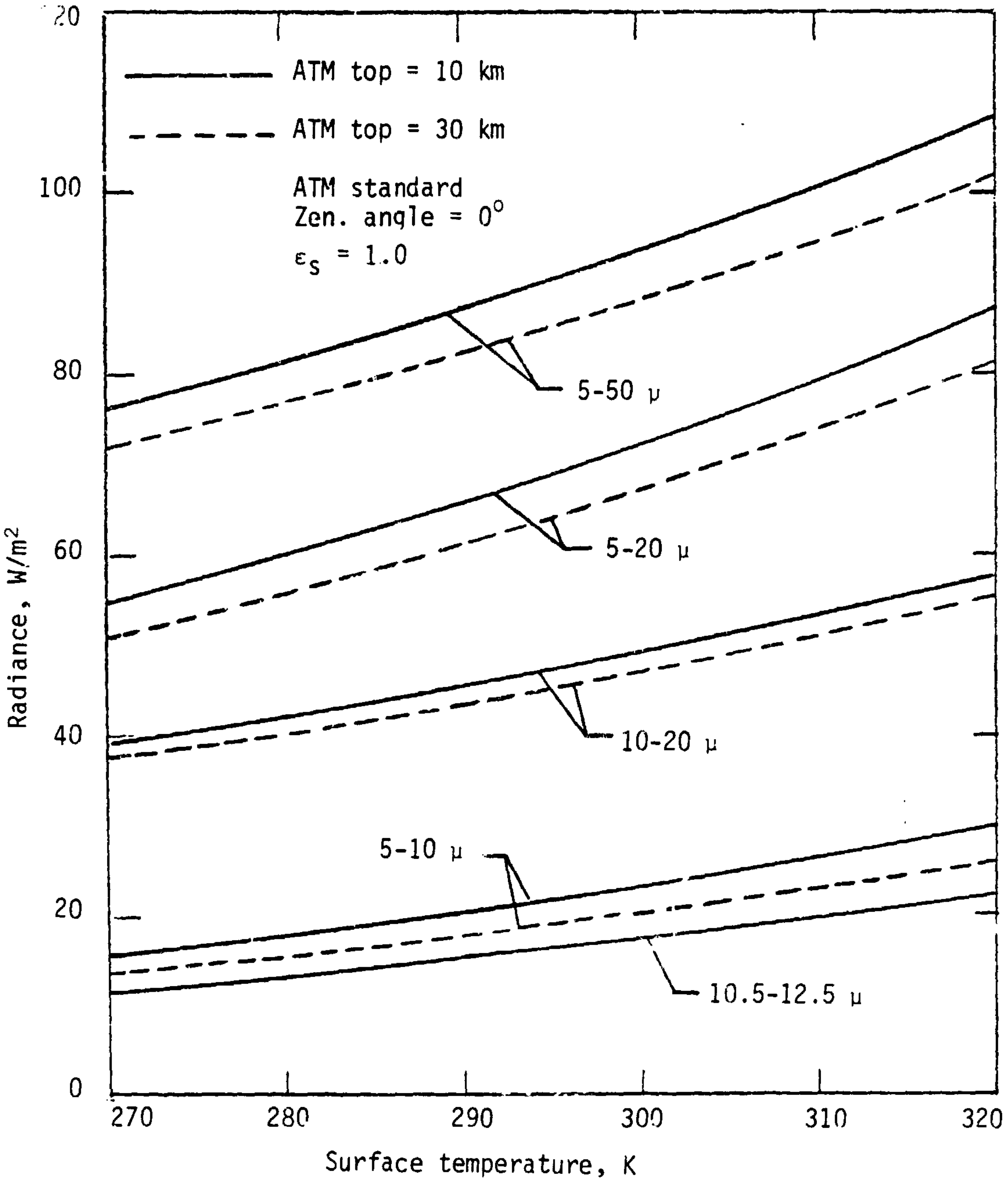

Figure 5.5 Variation in upwelling radiative with surface temperature for different spectral ranges.

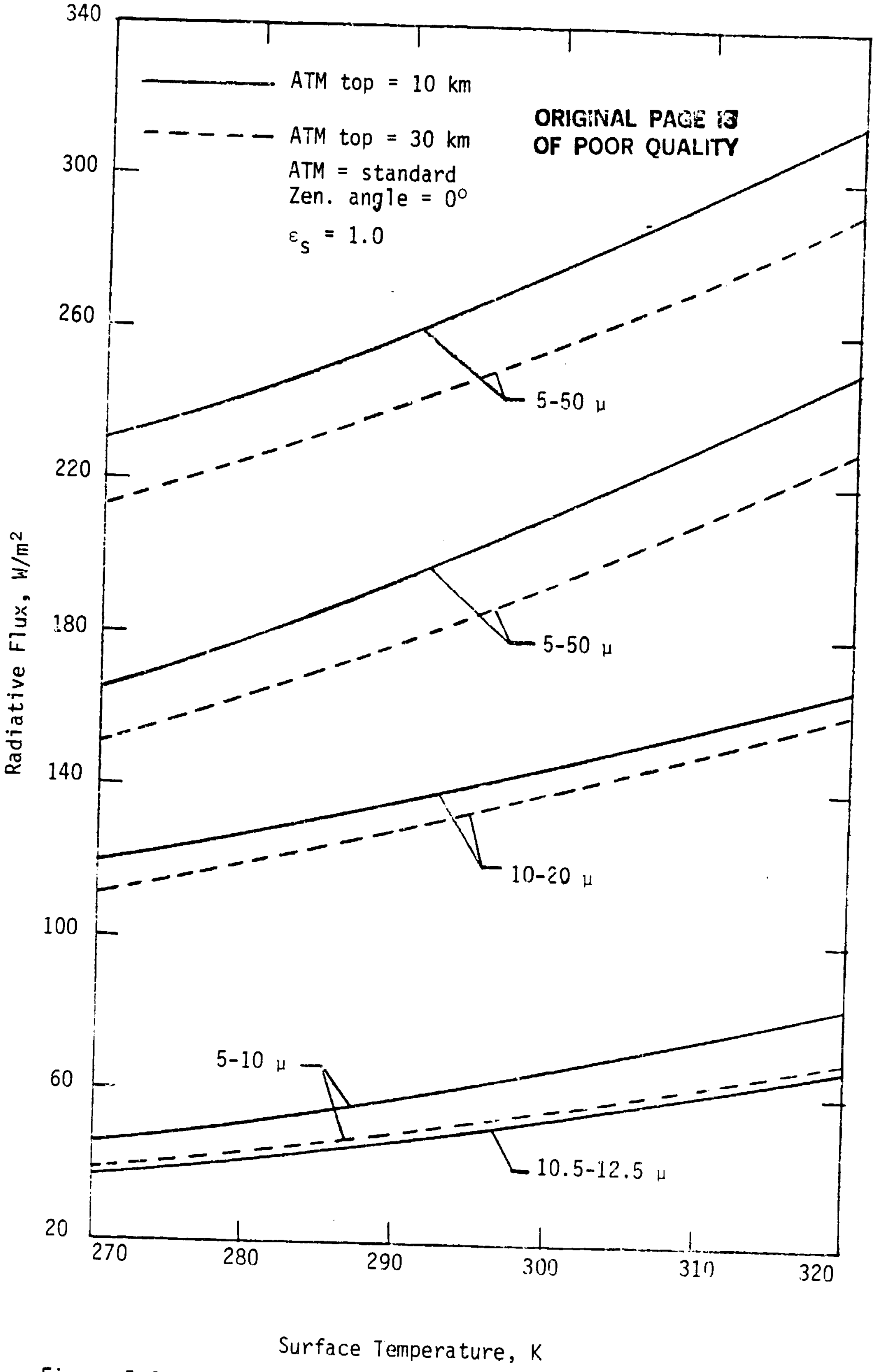

Figure 5.6 Variation in upwelling radiative flux with surface temperature for different spectral ranges.

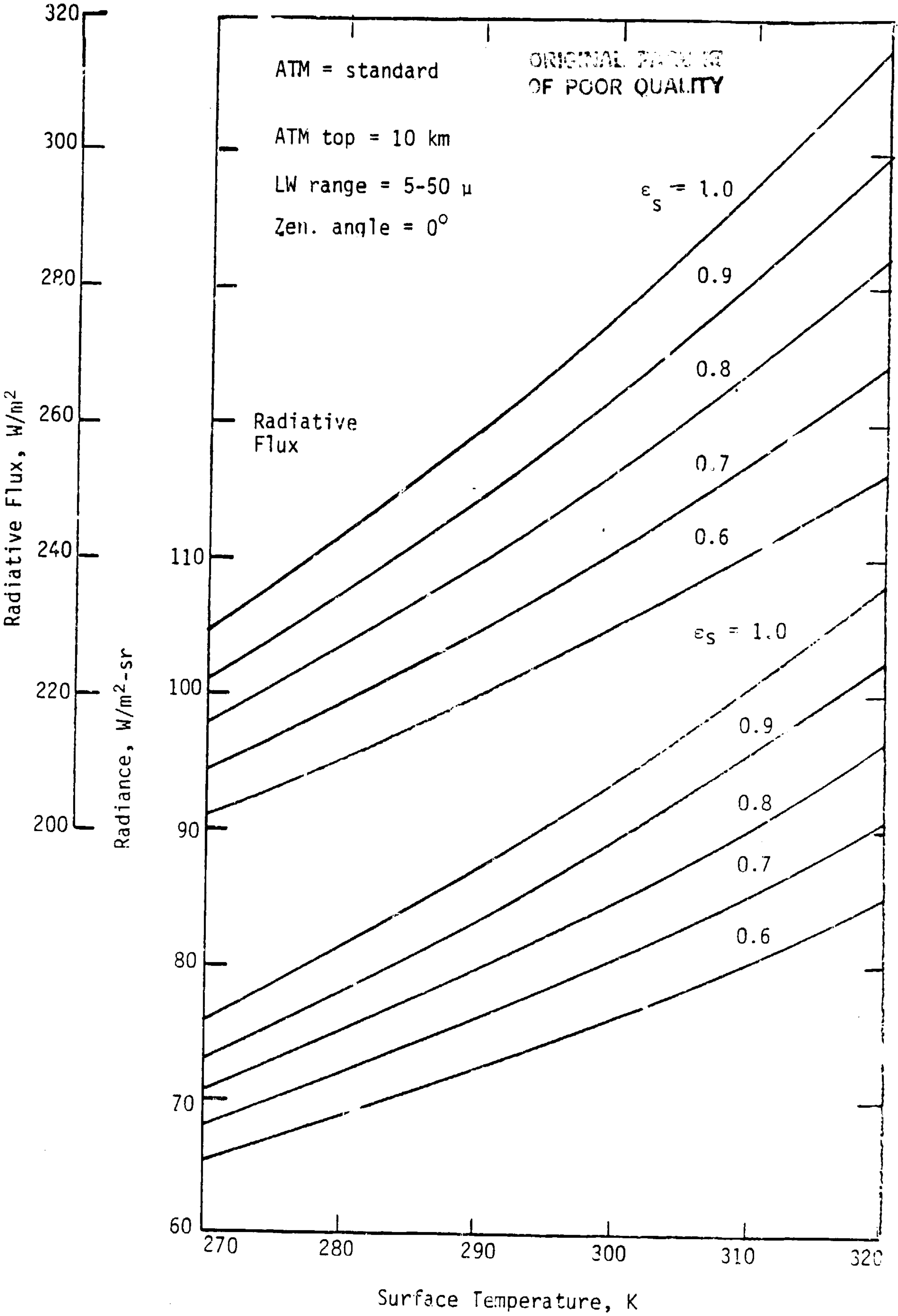

Figure 5.7 Variation in upwelling radiance and radiative flux with surface temperature for different surface emittances, LW Range = 5-50 μ, ATM top = 10 km.

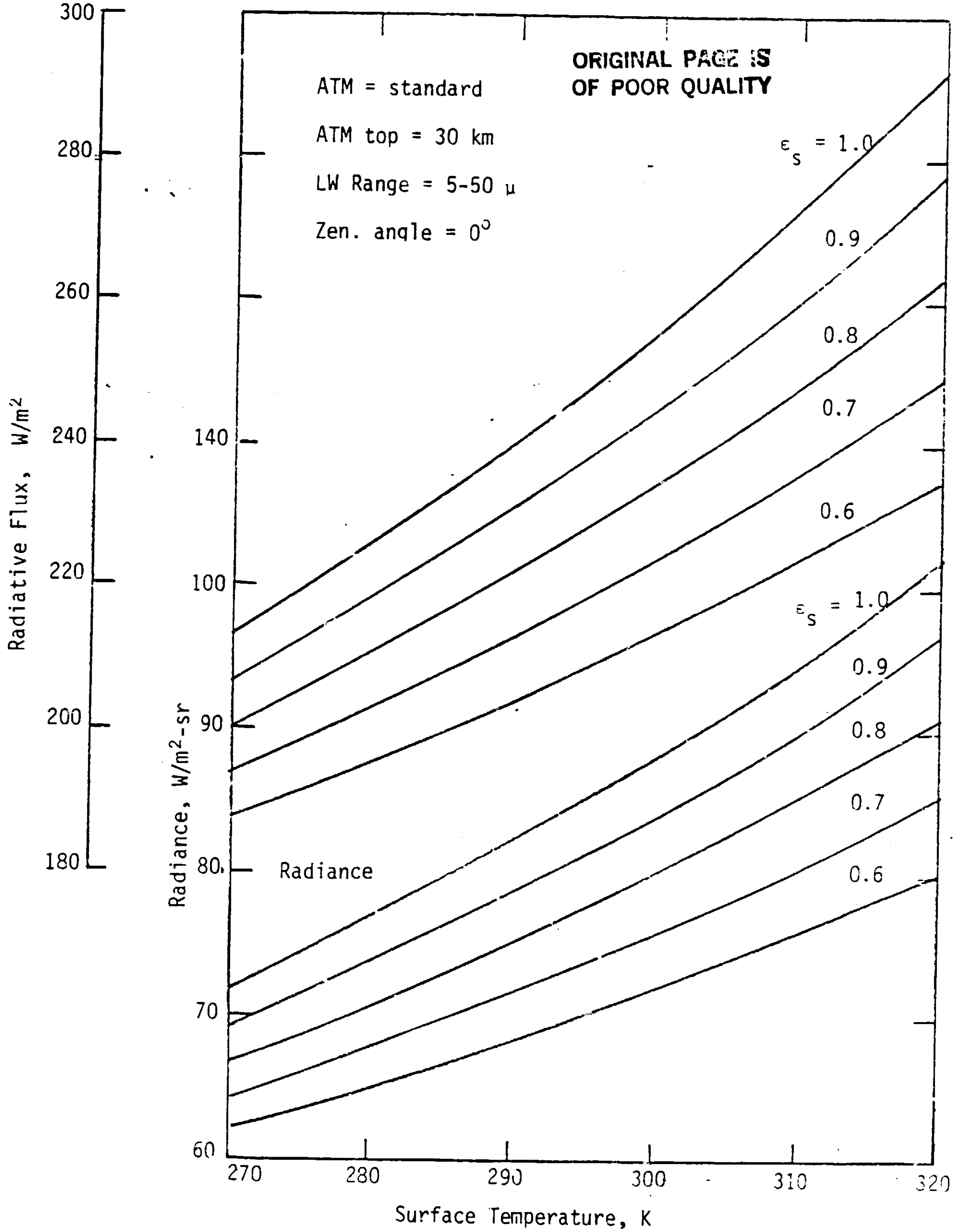

Figure 5.8 Variation in upwelling radiance and radiative flux with surface temperature for different surface emittances, LW Range = 5-50 μ, ATM top = 10 km.

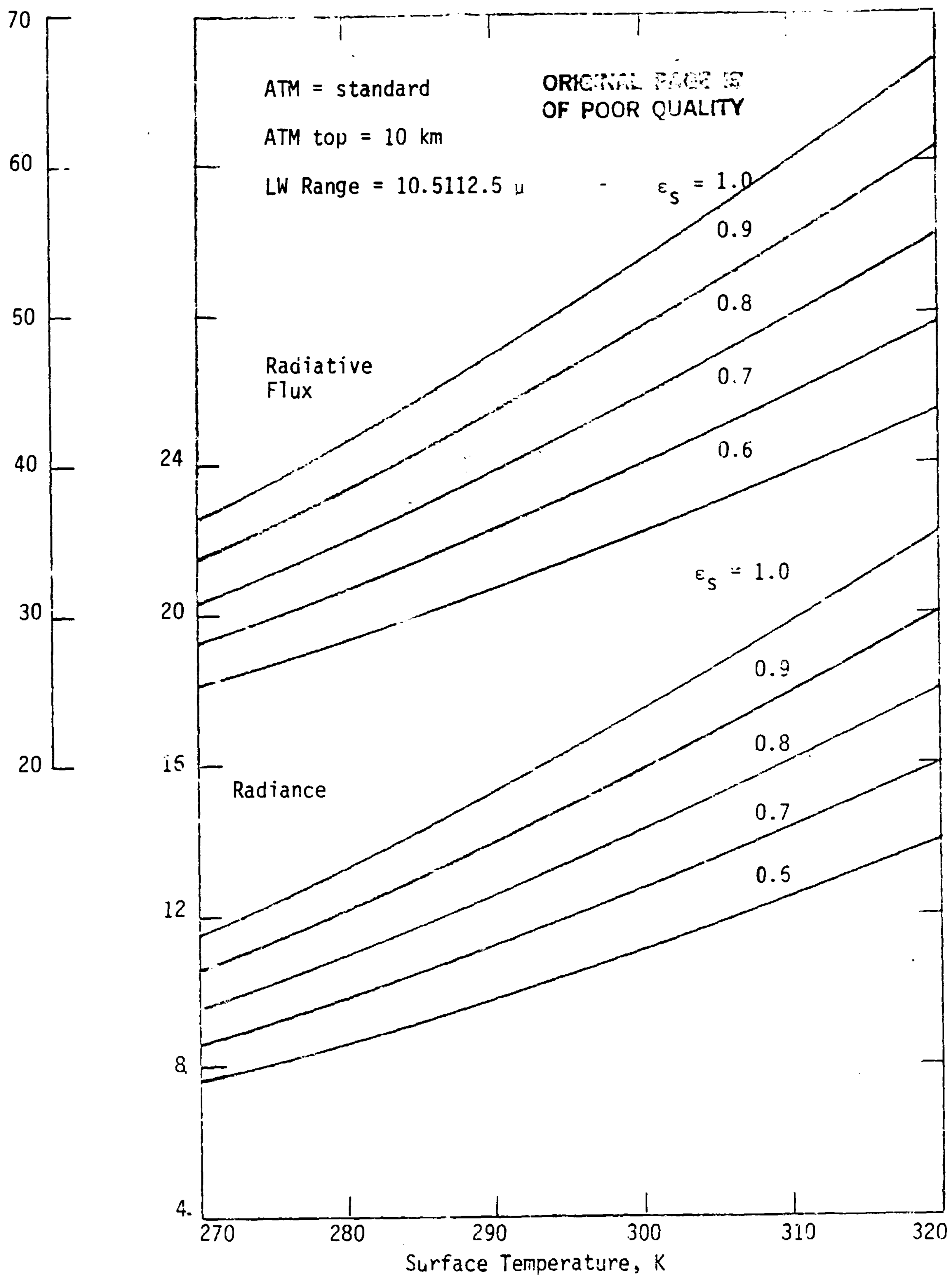

Figure 5.9 Variation in upwelling radiance and radiative flux with surface temperature for different surface emittances, LW Range = 10.5-125 μ, ATM top = 10 km.

6. SENSITIVITY ANALYSIS OF UPWELLING RADIANCE IN PRESENCE OF CLOUDS

The existing radiative transfer programs were modified to investigate the effects of clouds on the upwelling radiance. In order to study the sensitivity of upwelling radiance to variations in cloud height, cloud liquid water content, and cloud thickness, calculations were made in three different spectral ranges. They are the 5- to 10-μm, 10.5- to 12.5-μm (window), and 10- to 20-μm regions. These spectral regions include most of the strong absorption and emission bands of H_2O, CO_2, O_3, and N_2O. The QRB formulation was employed and results were obtained for the standard atmospheric conditions. The key results are discussed completely in reference 44, and a copy of this is attached as Appendix A1; the entire results are tabulated in Appendix B2.

As an example of the sensitivity analysis, the variation of radiance with cloud height is illustrated in figure 6.1 for different spectral range and surface emissivity. It is seen that the upwelling radiance decreases with increasing cloud height for all three spectral ranges. This is because the effective cloud top temperature at which the absorbed radiance is reemitted is lower for higher level clouds. It is noted that the maximum impact of the cloud layer is in the window region. Here, the reduction in upwelling radiance (from the clearsky value) by a cloud at z = 11 km is about 49 percent as compared to about 43 percent in the 5- to 10-μ range and 37 percent in the 10- to 20-μm range.

Other results of this study presented in Appendix A1 indicate that the difference between the clear and cloudy sky radiances is nearly 36 percent for the cloud base at 5 km and about 43 percent for the cloud base at 10 km; this difference increases with increasing surface emissivity and surface

temperature. Further sensitivity studies, however, are needed to study the formation of different types of clouds and their interaction with the atmosphere, study the influence of cloud height variations on the net upwelling flux, evaluate the total longwave flux and correlate this with the window flux by varying the cloud droplet-size distribution, and evaluate the variation of total and window region flux with the cloud liquid water content and cloud top temperature.

ORIGINAL PAGE IS
OF POOR QUALITY

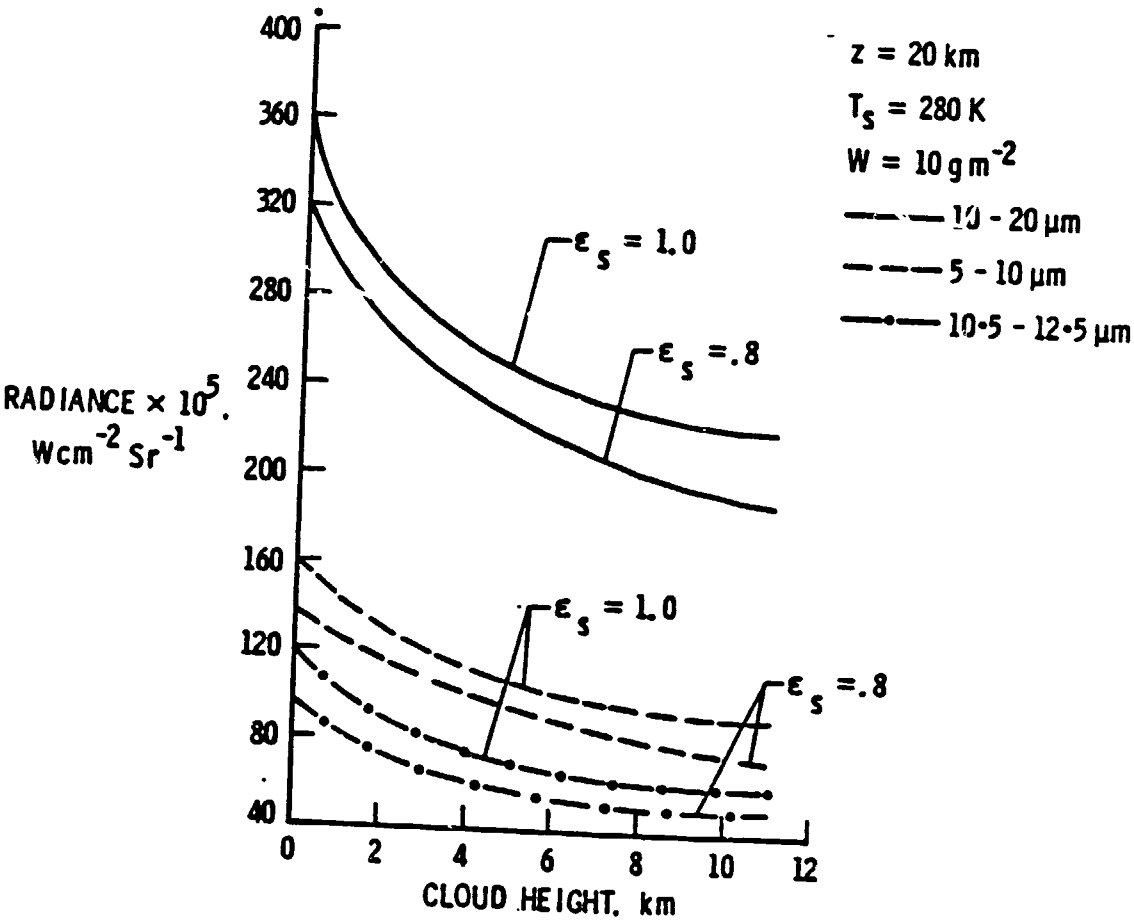

Figure 6.1 Upwelling radiance variation with cloud height.

7. EVALUATION OF ANISOTROPIC FUNCTIONS IN THE LONGWAVE REGION

7.1 Introduction

A study of the anisotropic function in the atmosphere has assumed greater importance recently because of its applicability for the Earth Radiation Budget Experiment (ERBE). This experiment is designed to measure the radiation budget of the Earth-atmosphere system at the top of the atmosphere. The scanning radiometer which is an important component of the instrument complement measures the radiance emanating at the top in a given direction. These directional radiances can be converted to the total outgoing flux density only if the anisotropic functions for the atmosphere are known.

In this study, anisotropic functions have been calculated for several model atmospheres. The effects of variability of various meteorological parameters on the anisotropic function are investigated. During the initial phases of this study, the spectral range considered for the longwave radiative transfer was 5-50μ. The results were presented at a national conference (AIAA Paper 83-0161) and the entire material is included in this report as Appendix A2. Some specific results discussed in Appendix A2 are tabulated in Appendix B3. Later, the computer code was modified to cover the longwave spectral range 5-200μ. Key results of this study are presented here and are compared with the results presented in Appendix A2.

7.2 Physical Conditions and Computational Procedure

The physical conditions, data source, and computation procedure are esentially the same as given in Appendix A_2; these are discussed here briefly.

The top of the atmosphere is considered to be at 30km. For calculation of the transmittance and radiance, the atmosphere is divided into 15 layers; the first ten layers are one-kilometer thick. The low altitude cloud is assumed to be at 2 km, middle-level cloud at 6 km, and high-level cloud at 10 km. The thickness of the cloud layers is assumed to be one kilometer.

Several climatological-average model atmospheres are used to establish the latitudinal and seasonal variability of the anisotropic functions. These are tropical, mid-latitude summer/winter, sub-arctic summer/winter in addition to the U.S. Standard Atmosphere (USSA) which represents the mean-annual mid-latitude conditions. Pressure, temperature, and ozone profiles for the above models are taken from McClatchey et al. (refs. 55 and 56). A climatological mean value for the surface relative humidity (RH) of 75% (ref. 59) is used for all of the above models and vertical distribution of water vapor is computed using the power law (ref. 60)

$$w_z = w_z(p_z/p_s)^\lambda \tag{7.1}$$

where λ is related to the water-vapor scale height and its average value is taken to be 3. The concentration of water vapor is calculated by

$$C = A \exp(18.9766-14.9595A-2.4388A^2) \tag{7.2}$$

where $A = 273.15/T_s$. Upon dividing by the density and multiplying by the ratio of air molecular weight to the water vapor molecular weight, the concentration of water vapor in ppmV is obtained. Data files are created for different surface relative humidities.

The computer code developed for this study has the following capabil-

ities:

1. The upwelling radiance and radiative flux in the longwave range from 5 to 200 μ (2000 to 50 cm^{-1}) can be calculated; the program can be used also in any specified spectral range between 5-200 μ.
2. The participating species considered for the calculation of the atmospheric transmittance are Ch_4, CO_2, H_2O, N_2O, and O_3. The effect of any particular gas (i.e., the radiative contribution of a specific molecular gas) can be investigated.
3. The atmosphere (with top at 30 km) is divided into 15 sublayers; the first ten kilometers is divided into ten equal layers. The cloud base can be considered anywhere below 10 km. It is assumed that most clouds lie below 10 km.
4. The parameters that can be changed easily in the program are surface temperature, surface emissivity (emittance), cloud height and cloud emissivity.
5. Radiances and fluxes can be calculated for different cloud-cover fractions and zenith angles.
6. Anisotropic functions can be calculated for different atmospheric models.

For a given atmospheric model, the computer program is capable of computing all results (including all information given in steps one through six) in one step. This reduces the computer time considerably as compared to the individual runs. For parametric and sensitivity studies, therefore, the present code is very economical. The information on the computer program is available in Appendices C1 and C2; Appendix C1 provides the listing of the program. Comment cards are inserted in the listing to ex-

plain each stage of the program.

7.3 Results and Discussion

The sensitivity of the anisotropic functions to meteorlogical variables like cloud cover, cloud height, surface relative humidity, surface emittance and temperature is examined for the U.S. Standard, Tropical, and Sub-Arctic Winter atmospheres.

The results of clearsky radiance and flux are tabulated in table 7.1 for the U.S. Standard Atmosphere for different longwave spectral ranges. These results are similar to those presented in chapter 5; but now the spectral range has been extended to cover 5-200μ. The results show that the radiance and flux for 5-200 μ range are only about three-and-one-half percent higher than the values for 5-50 μ range. This is not a significant increase, but this information may be essential for some specific applications.

For the standard atmosphere and spectral range 5-200μ, figure 7.1 shows the upwelling radiance as a function of the cloud cover fraction for differ- values of the zenith angle. The cloud top is assumed to be at 5 km and the cloud emissivity is taken to be unity. As would be expected, the results clearly show that the upwelling radiance decreases with increasing cloud cover and zenith angle. The radiance values for $\theta = 0°$ and 15° are seen to be quite close, but considerable decrease in radiance is noted for θ-values larger than 45°. As explained in Chapter 2, the difference between the maximum and minimum values of radiance represents the extent of limb darkening for most atmospheric models.

The significance of the anisotropic function and importance of the

Table 7.1 Clearsky radiance and flux for U.S. standard (mid-lat. average) atmosphere, Atm Top = 30 km, E_s = 1.0, T_s = 288.15 K surface relative humidity (RH) = 75%, θ = 0.

Spectral Range, μ	Clear Atm. Radiance, W/m^2-sr	Clear Atm. Flux, W/m^2
5 - 10	16.63	45.58
10 - 20	42.16	124.94
5 - 20	58.79	170.52
10.5 - 12.5	14.79	45.58
5 - 50	78.59	229.10
5 - 200	81.41	237.85

limb-darkening work are illustrated in figures 7.2 and 7.3. It is noted that the radiance emerging from the top of the atmosphere can be highly anisotropic (non Lambertian). For a given Earth-atmosphere system, if the radiation leaving the atmosphere is isotropic (Lambertian), the satellite instrument will receive the same radiation for all nadir viewing angle. However, because of the directional dependence of the upwelling radiation, different radiative energy is received by the instrument at different viewing angle. The extent of the limb darkening is expressed by the value of G which is the difference between the maximum and minmum values of the anisotropic function for a given atmospheric model. The results for anisotropic functions are tabulated in Appendices B3 and B4 for the spectral ranges 5-50 μ and 5-200 μ, respectively. The results for the spectral range 5-50 μ are discussed in Appendix A2 and some specific results for the spectral range 5-200 μ are discussed in this section.

The latitudinal variability of the anisotropic functions for the climatological-average model atmospheres is shown in figure 7.4; the values of G for different models are given within the parentheses. In comparison to the results for the mid-latitude average model, the values of the anisotropic function are found to be higher for the tropical atmosphere and lower for the sub-arctic winter atmosphere for lower nadir viewing angles; however, the reverse trend is observed for viewing angles greater than 50°. The value of G for the mid-latitude average clear atmosphere was found to be 0.2386 (instead of 0.2444 for the spectral range 5-50μ) and is used as a reference value in the following discussions. The values of G for the tropical and sub-arctic winter models were found to be 0.3073 and 0.1622, respectively. Similar latitudinal variability in anisotropic functions was observed when

radio-sonde-measured model atmospheres were used instead of the climatological-average models (see Appendix A2).

The sensitivity of the isotropic functions to changes in the values of various meteorological parameters was examined in detail for the U.S. standard (mid-latitude average), tropical and sub-arctic winter atmospheres. For all case considered, the top of the atmosphere was taken to be 30 km. The entire results are presented in Appendix B4, selected results are given in tables 7.2 and 7.3, and some specific results are illustrated in figures 7.5-7.8.

The effects of cloud height on the anisotropic functions were examined for the overcast (100% cloud cover) conditions and the results for the standard and tropical atmospheres are shown in figures 7.5a and 7.5b, respectively. It is seen that $R(\theta)$ decreases with θ sharply for the lower cloud heights than for the cloud at $z_c = 10$ km; the variation is steeper for the tropical atmosphere than the standard atmosphere. The value of G varies from 0.2013 ($z_c = 2$ km) to 0.0186 ($z_c = 10$ km) for the standard atmosphere and from 0.2646 ($z_c = 2$ km) to 0.1050 ($z_c = 10$ km) for the tropical atmosphere. The results clearly indicate that the anisotropic atmosphere functions are quite sensitive to the location of clouds in the atmosphere.

The sensitivity of the anisotropic function to cloud covers is illustrated in figures 7.6a and 7.6b for the standard and tropical atmospheres, respectively. The results are obtained for a cloud height of 6 km and the cloud emissivity is taken to be unity. It is noted that the value of G varies from 0.2386 (clear sky) to 0.1265 (overcast sky) for the standard atmosphere and from 0.3073 (clear sky) to 0.1958 (overcast sky) for the trop-

Table 7.2 Sensitivity of anisotropic functions to various meteorological parameters for a mid-latitude average atmosphere, Atm Top = 30 km.

No.	Meteorological Parameter	G-values	
		5-50 μ	5-200 μ
1.	Surface relative humidity, %		
	50	0.238	0.2331
	75	0.244	0.2386
	100	0.249	0.2438
2.	Water vapor scale-height parameter, λ		
	2	0.258	0.2490
	3	0.244	0.2386
	4	0.233	0.2280
3.	Surface emittance, ε_s		
	0.8	0.201	0.1966
	0.9	0.223	0.218[illegible]
	1.0	0.244	0.2386
4.	Cloud height (overcast), km		
	2	0.205	0.2013
	6	0.128	0.1265
	10	0.014	0.0186
5.	Cloud cover (z_c = 6 km), %		
	0	0.244	0.2386
	50	0.195	0.1906
	100	0.128	0.1265
6.	High-cloud emissivity, ε_c		
	0.5	0.162	0.1586
	1.0	0.014	0.0186

Table 7.3 Sensitivity of anisotropic functions to various meteorological parameters for a tropical atmosphere, Atm Top = 30 km.

No.	Meteorological Parameter	5-50 μ	5-200 μ
1.	Surface emittance, ε_s		
	0.8		0.2590
	0.9		0.2837
	1.0		0.3073
2.	Cloud height (overcast), km		
	2		0.2646
	6		0.1958
	10		0.1050
3.	High-cloud emissivity, ε_c		
4.	0.5		0.2318
	1.0		0.1050

ical atmosphere. The results show that the anisotropic functions are also quite sensitive to the changes in fractional cloud cover.

The sensitivity of the anisotropic function to the high-cloud emissivity is shown in figures 7.7a and 7.7b; the results are obtained for an overcast sky. The value of G is seen to vary from 0.1586 ($\varepsilon_c = 0.5$) to 0.0186 ($\varepsilon_c = 1.0$) for the standard atmosphere and from 0.2318 ($\varepsilon_c = 0.5$) to 0.1050 ($\varepsilon = 1.0$) for the tropical atmosphere. The anisotropic function is seen to be quite sensitive also to the high-cloud emissivity.

The strong dependence of G on cloud height is a combination of two effects. Firstly, the lower temperature of the cloud top reduces the temperature difference between the underlaying surface (cloud top) and top layers of the atmosphere. Secondly, there is much less water vapor above the cloud top. Variation of G with fractional cloud cover is simply a combination of the effects for clear and overcast cases. The large increase in G as the high-cloud emissivity decreases from 1.0 to 0.5 can be attributed to the fact that for the partly transmitting cloud, considerable part of the radiation emanating at the top originated at the surface. It should be noted that the values of G for 50% cloud cover and $\varepsilon_c = 1.0$ is equal to that for 100% cloud cover and $\varepsilon_c = 0.5$; this demonstrates that cloud emissivity and fractional cloud cover are equivalent parameters (i.e., the effective cloud cover is ε_c x actual cloud cover).

The sensitivity of the anisotropic function to the surface emittance (emissivity) is shown in figures 7.8a and 7.8b; the results are obtained for the clear-sky conditions. The value of G is found to vary from 0.1966 ($\varepsilon_s = 0.8$) to 0.2386 ($\varepsilon_s = 1.0$) for the standard atmosphere and from 0.2590

(ε_s = 0.8) to 0.3073 (ε_s = 1.0) for the tropical atmosphere. It is noted that the anisotropic function is also quite sensitive to the surface emissivity; an increase in surface emittance of 10% results in an increase of $\bar{G}$ value of about 11% (see table 7.2). The sensitivity of the isotropic function to the variation of surface temperature was examined for different models (see Appendices A2, B3, and B4). A 5 K change in the surface temperature (without changilng the temperature profile) was found to cause more than 6% change in the G value. It should be noted that the changes in surface emittance and temperature effectively amount to a change in the lapse rate and this, in turn, causes the change in G values. When atmospheric temperature profile was changed along with the surface temperature, insignificant changes in G were observed (Appendix B3).

The sensitivity of the isotropic function to the variation of surface relative humidity (at fixed surface temperature) water vapor scale-height parameter λ, and CO^2 concentration was examined for different models (see table 7.2 and Appendices A2, B3, and B4). It was found that G increased sharply from 0.091 for a dry atmosphere (no water vapor) to 0.221 for 5% relative humidity (Appendices A2 and B3), but increased very slowly thereafter. The variation of the scale-height parameter was found to have a small effect on G (table 7.2). The variation of carbon dioxide concentration between zero and twice the standard amount (i.e., 660 ppmV) has very small effect on G (Appendix B3).

7.4 Conclusions

The existing computer code for the 5-50 μ longwave range was modified

to cover the spectral range 5-200 μ. Other modifications were made to achieve higher efficiency and less computational costs. The revised code was used to investigate the effects of various meteorological parameters on the upwelling radiation and anisotropic function. The study shows that inclusion of the spectral range from 50 μ to 200 μ amounts to about 3% change in final results in most cases. This may not appear to be a significant change, but for some specific applications this information may be of vital importance. Other conclusions on "Evaluation of Anisotropic Functions in the Longwave Region" are essentially the same as given under "Concluding Remarks" of Appendix A2.

ORIGINAL PAGE IS
OF POOR QUALITY

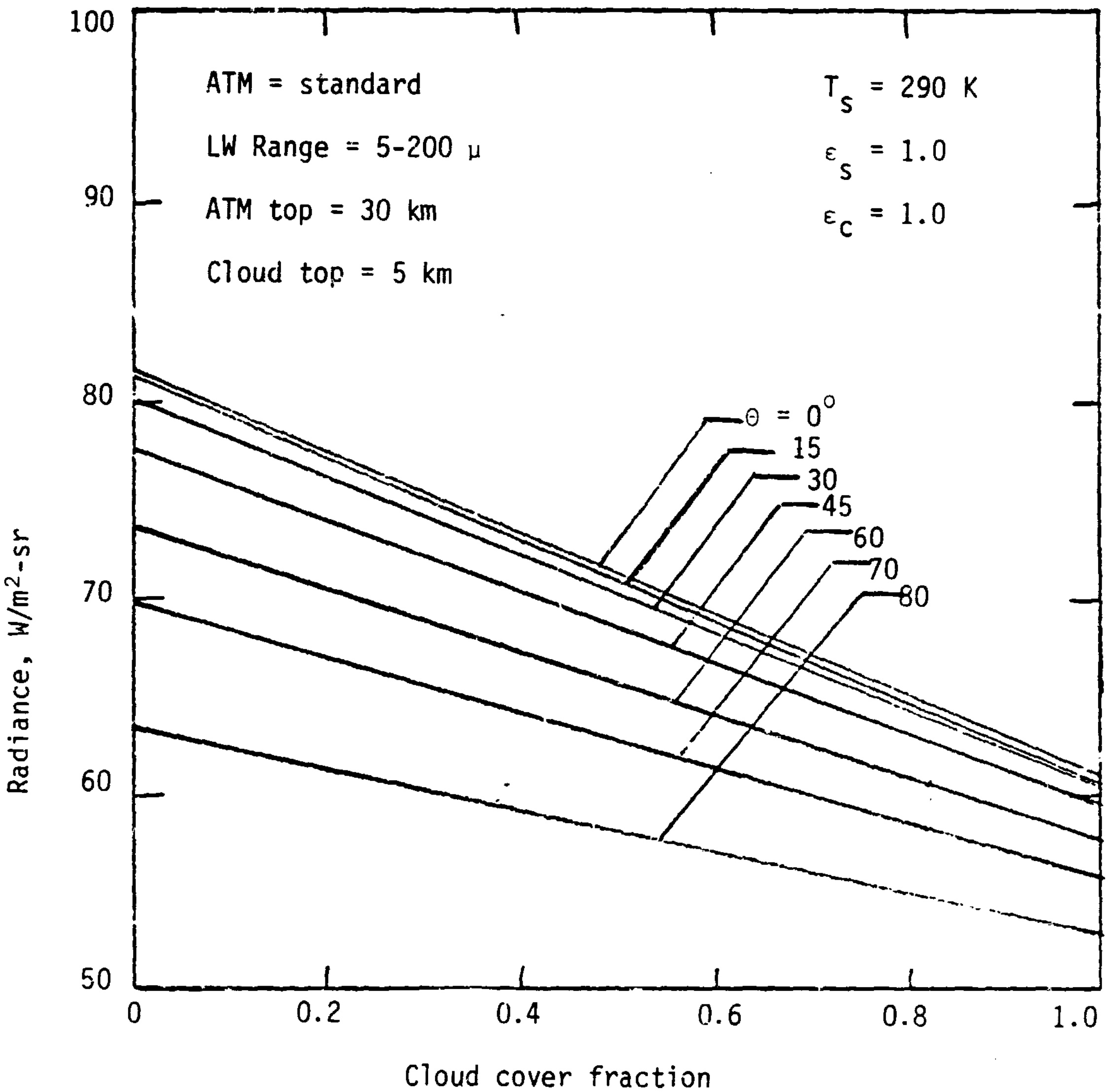

Figure 7.1 Upwelling radiance as a function of cloud-cover fraction for different zenith angles, LW Range = 5-200μ, Atm Top = 30 km.

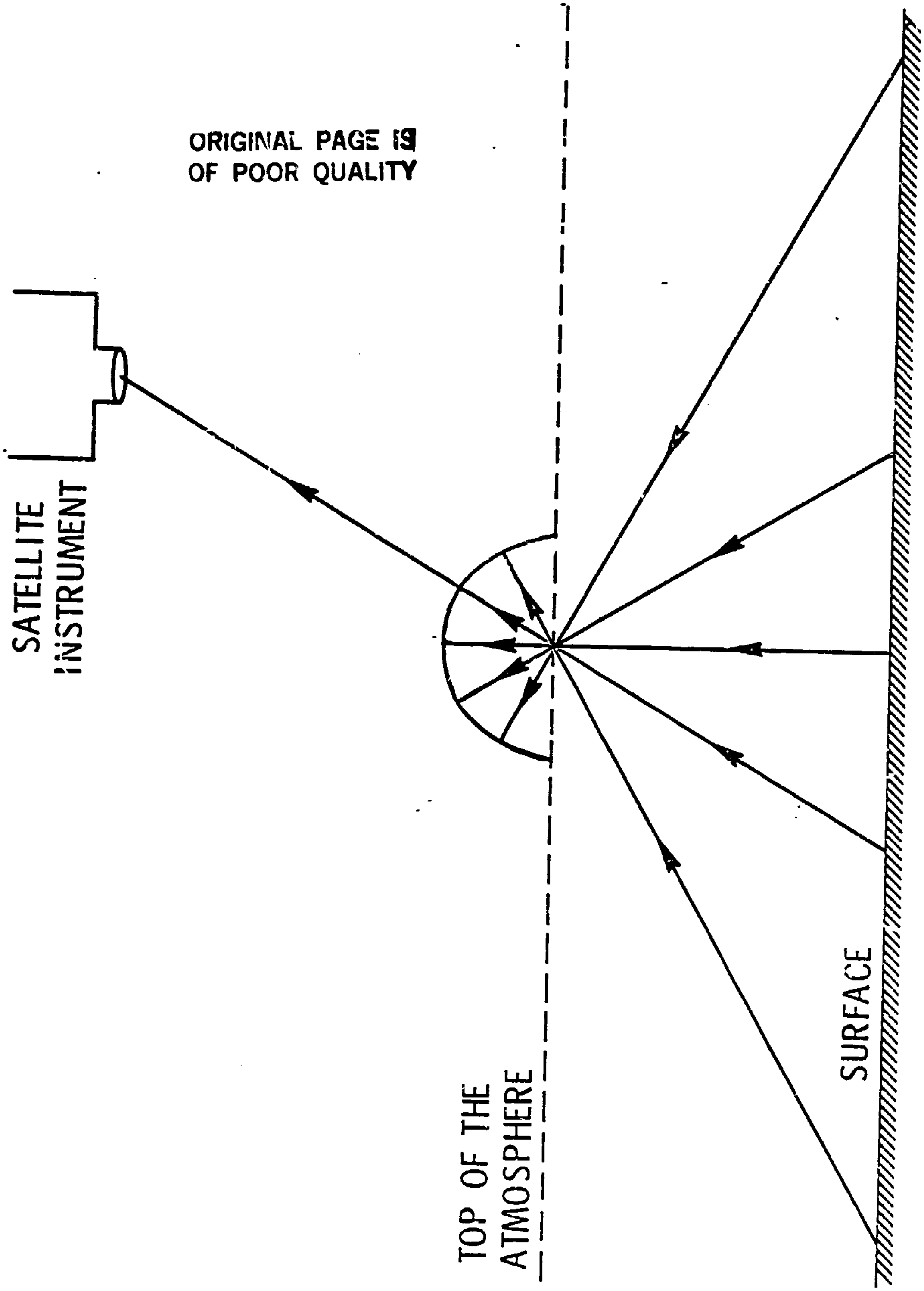

Figure 7.2 Illustration of importance of limb-darkening work.

ORIGINAL PAGE IS
OF POOR QUALITY

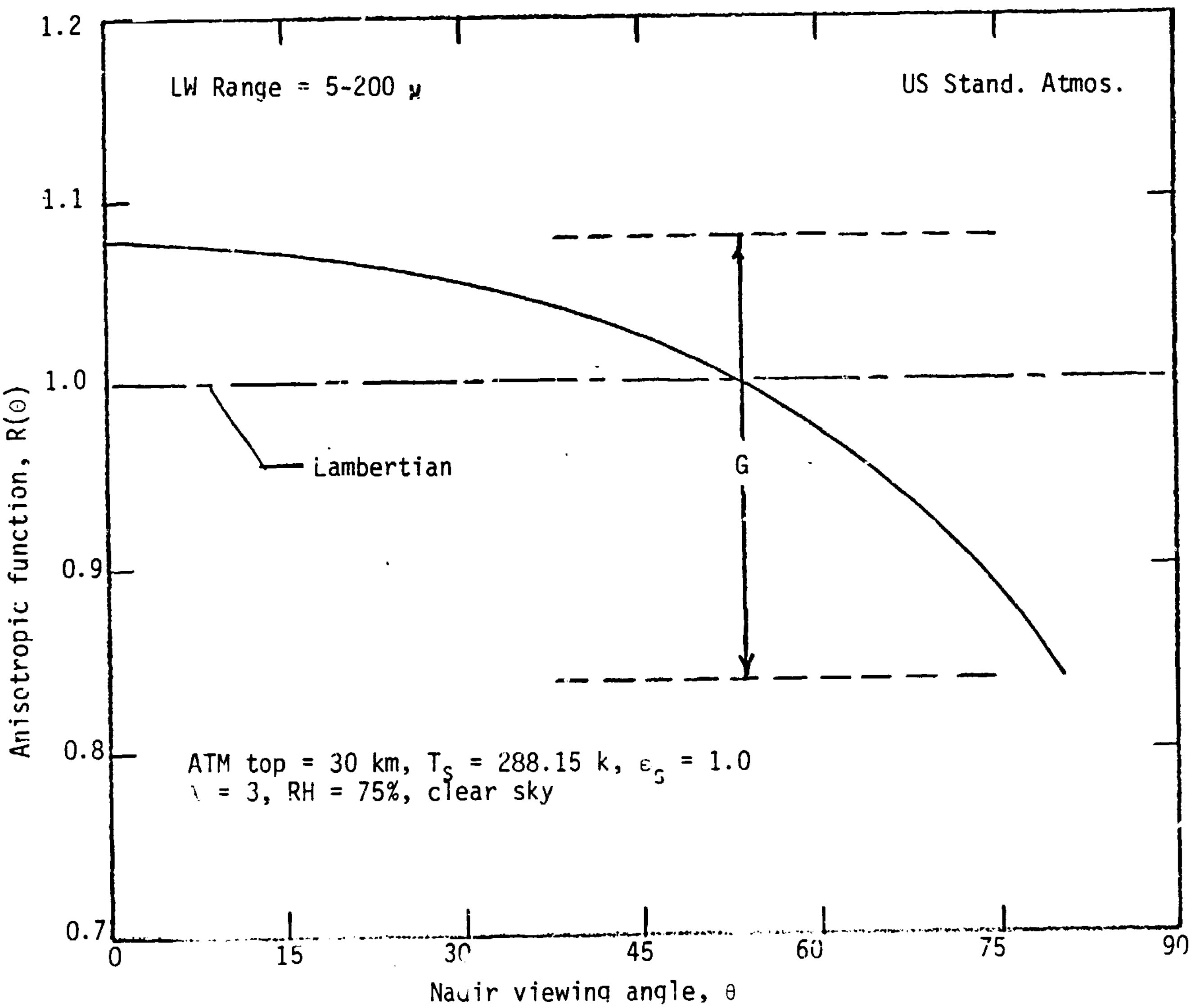

Figure 7.3 Significance of the anisotropic function and definition of G.

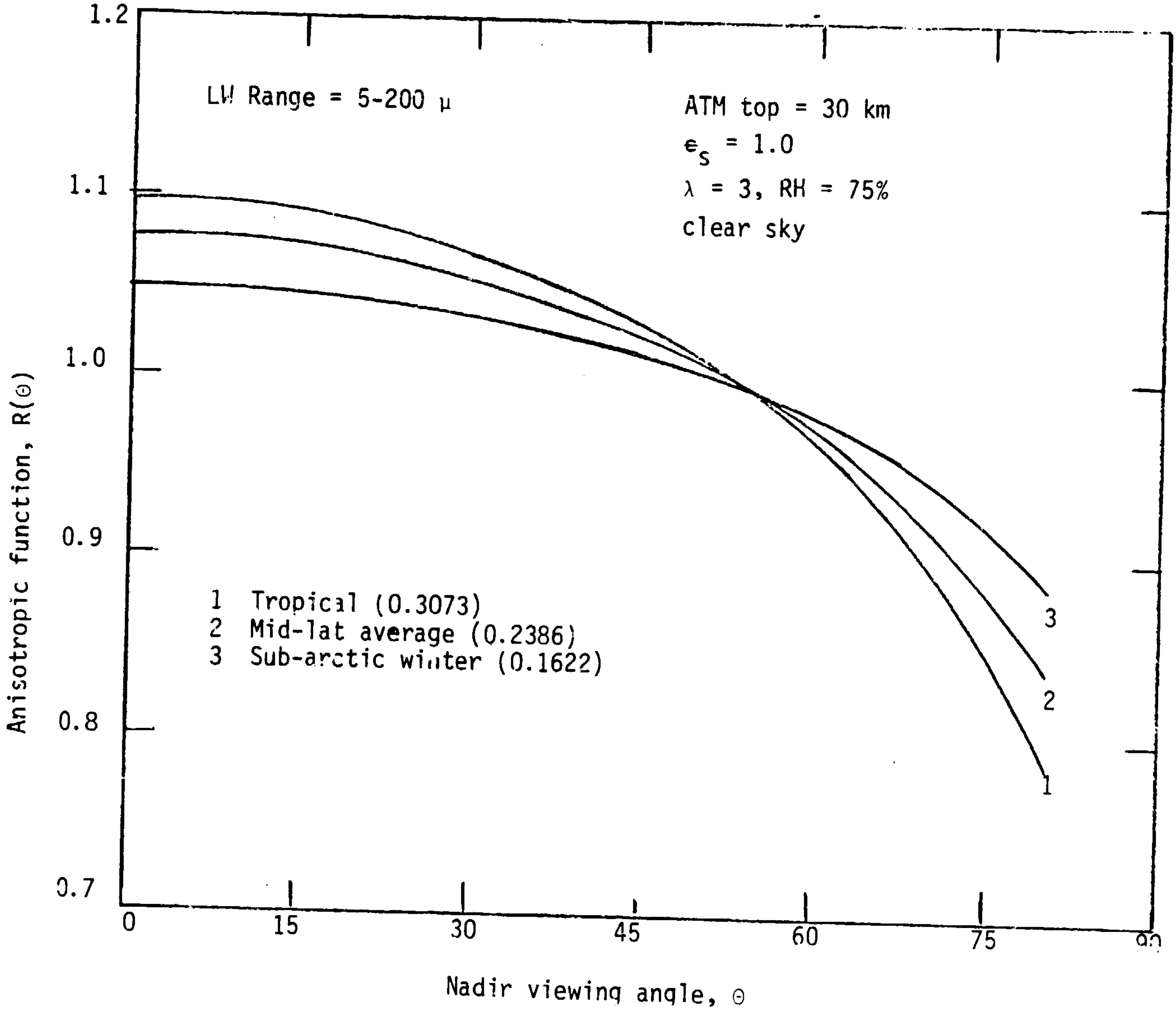

Figure 7.4 Latitudinal variability of the anisotropic functions for the climatological-average model atmospheres.

ORIGINAL PAGE IS
OF POOR QUALITY

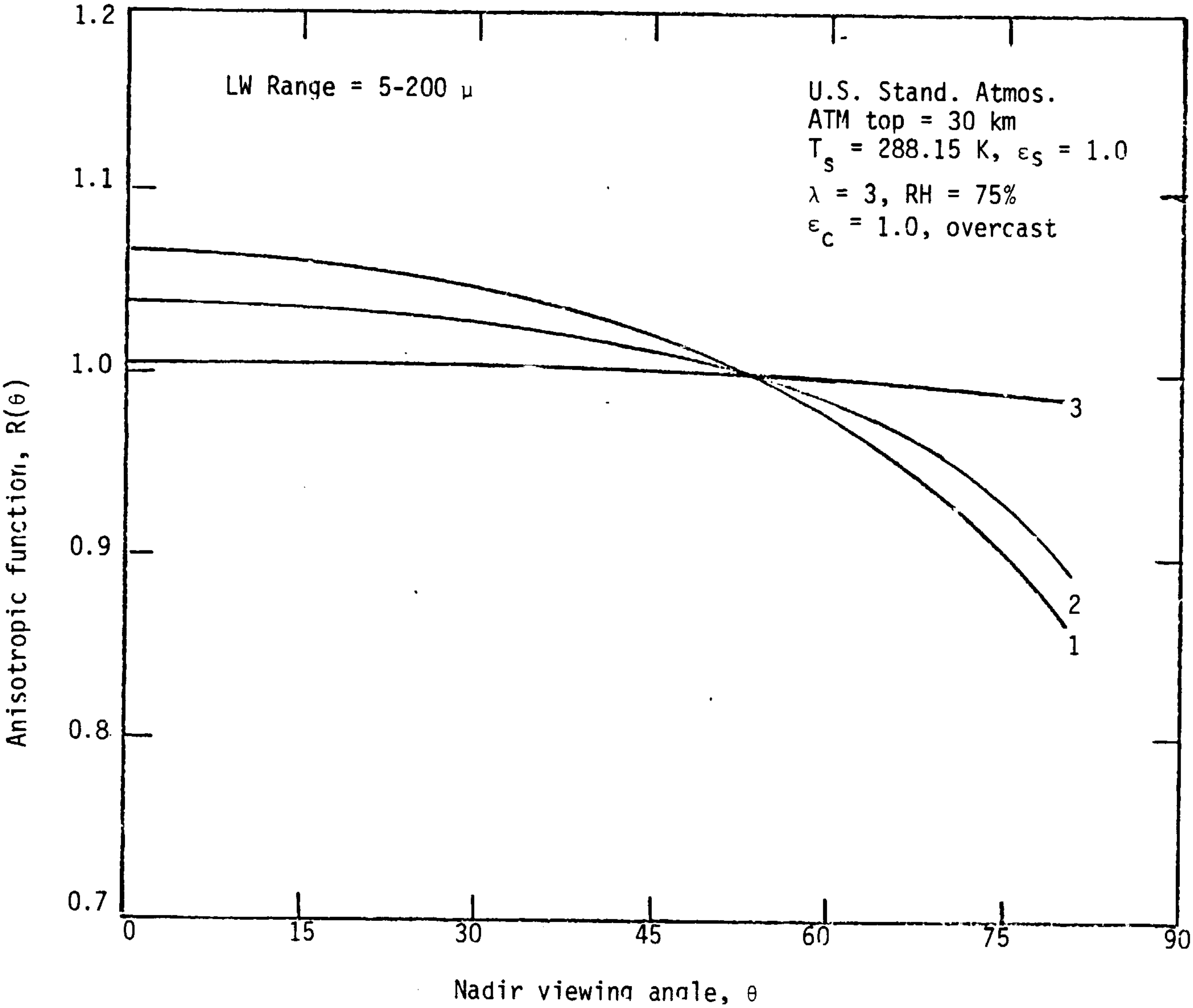

Figure 7.5a Anisotropic functions for selected values of cloud-top height, U.S. standard atmosphere.

ORIGINAL PAGE IS
OF POOR QUALITY

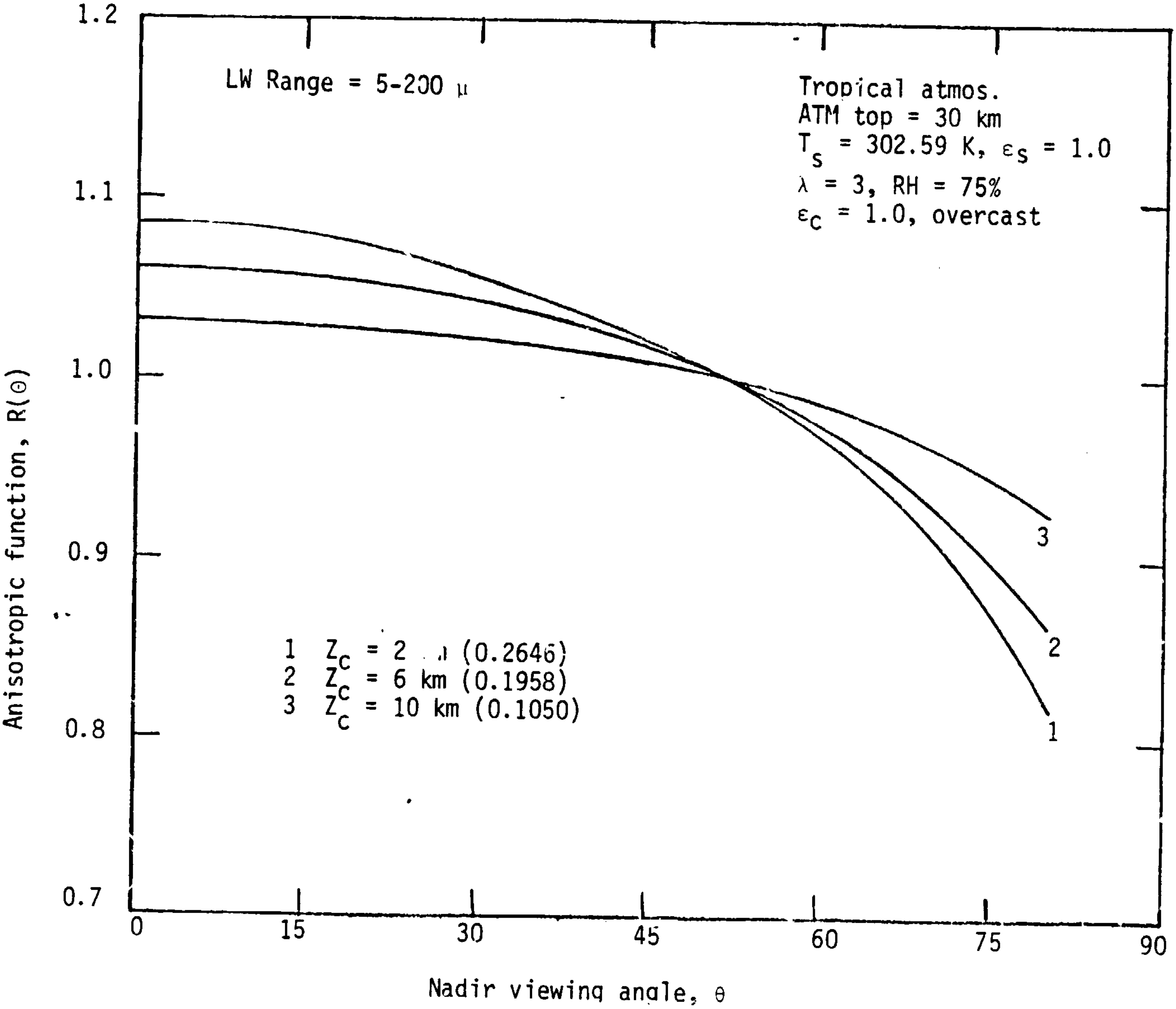

Figure 7.5b Anisotropic functions for selected values of cloud-top height, tropical atmosphere.

ORIGINAL PAGE IS
OF POOR QUALITY

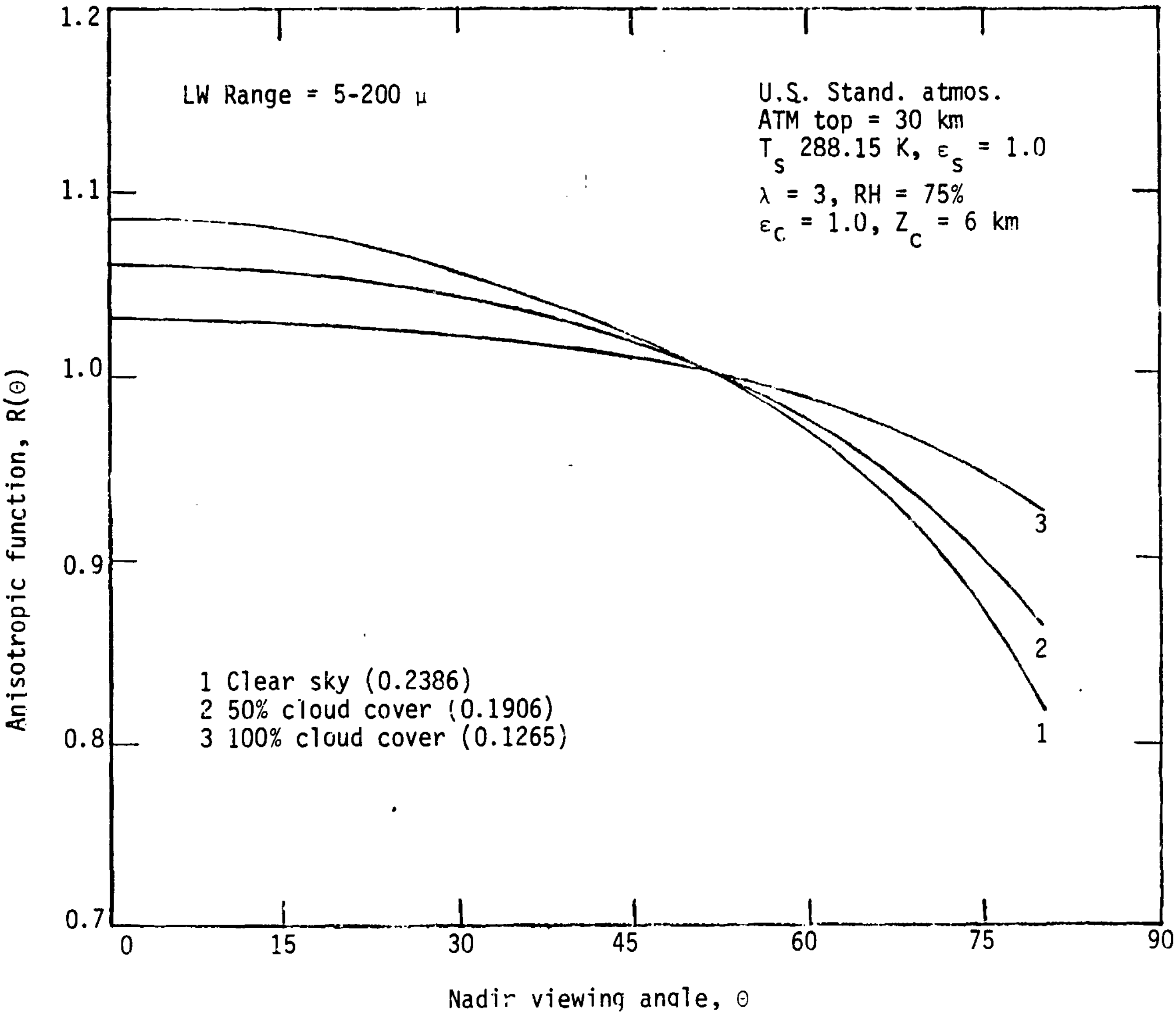

Figure 7.6a Anisotropic functions for different values of fractional-cloud cover, U.S. standard atmosphere.

ORIGINAL PAGE IS
OF POOR QUALITY

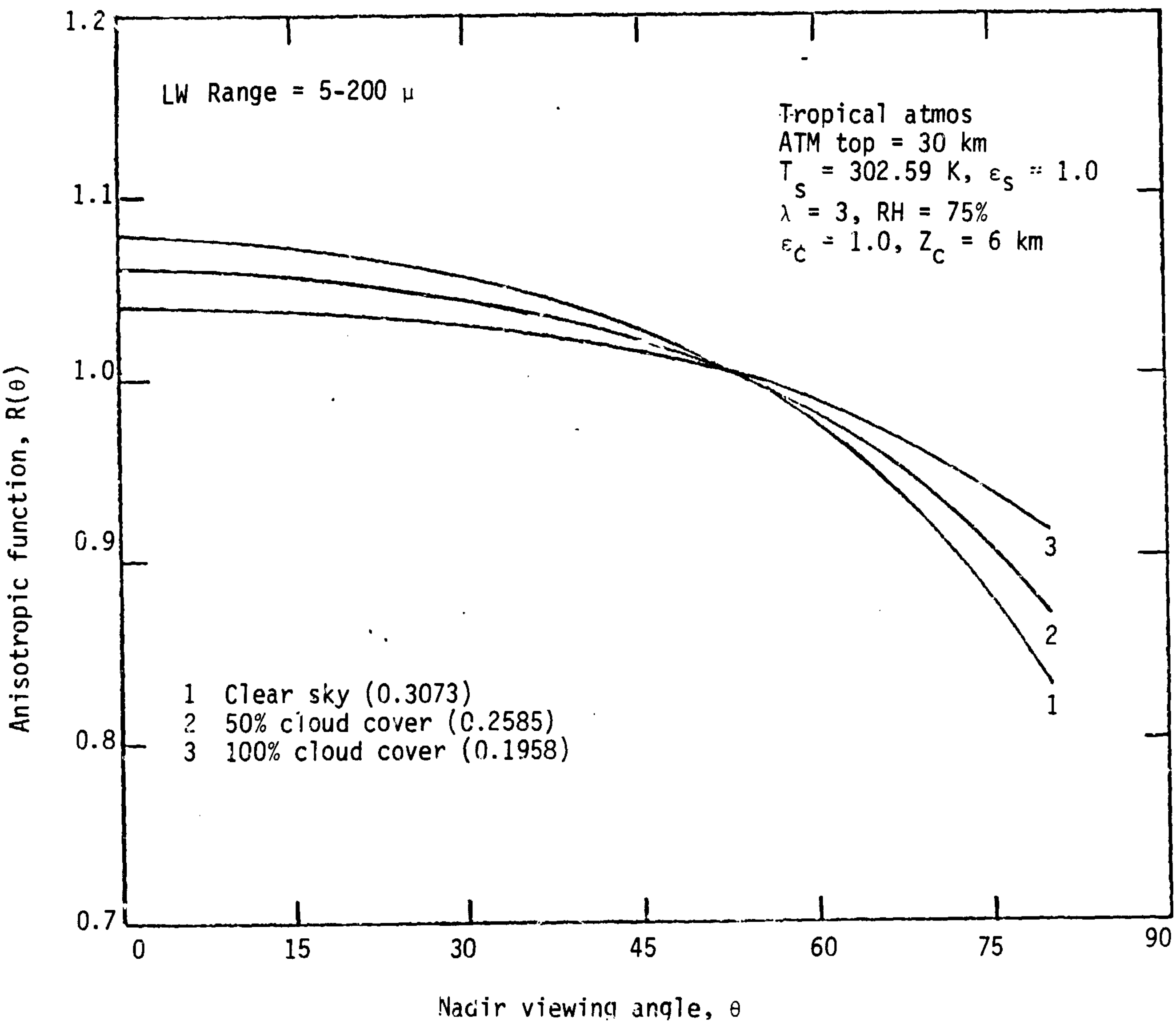

Figure 7.6b Anisotropic functions for different values of fractional-cloud cover, tropical atmosphere.

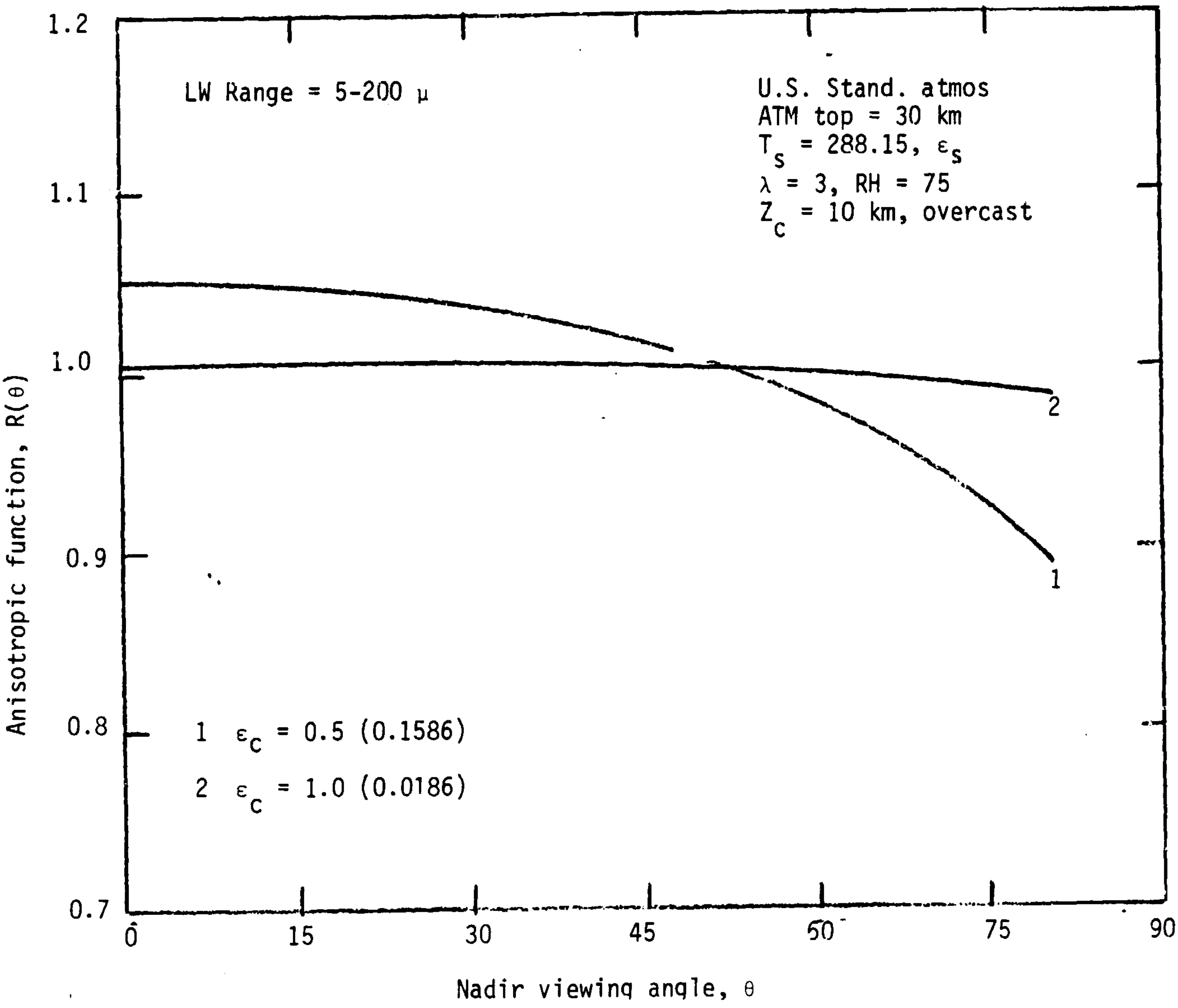

Figure 7.7a Sensitivity of the anisotropic function to the high-cloud emissivity, U.S. Standard atmosphere.

ORIGINAL PAGE IS
OF POOR QUALITY

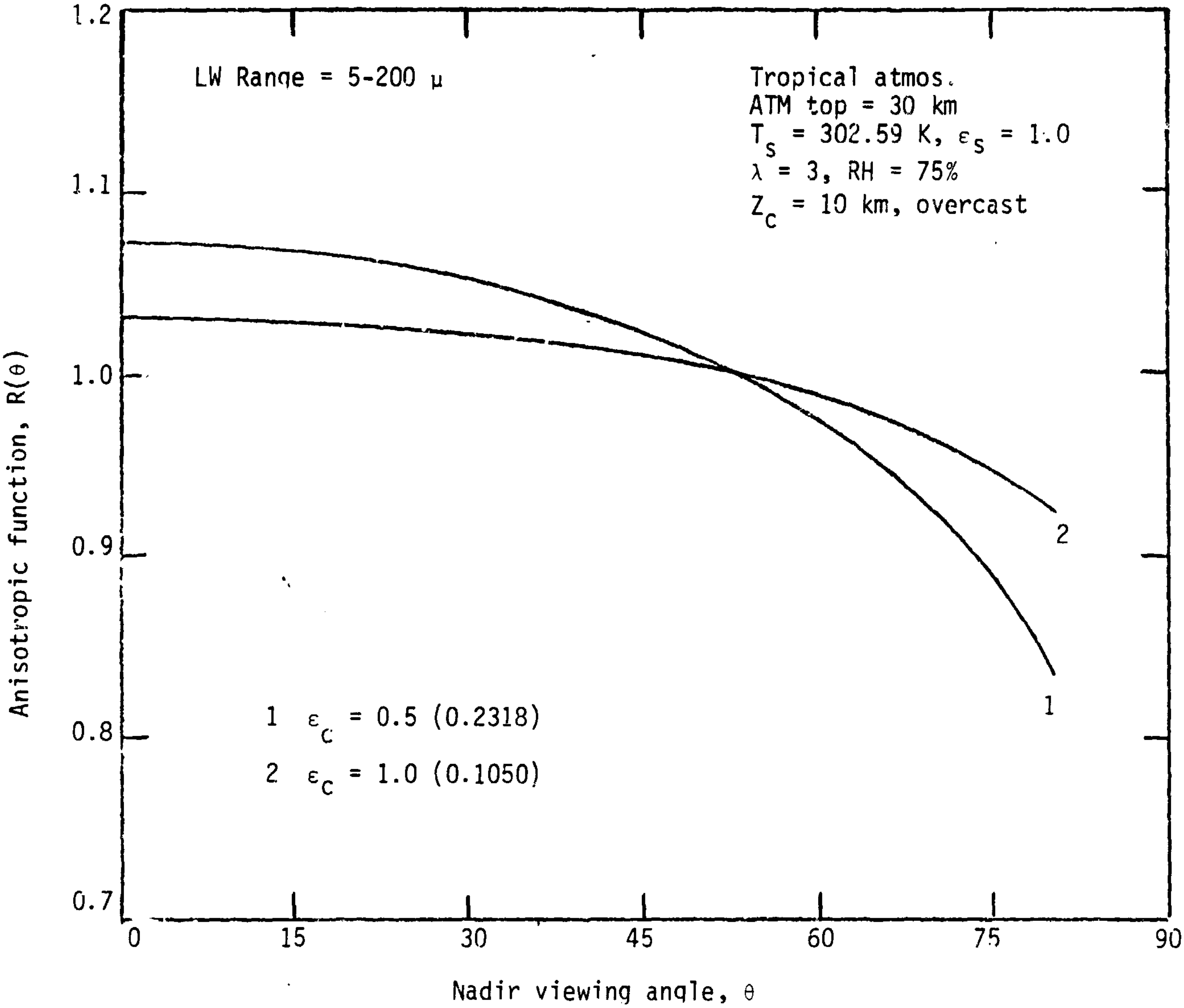

Figure 7.7b Sensitivity of the anisotropic function to the high-cloud emissivity, tropical atmosphere.

OF POOR QUALITY

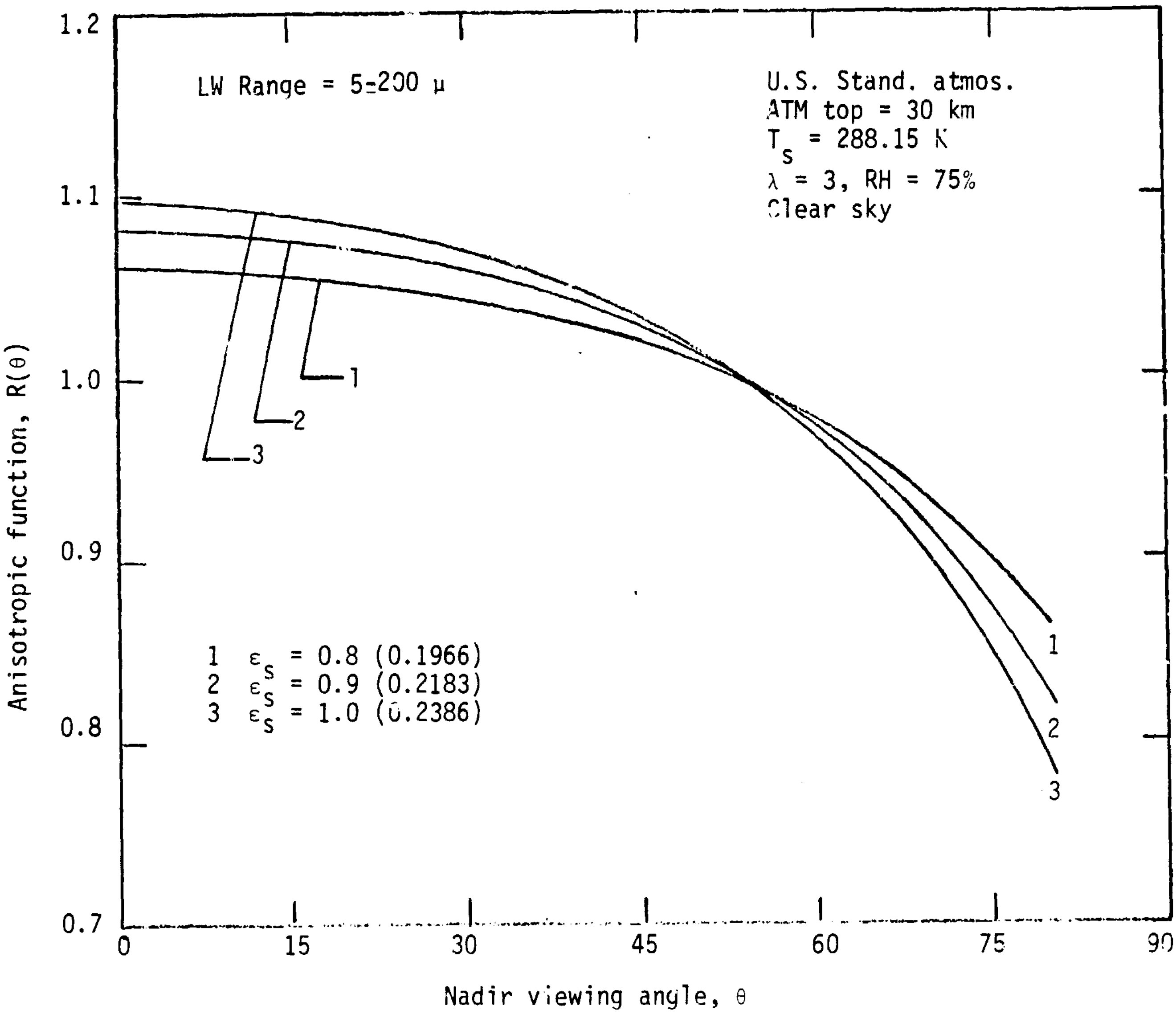

Figure 7.8a Sensitivity of the anisotropic function to the surface emittance, U.S. standard atmosphere.

ORIGINAL PAGE IS
OF POOR QUALITY

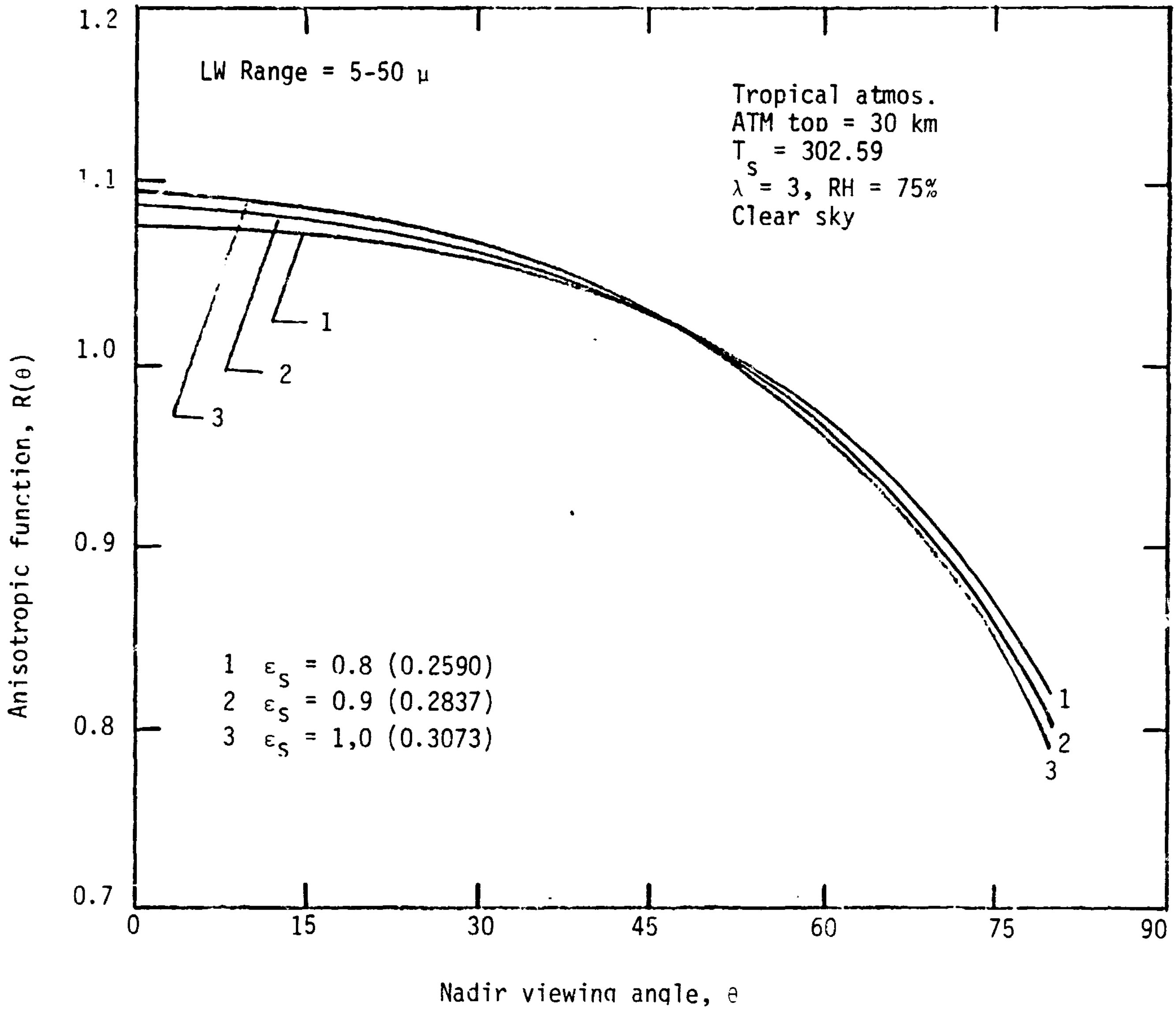

Figure 7.8b Sensitivity of the anisotropic function to the surface emittance, tropical atmosphere.

8. CONCLUDING REMARKS

Radiative transfer models and computer codes have been developed by employing the line-by-line and quasi-random band formulations to determine the gas emissivities, upwelling atmospheric radiance and radiative flux in the entire longwave spectral range (5-200 μ). The program is quite versatile and can be used to investigate the influence of various parameters and non-equilibrium radiation on the net radiative exchange.

In this study, the program was used to evaluate the radiative flux in clear atmosphere, provide sensitivity analysis of upwelling radiance in presence of clouds, and determine the effects of various climatological parameters on the upwelling radiation and anisotropic function. The results show that the QRB formulation is quite suitable for most atmospheric applications, the top of the atmosphere can be considered at 30 km, and the radiative contribution from the spectral range 50-200 μ amounts to about three percent. For a given surface and atmospheric conditions, the upwelling radiance and anisotropic function are found to be very sensitive to the variation in cloud parameters (liquid-water content, thickness, height, cover, and emissivity). Other studies, however, are needed to further investigate the specific influence of various cloud parameters. It is established that the limb-darkening in the atmosphere is caused primarily by the presence of water vapor and reaches saturation for very low values of water vapor burden.

REFERENCES

1. Wark, D.Q., Yamamoto, G. and Lienesch, J.H.: Methods of Estimating Infrared Flux and Surface Temperature from Meteorological Satellites. J. Atmos. Sci. vol. 19, Sept. 1962, pp. 369-384.

2. Lenschow, D.H. and Dutton, J.A.: Surface Temperature Variations from an Airplane over Several Surface Types. J. Appl. Meteor.. vol. 3, Feb. 1964, pp. 65-69.

3. Marlatt, W.E.; Harlan, J.C., and Cole, H.L.: Mathematical Models for Radiation Transfer. Dept. of Watershed Sciences, Colorado State Univ. (Fort Collins, CO), 1971.

4. Tiwari, S.N.: Models for Infrared Atmospheric Radiation. Final Report, NASA Grant NSG 11153, Jun. 1966. Also in Advances in Geophysics, vol. 20, Academic Press, 1978, pp. 1-85.

5. Cess, R.D.: Radiative Transfer Due to Atmospheric Water Vapor: Global Considerations of the Earth's Energy Balance. J. Quart. Spectrosc. Radiat. Transfer, vol. 14. no. 9, Sep. 1974. pp. 861-872.

6. Ramanathan, V.: Radiative Transfer within the Earth's Troposphere and Stratosphere. A Simplified Radiative-Convective Model. J. Atmos. Sci., vol. 33, no. 7, Jul. 1976, pp. 1330-1346.

7. Arking, A.; Chesters, D. and Chow, M.D.: Fast But Accurate Techniques for Calculating Radiative Terms in Numerical Atmospheric Models and in Remote Sensing Applications. Paper No. 35, Third NASA Weather and Climate Program Science Review, Conference Publication 2029, 1977, pp. 195-200.

8. Smith, W.L.; Hickey, J.; Howell, H.B.; Jacobwitz, H.; Hilleary, D.T. and Drummond, A.J.: Nimbus-6 Earth Radiation Budget Experiment. Appl. Opt. vol. 16, no. 2, Feb. 1977, pp. 306-318.

9. Woerner, C.V. and Cooper, J.E.: Earth Radiation Budget Satellite System Studies. NASA TM X-72776, 1977.

10. Wyatt, P.J.; Stull, V.R. and Plass, G.N.: Quasi-Random Model of Band Absorption. J. Opt. Soc. Amer., vol. 52, no. 11, Nov. 1962, pp. 1209-1217.

11. Kunde, V.G.: Theoretical Computations of the Outgoing Infrared Radiance from a Planetary Atmosphere. NASA TN D-4045, Aug. 1967.

12. Gupta, S.K. and Tiwari, S.N.: Evaluation of Upwelling Infrared Radiance Earth's Atmosphere. Progress Report, NASA Grant NSG 1153, Nov. 1975.

13. Wiscombe, W.J. and Evans, J.N.: Exponential-Sum Fitting of Radiative Transmission Functions. J. Comput. Phys.. vol. 24, no. 4. Aug. 1977, pp. 416-444.

14. Sasamori, T.: The Radiative Cooling Calculation for Application to General Circulation Experiments. J. Appl. Meteor., vol. 7, no. 5, Oct. 1968, pp. 721-729.

15. Sasamori, T.: Simplication of Radiative Cooling Calculation for Application to Atmospheric Dynamics. WMO Tech. Note 104, 1970, pp. 479-488.

16. Rasool, S.I. and Schneider, S.H.: Atmospheric Carbon Dioxide and Aerosols: Effects of Large Increases on Global Climate. Science, vol. 173, 1971, pp. 138-141.

17. Rodgers, C.D.: Modeling of Atmospheric Radiation for Climatic Studies. The Physical Basis of Climate and Climate Modeling. GARP Publication Series, no. 16, pp. 177-180. Also, Rodgers, C.D. and Walshaw, C.D.: The Computation of Infrared Cooling Rate in Planetary Atmosphere. Quarterly Journal of the Royal Meteorological Society, vol. 92, 1966, pp. 67-92.

18. Fels, S.B. and Kaplan, L.D.: A Test of the Role of Longwave Radiative Transfer in a General Circulation Model. J. Atmos. Sci., vol. 32, no. 4, Apr. 1975, pp. 779-789.

19. Kunde, V.G. and Maguire, W.C.: Direct Integration Transmittance Model. J. Quant. Spectrosc. Radiat. Transfer, vol. 14, no.8, Aug. 1974, pp. 806-814.

20. Tiwari, S.N. and Gupta, S.K.: Accurate Spectral Modeling for Infrared Radiation: J. Heat Transfer, vol. 100, May 1978, pp. 240-246.

21. Burch, E.E.; Grynak, D.A.; Singleton, E.B.; France, W.L. and Williams, D.: Infrared Absorption by Carbon Dioxide, Water Vapor, and Minor Atmospheric Constitutents. AFCRL-62-698, Air Force Cambridge Research Laboratories (Bedford, MA), Jul. 1962.

22. Selby, J.E.A. and McClatchey, R.A.: Atmospheric Transmittance from 0.25 to 28.5 m: Computer Code LOWTRAN 3. AFCRL-TR-75-0255, Air Force Cambridge Research Laboratories (Bedford, MA), 1975.

23. Arking, A. and Grossman, K.: The Influence of Line Shape and Band Structure on Temperatures in Planetary Atmospheres. J. Atmos. Sci., vol. 29, Jul. 1972, pp. 937-949.

24. Arking, A.; Chester, D. and Chou, M.D.: Fast But Accurate Techniques for Calculating Radiative Terms in Numerical Atmospheric Models and in Remote Sensing Applications. NASA CP-2029, Nov. 1977, pp. 195-200.

25. Chou, M.D. and Arking, A.: Computation of Infrared Cooling Rates in the Water Vapor Bands. J. Atmos. Sci. vol. 37, Apr. 1980, pp. 855-867.

26. Lacis, A.A. and Hansen, J.E.: A Parameterization of Solar Radiation in the Earth's Atmosphere. J. Atmos. Sci., vol. 31, Jan. 1974 pp. 118-133.

27. Lacis, A.A.; Wang, W.C. and Hansen, J.E.: Correlated K-Distribution Method for Radiative Transfer in Climate Models: Application to Effect of Cirrus Clouds on Climate. NASA CP-2076, Jan. 1979, pp. 309-314.

28. Smith, H.J.P.; Dube, D.J.; Gardner, M.E.; Clough, S.A.; Kneizys, F.X.; and Rothman, L.S.: FASCODE - Fast Atmospheric Signature Code (Spectral Transmittance and Radiance). AFGL-TR-78-0081, Air Force Geophysics Laboratory, Bedford, MA, 1978.

29. Clough, S.A.; Kneizys, F.X.; Rothman, L.S. and Gallery, W.O.: Atmospheric Spectral Transmittance and Radiance: FASCOD1B. The Society of Photo-Optical Instrumentation Engineers Vol. 277-Atmospheric Transmission, 1981.

30. Ludwig, C.B.; Griggs, M.; Malkmus, W. and Bartle, E.R.: Air Pollution Measurements from Satellites. NASA CR-2324, Nov. 1973.

31. Raschke, E.; Vonder Haar, T.H.,; Pasternak, M. and Bandeen, W.R.: The Radiation Balance of the Earth-Atmosphere System for Nimbus 3 Radiation Measurements. NASA TN D-7249, 1973.

32. Kunde, V.G.; Conrath, B.J.; Hanel, R.A.; Maguire, W.C.; Prabhakara, C. and Solomonson, U.V.: The Nimbus 4 Infrared Spectroscopy Experiment 2 - Comparison of Observed and Theoretical Radiances from 425-1450 cm^{-1}. J. Geophys. Res., vol. 79, COSPAR, 1974, pp. 265-269.

33. Ramanathan, V.: Satellite Radiation Budget Measurements in Spectral Bands. Earth Radiation Budget Science 1978, NASA Conference Publication 2100 (NASA CP-2100), Oct. 1979, pp. 66-68.

34. Yamamoto, G.; Tanaka, M. and Asano, S.: Radiative Transfer in Water Clouds in the Infrared Region. J. Atmos. Sci., vol. 2 1970, pp. 282-292.

35. Zdunkowski, W.G. and Crandall, W.K.: Radiative Transfer of Infrared Radiation in Model Clouds. Tellus, vol. 23, 1971, pp. 515-527.

36. Hunt, G.E.: Radiative Properties of Terrestrial Clouds at Visible and Infrared Thermal Window Wavelengths. Quart J. Roy. Meteor. Soc. vol. 99, 1973, pp. 346-369.

37. Kuhn, P.M.; Weickmann, H.K.; Lojko, J. and Stearns, L.P.: Transfer of Infrared Radiation Through Clouds. Appl. Opt., vol. 13, 1974, pp. 512-517.

38. Kuhn, W.R.: The Effects of Cloud Height, Thickness and Overlap on Tropospheric Terrestrial Radiation. J. Geophys. Res., vol. 83, 1978, pp. 1337-1346.

39. Barkstrom, B.R. Some Effects of 8-12 μm Radiant Energy Transfer on the Mass and Heat Budget of Cloud Droplets. J. Atmos. Sci., vol. 35, 1978 pp. 665-673.

40. Stephens, G.L.: Radiative Profiles in Extended Water Clouds - II. Parameterization Schemes. J. Atmos. Sci., vol 35, 1978, pp. 2123-2132.

41. Stephens, G.L.: Radiation Profiles in Extended Water Clouds - III. Observations. J. Atmos. Sci., vol. 35, 1978, pp. 2133-2141.

42. Liou, K.N. and Ou, S.C.S.: Infrared Radiative Transfer in Finite Cloud Layers, J. Atmos. Sci., vol. 36, 1979, pp. 1985-1996.

43. Stephens, G.L.: Radiative Properties of Cirrus Clouds in the Infrared Region. J. Atmos. Sci., vol. 37, Feb. 1980 pp. 435-446.

44. Subramanian, S.V.; Tiwari, S.N. and Suttles, J.T.: Sensivity Analysis of Upwelling Thermal Radiance in Presence of Clouds. AIAA Paper 81-1095, Jun. 1981.

45. Harshvardhan; Weinman, J.A. and Davies, R.: Transport of Infrared Radiation in Cuboidal Clouds. J. Atmos. Sci., vol. 38, Nov. 1981, pp. 2500-2513.

46. Liou, K.N. and OU, S.C.S.: Parameterization of Infrared Radiative Transfer in Cloudy Atmosphere. J. Atmos. Sci., vol. 8 Dec. 1 1981, pp. 2707-2716.

47. Chylek, P. and Ramaswamy, V.: Simple Approximation for Infrared Emissivity of Water Clouds. J. Atmos. Sci., vol. 39, Jan. 1982, pp. 171-177.

48. Harshvardhan and Weinman, J.A.: Infrared Radiative Transfer Through a Regular Array of Cuboidal Clouds. J. Atmos. Sci., vol. 39, Feb. 1982, pp. 431-439.

49. Ellingson, R.G.: On the Effects of Cumulus Dimensions on Longwave Irradiance and Heating Rate Calculations. J. Atmos. Sci., vol. 39 Apr. 1982, pp. 886-896.

50. Barkstrom, B.R. and Hall, J.B.: Earth Radiation Budget Experiment (ERBE): An Overview. Journal of Energy, vol. 6, No. 2, Mar./Apr. 1982, pp. 141-146.

51. Tiwari, S.N. and Subramanian, S.V.: Evaluation of Upwelling Radiance in a Nonhomogeneous Nonequilibrium Atmosphere. NASA CR-149090, Nov. 1976. Also Proceedings, 7th International Heat Transfer Conference, Munich, Germany, Sept. 1982.

52. Gupta, S.K.; Tiwari, S.N.; Vemuru, C.S. and Suttles, J.T.: Infrared Limb-Darkening Effects for the Earth-Atmosphere System. AIAA Paper 83-0161, Jan. 1983.

53. Gupta, S.K. and Tiwari, S.N.: Evaluation of Upwelling Infrared Radiance from Earth's Atmosphere. Progress Report, NASA Grant NSG 1153, Nov. 1975. Also available as TR-75-T14, School of Engineering, Old Dominion University, Norfolk, Va.. Nov. 1975.

54. Tiwari, S.N. and Mirakhur, N.: Feasibility of Quasi-Random Band Model in Evaluating Atmospheric Radiance. NASA CR-123456, Aug. 1980 Also ME Thesis by N. Mirakhur, School of Engineering, Old Dominion University Norfolk. Va., Dec. 1979.

55. McClatchey, R.A.; Fenn, R. [illegible] by, J.E.A.; Volz, F.E. and Garing, J.S.: Optical Properties [illegible] Atmosphere (3rd ed.). AFCRL-72-0497, Air Force Cambridge R[illegible] Laboratories (Bedford, Mass.), 1972.

56. McClatchey, R.A.; Bened[illegible] W.S.; Clough, S.A.; Burch, D.E.; Calfee, R.F.; Fox, K.; Rothman, L.S.; and Garing, J.S. AFCRL Atmospheric Line Parameters Compilation. AFCRL-TR-73-0096, Air Force Cambridge Research Laboratories (Bedford, Mass.), Jan. 1973.

57. U.S. Standard Atmosphere, 1962, U.S. Govt. Printing Office (Washington, D.C.), 1962.

58. Wark, D.Q.; Yamamoto, G. and Lienesch, J.: Infrared Flux and Surface Temperature Determinations from TIROS Radiometer Measurements. U.S. Department of Commerce-Weather Bureau, Washington, DC, Meteorological Satellite Laboratory Report No. 10, Aug. 1962.

59. Manabe, S. and Wetherald, R.T.: Thermal Equilibrium of the Atmosphere with a Given Distribution of Relative Humidity. Journal of the Atmospheric Sciences, vol. 24, 1967, pp. 241-259.

60. Smith, W.L.: Note on the Relationship Between Total Precipitable Water and Surface Dew Point. Journal of Applied Meteorology, vol. 5, 1966. pp. 726-727.

APPENDICES

APPENDIX B1

CLEARSKY UPWELLING RADIANCE AND RADIATIVE FLUX

TABLES B1.1 - B1.5

PRECEDING PAGE BLANK NOT FILMED

70, 71, 72, 73, 74, 75, 76, 77, 78, 79, 80, 81, 82, 83, 84, 85

Table B1-1 Clearsky upwelling radiance and radiative flux for spect~al range 5-50 μ.

Z, km and ϵ_s	Radiance, W/m^2-sr Surface Temperature, K						Radiative Flux, W/m^2 Surface Temperature, K					
	270	280	290	300	310	320	270	280	290	300	310	320
Z = 10												
ϵ_s = 0.6	64.642	67.766	71.256	75.122	79.372	84.012	198.15	206.47	215.76	226.07	237.39	249.76
0.7	67.255	70.899	74.971	79.481	84.440	89.852	205.01	214.71	225.55	237.57	250.78	265.21
0.8	69.867	74.032	78.685	83.840	89.507	95.693	211.86	222.94	235.34	249.07	264.18	280.66
0.9	72.479	77.165	82.40	88.199	94.574	101.53	218.71	231.18	245.12	260.58	277.57	296.12
1.0	75.091	80.297	86.114	92.558	99.641	107.37	225.56	239.42	254.91	272.08	290.96	311.57
Z = 20												
ϵ_s = 0.6	61.553	64.557	67.910	71.623	75.701	80.151	186.14	194.00	202.78	212.50	223.19	234.84
0.7	64.081	67.585	71.497	75.828	80.586	85.778	192.66	201.83	212.08	223.42	235.88	249.48
0.8	66.608	70.613	75.084	80.034	85.472	91.405	199.19	209.67	221.37	234.34	248.58	264.12
0.9	69.136	73.641	78.671	84.239	90.357	97.032	205.71	217.50	230.67	245.26	261.28	278.76
1.0	71.663	76.668	82.257	88.445	95.242	102.66	212.24	225.33	239.97	256.17	273.98	293.41
Z = 30												
ϵ_s = 0.6	61.536	64.471	67.747	71.373	75.355	79.699	186.26	193.89	202.41	211.84	222.20	233.50
0.7	64.012	67.437	71.258	75.489	80.135	85.203	192.61	201.51	211.45	222.45	234.54	247.73
0.8	66.489	70.402	74.770	79.605	84.914	90.707	198.96	209.13	220.49	233.07	246.88	261.95
0.9	68.965	73.368	78.282	83.721	39.694	96.210	205.31	216.76	229.54	243.69	259.23	276.18
1.0	71.442	76.334	81.794	87.837	94.474	101.71	211.67	224.38	238.58	254.30	271.57	290.40

Table B1.2 Clearsky upwelling radiance and radiative flux for spectral range 5-50 μ.

Z, km and ϵ_s	Radiance, W/m^2-sr Surface Temperature, K						Radiative Flux, W/m^2 Surface Temperature, K					
	270	280	290	300	310	320	270	280	290	300	310	320
Z = 10												
ϵ_s = 0.6	11.618	12.923	14.421	16.121	18.033	20.164	35.428	38.904	42.887	47.398	52.461	58.091
0.7	12.528	14.050	15.798	17.782	20.012	22.498	37.873	41.929	46.575	51.839	57.745	64.313
0.8	13.438	15.178	17.175	19.442	21.991	24.832	40.319	44.954	50.264	56.279	63.029	70.536
0.9	14.348	16.305	18.552	21.103	23.970	27.167	42.764	47.979	53.952	60.720	68.313	76.758
1.0	15.258	17.433	19.929	22.763	25.950	29.501	45.210	51.003	57.640	65.160	73.597	82.980
Z = 20												
ϵ_s = 0.6	10.802	11.971	13.316	14.844	16.566	18.487	31.648	34.607	38.004	41.861	46.199	51.031
0.7	11.610	12.974	14.542	16.326	18.344	20.576	33.703	37.154	44.118	45.618	50.678	56.316
0.8	12.418	13.977	15.769	17.808	20.103	22.665	35.757	39.702	43.231	49.375	55.157	61.601
0.9	13.226	14.979	16.996	19.289	21.871	24.753	37.811	42.249	47.345	53.131	59.637	66.886
1.0	14.034	15.982	18.223	20.771	23.640	26.842	39.866	44.797	50.459	56.888	64.116	72.171
Z = 30												
ϵ_s = 0.6	10.638	11.740	13.008	14.451	16.078	17.895	30.996	33.732	36.977	40.452	44.477	48.966
0.7	11.395	12.680	14.159	15.843	17.741	19.862	32.883	36.074	39.743	43.915	48.610	53.847
0.8	12.152	13.621	15.311	17.236	19.405	21.828	34.769	38.416	48.610	47.377	52.743	58.729
0.9	12.909	14.561	16.463	18.628	21.068	23.794	36.6551	40.759	45.476	50.839	56.876	63.610
1.0	13.666	15.502	17.615	20.021	22.732	25.761	38.5427	43.101	48.342	54.302	61.009	68.491

ORIGINAL PAGE IS OF POOR QUALITY

Table B1.3 Clearsky upwelling radiance and radiative flux for spectral range 10-20 μ.

Z, km and ϵ_s	Radiance, W/m^2-sr Surface Temperature, K						Radiative Flux, W/m^2 Surface Temperature, K					
	270	280	290	300	310	320	270	280	290	300	310	320
Z = 10												
ϵ_s = 0.6	31.953	33.766	35.752	37.911	40.242	42.743	99.586	104.42	109.73	115.52	121.78	128.51
0.7	33.646	35.760	38.077	40.596	43.316	46.234	103.99	109.63	115.83	122.58	129.88	137.74
0.8	35.338	37.755	40.403	43.281	46.389	49.724	108.39	114.84	121.92	129.64	[illegible]	146.96
0.9	37.030	39.749	42.728	45.966	49.463	53.215	112.80	120.05	128.01	136.70	[illegible]	156.19
1.0	38.723	41.744	45.053	48.652	52.537	56.706	117.20	125.26	134.11	143.76	154.19	165.41
Z = 20												
ϵ_s = 0.6	30.121	31.948	33.949	36.124	38.473	40.993	93.267	98.165	103.55	109.41	115.75	122.57
0.7	31.828	33.960	36.295	38.833	41.573	44.513	97.732	103.45	109.72	116.56	123.96	131.92
0.8	33.536	35.972	38.640	41.541	44.673	48.033	102.20	108.73	115.90	123.72	132.18	141.27
0.9	35.244	37.984	40.986	44.249	47.773	51.553	106.66	114.01	122.08	130.87	140.39	150.62
1.0	36.951	39.996	43.332	46.958	50.872	55.073	111.13	119.29	128.26	138.03	148.60	159.97
Z = 30												
ϵ_s = 0.6	30.242	32.067	34.068	36.242	38.589	41.107	93.890	98.782	104.15	110.01	116.34	123.15
0.7	31.949	34.079	36.413	38.949	41.587	44.625	98.352	104.06	110.33	117.16	124.54	132.49
0.8	33.657	36.091	38.758	41.657	44.786	48.144	102.816	109.34	116.50	124.30	132.75	141.82
0.9	35.364	38.103	41.103	44.364	47.885	51.662	107.27	114.61	122.67	131.45	140.95	151.16
1.0	37.072	40.115	43.448	47.072	50.983	55.180	111.74	119.898	128.84	138.60	149.15	160.50

ORIGINAL PAGE IS
OF POOR QUALITY

Table B1.4 Clearsky upwelling radiance and radiative flux for spectral range 5-20 μ

Z, km and ϵ_s	Radiance, W/m^2-sr Surface Temperature, K						Radiative Flux, W/m^2 Surface Temperature, K					
	270	280	290	300	310	320	270	280	290	300	310	320
Z = 10												
ϵ_s = 0.6	43.571	46.689	50.172	54.032	58.275	62.907	135.01	143.33	152.62	162.92	174.24	186.61
0.7	46.174	49.811	53.875	58.378	63.328	68.732	141.86	151.56	162.40	174.42	187.63	202.05
0.8	48.776	52.932	57.577	62.723	68.381	74.557	148.71	159.79	172.18	185.92	201.02	217.50
0.9	51.378	56.054	61.280	67.069	73.434	80.382	155.56	168.03	181.97	197.42	214.40	232.95
1.0	53.981	59.176	64.982	71.415	78.486	86.207	162.41	176.26	191.75	208.92	227.79	248.39
Z = 20												
ϵ_s = 0.6	40.923	43.919	47.265	50.969	55.039	59.481	124.92	132.77	141.55	151.27	161.95	173.60
0.7	43.439	46.934	50.837	55.159	59.907	65.089	131.43	140.60	150.84	162.18	174.64	188.24
0.8	45.954	49.949	54.409	59.349	64.776	70.698	137.95	148.43	160.13	173.09	187.33	202.87
0.9	48.470	52.963	57.982	63.538	69.644	76.306	144.47	156.26	169.42	184.01	200.03	217.50
1.0	50.985	55.978	61 54	67.728	74.512	81.914	150.99	169.09	178.72	194.92	212.72	232.14
Z = 30												
ϵ_s = 0.6	40.880	43.807	47.075	50.693	54.666	59.002	124.89	132.51	141.03	150.46	160.82	172.11
0.7	43.344	46.759	50.572	54.792	59.429	64.487	131.23	140.13	150.07	161.07	173.15	186.33
0.8	45.809	49.712	54.059	58.892	64.191	69.971	137.58	147.75	159.11	171.68	185.49	200.55
0.9	48.273	52.664	57.566	62.992	68.953	75.456	143.93	155.37	168.15	182.29	197.83	214.77
1.0	50.737	55.616	61.063	67.092	73.715	80.941	150.28	162.99	192.90	210.16	27[illegible].57	228.99

Table B1.5 Clearsky upwelling radiance and radiative flux for spectral range 10.5-12.5 μ

Z, km and ϵ_s	Radiance, W/m^2-sr Surface Temperature, K						Radiative Flux, W/m^2 Surface Temperature, K					
	270	280	290	300	310	320	270	280	290	300	310	320
Z = 10												
ϵ_s = 0.6	7.622	8.694	[illegible]870	11.151	12.515	14.022	25.324	28.376	31.726	35.374	39.318	43.556
0.7	8.598	9.848	11.220	12.714	14.329	16.064	28.097	31.657	35.566	39.822	44.424	49.367
0.8	9.573	11.002	12.570	14.277	16.123	18.105	30.870	34.938	39.405	44.270	49.529	55.179
0.9	10.55	12.155	13.920	15.840	17.917	20.147	33.642	38.220	43.245	48.717	54.634	60.990
1.0	11.52	13.309	15.2694	17.404	19.711	22.189	36.415	41.501	47.085	53.165	59.739	66.802
Z = 20												
ϵ_s = 0.6	7.559	8.643	9.833	11.129	12.530	14.035	25.029	28.141	31.557	35.278	39.300	43.621
0.7	8.546	9.811	11.200	12.711	14.346	16.101	27.857	31.488	35.474	39.814	44.507	49.548
0.8	9.533	10.979	12.566	14.293	16.161	18.167	30.685	34.835	39.390	44.350	49.714	55.475
0.9	10.520	12.146	13.932	15.875	17.977	20.233	33.514	38.182	43.306	48.887	54.920	61.402
1.0	11.507	13.314	15.298	17.458	19.792	22.300	36.342	41.529	47.223	53.423	60.127	67.329
Z = 30												
ϵ_s = 0.6	7.549	8.635	9.827	11.126	12.529	14.036	24.981	28.103	31.529	35.261	39.296	43.630
0.7	8.537	9.805	11.196	12.711	14.348	16.106	27.818	31.460	35.458	39.458	44.518	49.575
0.8	9.526	10.975	12.565	14.296	16.167	18.177	30.655	34.817	39.386	44.362	49.741	55.575
0.9	10.515	12.145	13.933	15.881	17.986	20.247	33.492	38.174	43.315	48.912	54.964	61.465
1.0	11.5042	13.315	15.302	17.466	19.805	22.317	36.329	41.532	47.243	53.462	60.187	67.410

ORIGINAL PAGE IS
OF POOR QUALITY

APPENDIX B2
UPWELLING RADIANCE IN PRESENCE OF CLOUDS
TABLES B2.1 - B2.4

Table B2.1 Upwelling radiance in presence of clouds [(W/cm^2-sr) x 10^{-5}] for T_s = 280 K and spectral range = 5-10 μ (1,000 - 2,000 cm^{-1})

Z, (Z_b), km	ϵ_s	Clearsky LWC = 0	Liquid Water Content (LWC), gm/m^2 10	20	30	40	50	60	70	80	90
10 (5)	0.5	113.35	79.31	55.91	43.07	36.02	32.15	30.03	28.87	28.23	27.87
	0.6	123.86	85.20	59.14	44.84	36.99	32.69	30.32	29.03	28.31	27.92
	0.7	134.37	91.08	62.37	46.61	37.97	33.22	30.62	29.19	28.40	27.97
	0.8	144.88	96.97	65.60	48.39	38.94	33.75	30.91	29.35	28.49	28.02
	0.9	155.39	102.86	68.84	50.16	39.91	34.23	31.20	29.51	28.58	28.07
	1.0	165.90	108.75	72.07	51.93	40.89	34.82	31.50	29.67	28.67	28.12
20 (5)	0.5	107.60	76.53	54.91	43.04	36.52	32.95	30.99	29.91	29.32	29.00
	0.6	117.02	81.81	57.80	44.63	37.40	33.43	31.25	30.06	29.40	29.04
	0.7	126.43	87.08	60.70	46.22	38.27	33.91	31.51	30.20	29.48	29.08
	0.8	135.84	92.36	63.59	47.80	39.14	34.39	31.78	30.34	29.56	29.13
	0.9	145.26	97.64	66.49	49.39	40.01	34.86	32.04	30.40	29.64	29.17
	1.0	154.67	102.91	69.38	50.98	40.88	35.34	32.20	30.63	29.72	29.20
30 (5)	0.5	108.12	77.57	56.13	44.36	37.90	34.36	32.41	31.39	30.76	30.44
	0.6	117.33	82.73	58.96	45.91	38.76	34.83	32.67	31.49	30.48	30.48
	0.7	126.54	88.89	61.79	47.47	39.61	35.30	32.93	31.63	30.91	30.52
	0.8	135.75	93.05	64.62	49.02	40.46	35.76	33.18	31.77	30.99	30.56
	0.9	144.96	98.21	67.46	50.58	41.32	36.23	33.44	31.91	31.07	30.61
	1.0	154.17	103.37	70.29	52.13	42.17	36.70	33.70	32.05	31.15	30.65

Table B2.1 (continued)

Z, (Z_b), km	ϵ_s	Clearsky LWC = 0	Liquid Water Content (LWC), gm/m²								
			10	20	30	40	50	60	70	80	90
20 (10)	0.5	107.60	88.25	70.61	56.74	45.83	37.24	30.49	25.18	21.00	17.71
	0.6	117.02	95.70	76.48	61.35	49.45	40.10	32.73	26.94	22.39	18.80
	0.7	126.43	103.15	82.34	65.96	53.08	42.95	34.98	28.71	23.78	19.90
	0.8	135.84	110.60	88.20	70.57	56.71	45.80	37.22	30.47	25.16	20.99
	0.9	145.26	118.05	94.06	75.18	60.33	48.65	39.47	32.24	25.55	22.08
	1.0	154.67	125.51	99.02	79.79	63.96	51.51	41.71	34.00	27.94	23.17
30 (10)	0.5	108.12	98.58	71.05	57.26	46.42	37.88	31.17	25.89	21.74	18.47
	0.6	117.33	95.86	76.78	61.77	49.96	40.67	33.36	27.62	23.09	19.54
	0.7	126.54	103.15	82.51	66.28	53.51	43.46	35.56	29.34	24.45	20.61
	0.8	135.75	110.43	88.24	70.78	57.05	46.25	37.75	31.07	25.81	21.67
	0.9	144.96	117.71	93.97	75.29	60.59	49.04	39.94	32.79	27.17	22.74
	1.0	154.17	125.00	99.70	79.80	64.14	51.82	42.14	34.52	28.52	23.81
30 (20)	0.5	108.12	86.13	68.49	54.61	43.69	35.11	28.35	23.03	18.85	15.56
	0.6	117.33	93.42	74.22	59.12	47.24	37.89	30.54	24.76	20.21	16.63
	0.7	126.54	100.71	79.95	63.62	50.78	40.68	32.73	26.48	21.57	17.70
	0.8	135.75	107.99	85.68	68.13	54.33	43.47	34.93	28.21	22.92	18.77
	0.9	144.96	115.28	91.41	72.64	57.88	46.26	37.12	29.94	24.28	19.83
	1.0	154.17	122.57	97.14	77.15	61.42	49.05	39.32	31.66	25.64	20.90

ORIGINAL PAGE IS
OF POOR QUALITY

Table B2.2 Upwelling radiance in presence of clouds [(W/cm^2-sr) x 10^{-5}] for T_s = 280 K and spectral range = 5-10 μ (1,000-2,000 cm^{-1})

Z, (Z_b), km	ϵ_s	Clearsky LWC = 0	Liquid Water Content (LWC), gm/m^2								
			10	20	30	40	50	60	70	80	90
10 (5)	0.5	310.49	29.631	175.93	146.46	130.29	121.42	116.54	113.87	112.40	111.60
	0.6	332.89	242.27	182.87	150.27	132.38	122.56	117.17	114.22	112.59	111.70
	0.7	355.29	254.92	189.81	154.08	134.47	123.71	117.80	114.56	112.78	111.81
	0.8	377.69	267.56	196.75	157.89	136.56	124.86	118.43	114.91	112.97	111.91
	0.9	400.09	280.20	203.69	161.70	138.65	126.00	119.06	115.25	113.16	112.01
	1.0	422.09	292.84	210.62	165.50	140.74	127.15	119.69	115.60	113.35	112.12
20 (5)	0.5	296.34	213.83	160.48	131.20	115.13	106.31	101.47	98.811	97.353	96.553
	0.6	319.31	226.79	167.59	135.10	117.27	107.48	102.11	99.165	97.547	96.660
	0.7	342.28	239.74	174.70	139.00	119.41	108.66	102.76	99.519	97.742	96.766
	0.8	365.25	252.69	181.80	142.90	121.55	109.83	103.40	99.873	97.936	96.873
	0.9	388.23	265.64	188.91	146.80	123.69	111.01	104.05	100.23	98.130	96.980
	1.0	411.20	278.60	196.02	150.70	125.83	112.18	104.69	100.58	98.324	97.086
30 (5)	0.5	299.84	215.36	161.00	131.17	114.80	105.82	100.89	98.179	96.694	95.879
	0.6	323.21	228.59	168.27	135.16	116.99	107.02	101.54	98.541	96.892	95.988
	0.7	346.78	241.83	175.53	139.15	119.18	108.22	102.20	98.902	97.091	96.097
	0.8	370.25	255.06	182.79	143.13	121.36	109.42	102.86	99.264	97.289	96.206
	0.9	393.71	268.30	190.06	147.12	123.55	110.62	103.52	99.626	97.488	96.315
	1.0	417.18	281.53	197.32	151.10	125.74	111.82	104.18	99.987	97.686	96.423

Table B2.2 (continued)

Z, (Z_b), km	ε_s	Clearsky LWC = 0	Liquid Water Content (LWC), gm/m^2								
			10	20	30	40	50	60	70	80	90
20 (10)	0.5	296.34	248.63	205.69	171.92	145.35	124.45	108.01	95.082	84.913	76.908
	0.6	319.31	266.79	219.98	183.16	154.19	131.41	113.48	99.385	88.295	79.570
	0.7	342.28	284.95	234.27	194.40	163.03	138.36	118.95	103.69	91.679	82.233
	0.8	365.25	303.11	248.55	205.63	171.87	145.32	124.42	107.99	95.064	84.396
	0.9	388.23	321.27	262.84	216.87	180.71	152.27	129.89	112.29	98.449	87.558
	1.0	411.20	339.44	277.13	228.11	189.55	159.22	135.36	116.60	101.83	90.221
30 (10)	0.5	299.84	251.05	207.77	173.74	146.96	125.90	109.33	96.294	86.04	77.98
	0.6	323.31	269.60	222.37	185.22	155.99	133.00	114.92	100.69	89.50	80.697
	0.7	346.78	288.16	236.97	196.70	165.02	140.11	120.50	105.09	92.96	83.417
	0.8	370.25	306.71	251.56	208.18	174.05	147.21	126.09	109.48	96.42	86.137
	0.9	393.71	325.27	266.16	219.66	183.09	154.31	131.68	113.88	99.87	88.858
	1.0	417.18	343.87	280.75	231.14	192.12	161.42	137.27	118.27	103.33	91.578
30 (5)	0.5	299.84	242.94	196.34	159.69	130.86	108.18	90.337	76.303	65.263	56.579
	0.6	323.31	261.41	210.88	171.12	139.85	115.25	95.902	80.68	68.707	59.288
	0.7	346.78	279.89	225.41	182.56	148.85	122.33	101.47	85.06	72.151	61.997
	0.8	370.25	298.37	239.95	193.99	157.84	129.40	107.03	89.44	75.154	64.706
	0.9	393.71	316.85	254.48	205.42	166.83	136.48	112.60	93.81	79.038	67.415
	1.0	417.18	335.32	269.02	216.86	175.83	143.55	118.160	98.19	82.482	70.124

Table B2.3 Upwelling radiance in presence of clouds [(W/cm^2-sr) x 10^{-5}] for T_s = 280 K and spectral range = 5-10 μ (1,000-2,000 cm^{-1})

Z, (Z_b), km	ε_s	Clearsky LWC = 0	Liquid Water Content (LWC), gm/m^2								
			10	20	30	40	50	60	70	80	90
10 (5)	0.5	423.84	308.936	231.84	189.53	166.31	153.57	146.57	142.74	140.63	139.47
	0.6	456.75	327.465	242.01	195.11	169.37	155.25	147.49	143.25	140.9	139.62
	0.7	489.66	346.00	252.18	200.69	172.44	156.93	148.42	143.75	141.18	139.78
	0.8	522.57	364.53	262.35	206.28	175.5	158.61	149.34	144.26	141.46	139.93
	0.9	555.48	383.06	272.53	211.86	178.56	160.29	150.26	144.76	141.76	140.0[illegible]
	1.0	587.99	401.59	282.69	217.43	181.63	161.97	151.19	145.27	142.02	140.2[illegible]
20 (5)	0.5	403.94	290.36	215.39	174.24	151.65	139.26	132.46	128.72	126.673	125.55
	0.6	436.33	308.61	225.3[illegible]	179.73	154.67	140.91	133.36	129.22	126.95	125.70
	0.7	468.71	326.82	235.4	185.22	157.68	142.57	134.27	129.72	127.22	125.85
	0.8	501.09	345.05	24[illegible].39	190.7	160.69	144.22	135.18	130.21	127.50	126.00
	0.9	533.49	363.28	255.4	196.19	163.70	145.87	136.09	130.72	127.77	126.15
	1.0	565.87	381.51	265.4	201.68	166.71	147.52	136.99	131.21	128.04	126.29
30 (5)	0.5	407.96	292.93	217.13	175.53	152.70	140.18	133.30	128.04	127.45	126.32
	0.6	440.64	311.32	227.23	181.07	155.75	141.85	134.2[illegible]			
	0.7	473.32	329.72	237.32	186.62	158.79	143.52	135.13			
	0.8	506.00	348.11	247.41	192.15	161.82	145.18	136.04			
	0.9	538.67	366.51	257.52	197.70	164.87	146.85	136.96			
	1.0	571.35	384.90	267.61	203.23	167.91	148.52	137.88			

Table B2.4 Upwelling radiance in presence of clouds [(W/cm^2-sr) x 10^{-5}] for T_s = 280 K and spectral range = 10.5 - 12.5 μ (800-950 cm^{-1})

Z, (Z_b), km	ε_s	Clearsky LWC = 0	Liquid Water Content (LWC), gm/m^2								
			10	20	30	40	50	60	70	80	90
10 (5)	0.5	71.044	39.552	22.087	12.501	7.241	4.354	2.769	1.900	1.423	1.161
	0.6	83.578	46.462	23.879	14.583	8.383	4.981	3.113	2.088	1.526	1.218
	0.7	96.113	53.372	29.671	16.664	9.525	5.607	3.457	2.277	1.630	1.274
	0.8	108.65	60.282	33.464	18.745	10.668	6.234	3.801	2.466	1.733	1.331
	0.9	121.18	67.192	37.256	20.826	11.810	6.861	4.145	2.655	1.837	1.388
	1.0	133.72	74.103	41.048	22.908	12.952	7.488	4.489	2.844	1.941	1.445
20 (5)	0.5	70.934	39.468	22.026	12.453	7.199	4.317	2.734	1.866	1.389	1.127
	0.6	83.491	46.389	25.824	14.538	8.344	4.944	3.079	2.055	1.493	1.185
	0.7	96.048	53.311	29.623	16.623	9.488	5.572	3.423	2.244	1.5978	1.242
	0.8	108.61	60.232	33.421	18.707	10.632	6.200	3.768	2.433	1.700	1.298
	0.9	121.166	67.153	37.220	20.792	11.776	6.828	4.112	2.622	1.804	1.355
	1.0	133.72	74.074	41.018	22.876	12.920	7.456	4.457	2.811	1.9082	1.412
30 (5)	0.5	70.869	39.415	21.984	12.418	7.168	4.287	2.706	1.838	1.362	1.100
	0.6	83.443	46.344	25.787	14.505	8.313	4.915	3.051	2.027	1.466	1.157
	0.7	96.016	53.273	29.590	16.592	9.459	5.544	3.396	2.217	1.570	1.214
	0.8	108.59	60.202	33.393	18.679	10.604	6.173	3.741	2.406	1.673	1.217
	0.9	121.16	67.131	37.195	20.766	11.750	6.801	4.086	2.595	1.777	1.328
	1.0	133.74	74.060	40.998	22.853	12.895	7.430	4.431	2.785	1.881	1.385

ORIGINAL PAGE IS
OF POOR QUALITY

Table B2.4 (continued)

Z, (Z_b), km	ε_s	Clearsky LWC = 0	Liquid Water Content (LWC), gm/m^2								
			10	20	30	40	50	60	70	80	90
20 (10)	0.5	70.934	55.813	43.909	34.545	27.179	21.385	16.827	13.242	10.421	8.203
	0.6	83.491	65.692	51.680	40.658	31.988	25.168	19.603	15.582	12.263	9.651
	0.7	96.048	75.572	59.452	46.772	36.797	28.951	22.778	17.923	14.104	1.100
	0.8	108.618	85.451	67.224	52.885	41.606	32.733	25.754	20.264	15.945	1.255
	0.9	121.16	95.331	74.995	58.998	46.419	36.516	28.730	2.605	17.786	1.400
	1.0	133.72	105.21	82.767	65.112	51.224	40.299	31.705	24.945	19.628	1.544
30 (10)	0.5	70.869	55.763	43.871	34.516	27.158	21.369	16.816	13.234	10.417	8.200
	0.6	83.443	65.655	51.652	40.637	31.973	25.157	19.795	15.578	12.260	9.650
	0.7	96.016	75.547	59.434	46.759	36.788	28.945	22.775	17.922	14.104	11.101
	0.8	108.59	85.439	67.215	52.880	41.603	32.732	25.754	20.265	15.947	12.551
	0.9	121.16	95.332	74.997	59.001	46.418	36.520	28.734	22.609	17.791	14.001
	1.0	133.74	105.221	82.778	65.122	51.122	51.233	40.307	31.713	24.953	19.635
30 (20)	0.5	70.869	55.750	43.856	34.500	27.140	21.351	16.796	13.214	10.396	8.179
	0.6	83.443	65.641	51.641	51.637	40.620	25.138	19.775	15.557	12.239	9.629
	0.7	96.016	75.532	59.417	46.740	36.769	28.925	22.754	17.901	14.083	11.079
	0.8	108.59	85.423	67.197	52.861	41.583	32.712	25.734	17.901	14.083	12.529
	0.9	121.16	95.314	74.978	58.981	46.398	35.499	28.713	22.588	17.769	13.979
	1.0	133.747	105.207	82.758	65.101	51.212	40.286	31.692	24.931	19.613	15.429

APPENDIX B3

ANISOTROPIC FUNCTIONS FOR SPECTRAL

RANGE 5 - 50 - Tables B3.1 - B3.12

Table B3.1 Variation of anisotropic function with cloud cover fraction for standard atmosphere; Atm Top = 30 km, spectral range = 5-50 μ, T_s = 288.15 K, ε_s = 1.0, λ = 3, ε_c = 1.0, Z_c = 6 km, RH

Zenith Angle, θ	Cloud Cover, %		
	0	50	100
0	1.079	1.062	1.040
15	1.073	1.058	1.037
30	1.056	1.044	1.029
45	1.024	1.019	1.013
60	0.972	0.978	0.985
70	0.919	0.935	0.957
80	0.835	0.867	0.912
G	0.244	0.195	0.128

Table B3.2 Variation of anisotropic function with cloud height for standard atmosphere; Atm Top = 30 km, spectral range = 5-50 μ, T_s = 288.15 K, ε_s = 1.0, λ = 3, ε_c = 1.0, RH = 75%

Zenith Angle, θ	Cloud Height (Z_c), km					
	50% Cloud Cover			100% Cloud Cover		
	2	6	10	2	6	10
0	1.073	1.062	1.092	1.067	1.040	1.005
15	1.068	1.058	1.049	1.063	1.040	1.005
30	1.052	1.044	1.037	1.048	1.029	1.004
45	1.023	1.019	1.016	1.021	1.013	1.002
60	0.974	0.978	0.982	0.976	0.985	0.998
70	0.925	0.935	0.946	0.931	0.957	0.995
80	0.848	0.867	0.890	0.862	0.912	0.991
G	0.225	0.195	0.162	0.205	0.128	0.014

Table B3.3 Variation of anisotropic function with high-cloud emissivity for standard atmosphere; Atm Top = 30 km, spectral range = 5-50 μ, T_s = 288.15 K, ε_s = 1.0, λ = 3, RH = 75%

Zenith Angle, θ	High Cloud (Z_c = 10 km) Emissivity, ε_c			
	50% Cloud Cover		100% Cloud Cover	
	0.5	1.0	0.5	1.0
0	1.067	1.052	1.052	1.005
15	1.067	1.052	1.049	1.005
30	1.048	1.037	1.037	1.004
45	1.021	1.016	1.016	1.002
60	0.976	0.982	0.982	0.998
70	0.931	0.946	0.946	0.995
80	0.859	0.890	0.890	0.991
G	0.208	0.162	0.162	0.014

Table B3.4a Variation of anisotropic function with surface relative humidity for standard atmosphere; Atm Top = 30 km, spectral range = 5-50 μ, T_s = 288.15 K, ε_s = 1.0, λ = 3, ε_c = 1.0, Z_c = 6 km

Zenith Angle, θ	Surface Relative Humidity (RH), %							
	Clear Sky				Overcast sky			
	25	50	75	100	25	50	75	100
0	1.075	1.077	1.079	1.080	1.036	1.039	1.040	1.041
15	1.069	1.072	1.073	1.075	1.034	1.036	1.037	1.038
30	1.053	1.055	1.056	1.057	1.026	1.028	1.029	1.029
45	1.023	1.024	1.024	1.025	1.012	1.012	1.013	1.013
60	0.974	0.973	0.972	0.972	0.986	0.986	0.985	0.985
70	0.923	0.921	0.919	0.917	0.959	0.957	0.957	0.956
80	0.843	0.839	0.835	0.831	0.914	0.912	0.912	0.912
G	[illegible]	0.238	0.244	0.249	0.122	0.127	0.128	0.129

Table B3.4b Variation of anisotropic function with surface relative humidity (low range) for standard atmosphere; Atm Top = 30 km, spectral range = 5-50μ, T_s = 288.15 K, ε_s = 1.0, λ = 3, clear sky

Zenith Angle, θ	Surface Relative Humidity (RH), %					
	0	5	10	15	20	25
0	1.028	1.068	1.071	1.073	1.074	1.075
15	1.026	1.063	1.066	1.068	1.069	1.069
30	1.020	1.[illegible]37	1.051	1.052	1.053	1.053
45	1.009	1.022	1.022	1.023	1.023	1.023
60	0.990	0.975	0.974	0.974	0.974	0.974
70	0.970	0.926	0.924	0.924	0.923	0.923
80	0.937	0.847	0.845	0.844	0.843	0.843
G	0.091	0.221	0.226	0.229	0.231	0.232

Table B3.5 Variation of anisotropic function with water vapor scale-height parameter for standard atmosphere; Atm Top = 30 km, spectral range = 5-50 μ, T_s = 288.15 K, ε_s = 1.0, Z_c = 6 km, RH = 75%

Zenith Angle, θ	Water Vapor Scale-Height Parameter, λ					
	Clear Sky			Overcast Sky		
	2	3	4	2	3	4
0	1.084	1.079	1.074	1.044	1.040	1.035
15	1.078	1.073	1.069	1.041	1.037	1.033
30	1.060	1.056	1.053	1.031	1.029	1.026
45	1.026	1.024	1.023	1.014	1.013	1.011
60	0.971	0.972	0.974	0.985	0.985	0.987
70	0.915	0.919	0.923	0.956	0.957	0.960
80	0.826	0.835	0.841	0.914	0.912	0.915
G	0.258	0.244	0.233	0.130	0.128	0.120

C-2

Table B3.6 Variation of anisotropic function with surface emissivity for standard atmosphere; Atm Top = 30 km, spectral range = 5-50 μ, T_s = 288.15, λ = 3, ε_c = 1.0, Z_c = 6 km, RH = 75%.

Zenith Angle,	Surface Emissivity, ε_s					
	Clear Sky			50% Cloud Cover		
θ	0.8	0.9	1.0	0.8	0.9	1.0
0	1.066	1.073	1.079	1.055	1.059	1.062
15	1.062	1.068	1.073	1.051	1.055	1.058
30	1.047	1.052	1.056	1.039	1.042	1.044
45	1.021	1.023	1.024	1.017	1.044	1.019
60	0.977	0.975	0.972	0.981	1.019	0.978
70	0.933	0.926	0.919	0.944	0.979	0.935
80	0.865	0.850	0.835	0.886	0.939	0.867
G	0.201	0.223	0.244	0.169	0.182	0.195

Table B3.7 Variation of anisotropic function with surface skin temperature for standard atmosphere; Atm Top = 30 km, spectral range = 5-50 km, λ = 3, RH = 75%, clear sky.

Zenith Angle, θ	Surface Skin Temperature, K					
	$T'_s = T_s - 5$		Standard, T_s = 288.15		$T'_s = T_s + 5$	
	T_z	$T'_z=T_z-5$	T_z	T_z (CO_2 only)	T_z	$T'_z = T_z + 5$
0	1.074	1.081	1.079	1.013	1.083	1.077
15	1.069	1.075	1.073	1.012	1.078	1.071
30	1.053	1.057	1.056	1.009	1.059	1.055
45	1.023	1.025	1.024	1.004	1.026	1.024
60	0.974	0.972	0.972	0.996	0.971	0.973
70	0.925	0.917	0.919	0.988	0.914	0.921
80	0.847	0.830	0.835	0.976	0.823	0.839
G	0.227	0.251	0.244	0.037	0.260	0.238

Table B3.8 Variation of anisotropic function with carbon dioxide concentration for wet and dry standard atmosphere; Atm Top = 5-50 μ, T_s = 288.15 K, ε_s = 1.0, λ = 3, RH = 75%, clear sky.

Zenith Angle,	Carbon Dioxide Concentration					
	Dry Atmosphere			Standard Water Vapor		
θ	Zero	Stand.	Double	Zero	Stand.	Double
0	1.013	1.028	1.027	1.072	1.079	1.077
15	1.012	1.026	1.025	1.067	1.073	1.072
30	1.009	1.020	1.019	1.052	1.056	1.055
45	1.004	1.009	1.009	1.023	1.024	1.024
60	0.995	0.990	0.990	0.973	0.972	0.973
70	0.985	0.970	0.971	0.918	0.919	0.921
80	0.967	0.937	0.938	0.823	0.835	0.838
G	0.046	0.091	0.089	0.249	0.244	0.239

Table B3.9 Latitudinal variation of anisotropic function for climatological-average model atmospheres; Atm Top = 30 km, spectral range = 5-50 μ, ε_s = 1.0, λ = 3, ε_c = 1.0, Z_c = 6 km

Zenith Angle,	Climatological-Average Model Atmospheres					
	Tropical		Sub-Arctic Winter		Mid-Lat. Ave.	
θ	Clear	Overcast	Clear	Overcast	Clear	Overcast
0	1.097	1.062	1.053	1.025	1.079	1.040
15	1.090	1.057	1.049	1.023	1.073	1.037
30	1.069	1.044	1.038	1.018	1.056	1.029
45	1.030	1.019	1.017	1.008	1.024	1.013
60	0.965	0.978	0.981	0.991	0.972	0.985
70	0.898	0.933	0.943	0.971	0.919	0.957
80	0.789	0.864	0.882	0.936	0.835	0.912
G	0.308	0.198	0.171	0.089	0.244	0.128

Table B3.10 Variation of anisotropic function for different model atmospheres; Atm Top = 30 km, spectral range = 5-50 μ, ε_s = 1.0, λ = 3, ε_c = 1.0, Z_c = 6 km.

Zenith Angle, θ	Model Atmosphere					
	Sub-Arc. Summer, T_s = 288.45 K		Mid-Lat. Winter, T_s = 272.59 K		Mid-Lat. Summer T_s = 296.22 K	
	Clear	Overcast	Clear	Overcast	Clear	Overcast
0	1.071	1.035	1.065	1.034	1.083	1.050
15	1.066	1.033	1.061	1.032	1.077	1.047
30	1.050	1.025	1.047	1.025	1.059	1.036
45	1.022	1.011	1.020	1.011	1.026	1.016
60	0.975	0.987	0.977	0.987	0.971	0.982
70	0.928	0.963	0.931	0.961	0.914	0.947
80	0.855	0.926	0.859	0.915	0.824	0.892
G	0.216	0.109	0.206	0.119	0.259	0.158

Table B3.11 Latitudinal variation of anisotropic function for radiosonde-measured atmospheric models (Data 106 models, 9/29/58); Atm Top = 30 km, spectral range = 5-50 μ, ε_s = 1.0, clear sky.

Zenith Angle, θ	Atmospheric Model		
	Havana, Cuba	Nantucket, Mass.	Thule, Greenland
0	1.0834	1.0704	1.0501
15	1.0776	1.0655	1.0467
30	1.0595	1.0502	1.0360
45	1.0261	1.0220	1.0159
60	0.9703	0.9750	0.9816
70	0.9125	0.9266	0.9448
80	0.8219	0.8500	0.8854
G	0.2615	0.2204	0.1647

Table B3.12 Seasonal variation of anisotropic function for radiosonde-measured atmospheric models (Data 106 model); Atm Top = 30 km, spectral range = 5-50 μ, ε_s = 1.0, clear sky.

Zenith Angle, θ	Tropical		Mid-Lat. Const.		Sub-Arctic	
	Keywest, Florida		Grand Jn., Colo.	Denver, Colo.	Eureka, NWT	
	08/01/58	02/01/58	08/01/58	01/01/58	08/01/58	03/01/58
0	1.0835	1.0815	1.0718	1.0565	1.0561	1.0322
15	1.0777	1.0759	1.0668	1.0527	1.0522	1.0301
30	1.0594	1.0581	1.0512	1.0406	1.0398	1.0234
45	1.0260	1.0254	1.0224	1.0179	1.0173	1.0105
60	0.9706	0.9711	0.9746	0.9794	0.9806	0.9875
70	0.9134	0.9151	0.9256	0.9388	0.9442	0.9615
80	0.8226	0.8278	0.8489	0.8749	0.8906	0.9150
G	0.2609	0.2538	0.2229	0.1816	0.1655	0.1172

APPENDIX B4

ANISOTROPIC FUNCTIONS FOR SPECTRAL

RANGE 5-200 μ - Tables B4.1 - B4.16

Table B4.1 Variation of anisotropic function with high-cloud cover fraction for standard atmosphere; spectral range = 5-200 μ, Atm Top = 30 km, T_s = 288.15 K, ε_s = 1.0, λ = 3. ε_c = 1.0, Z_c = 6 km, RH = 75%.

Zenith Angle, θ	Cloud Cover, %		
	0	50	100
0	1.0768	1.0608	1.0395
15	1.0714	1.0566	1.0368
30	1.0546	1.0433	1.0283
45	1.0238	1.0189	1.0125
60	0.9731	0.9785	0.9857
70	0.9212	0.9367	0.9575
80	0.8382	0.8702	0.9130
G	0.2385	0.1906	0.1265

Table B4.2 Variation of anisotropic function with cloud height for standard atmosphere; spectral range = 5-200 μ, Atm Top = 30 km, T_s = 228.15 K, ε_s = 1.0, λ_s = 3, ε_c = 1.0, RH = 75%.

Zenith Angle, θ	Cloud Height (Z_c), km					
	50% Cloud Cover			100% Cloud Cover		
	2	6	10	2	6	10
0	1.0715	1.0608	1.0511	1.0658	1.0395	1.0060
15	1.0665	1.0566	1.0475	1.0612	1.0368	1.0056
30	1.0580	1.0433	1.0363	1.0468	1.0283	1.0043
45	1.0221	1.0189	1.0158	1.0204	1.0125	1.0019
60	0.9750	0.9785	0.9821	0.9770	0.9857	0.9978
70	0.9268	0.9367	0.9475	0.9329	0.9575	0.9936
80	0.8508	0.8702	0.8925	0.8645	0.9130	0.9874
G	0.2207	0.1906	0.1586	0.2013	0.1265	0.0186

Table B4.3 Variation of anisotropic function with high-cloud emissivity for standard atmosphere; spectral range = 5-200 μ, Atm Top = 30 km, T_s = 288.15 K, ε_s = 1.0, λ = 3, RH = 75%.

Zenith Angle, θ	High Cloud (Z_c = 10 km) Emissivity, ε_c			
	50% Cloud Cover		100% Cloud Cover	
	0.5	1.0	0.5	1.0
0	1.0655	1.0511	1.0511	1.0060
15	1.0609	1.0475	1.0475	1.0056
30	1.0465	1.0363	1.0363	1.0043
45	1.0203	1.0158	1.0158	1.0019
60	0.9771	0.9821	0.9821	0.9978
70	0.9328	0.9475	0.9475	0.9936
80	0.8621	0.8925	0.8925	0.9874
G	0.2034	0.1586	0.1586	0.0186

Table B4.4 Variation of anisotropic function with surface relative humidity for standard atmosphere; spectral range = 5-200 μ, Atm Top = 30 km, T_s = 288.15 K, ε_s = 1.0, λ = 3, ε_c = 1.0, Z_c = 6 km.

Zenith Angle, θ	Surface Relative Humidity (RH), %					
	Clear Sky			Overcast sky		
	50	75	100	50	75	100
0	1.0753	1.0768	1.0784	1.0384	1.0395	1.0401
15	1.0700	1.0714	1.0729	1.0358	1.0368	1.0374
30	1.0535	1.0546	1.0557	1.0276	1.0276	1.0287
45	1.0233	1.0238	1.0243	1.0122	1.0125	1.0126
60	0.9737	0.9731	0.8725	0.9859	0.9857	0.9855
70	0.9229	0.9212	0.9194	0.9579	0.9575	0.9573
80	0.8422	0.8382	0.8346	0.9128	0.9130	0.9134
G	0.2331	0.2386	0.2438	0.1256	0.1265	0.1267

Table B4.5 Variation of anisotropic function with water vapor scale-height for standard atmosphere; spectral range = 5-200 μ, Atm Top = 30 km, T_s = 288.15 K, ϵ_s = 1.0, ϵ_c = 1.0, Z_c = 6 km, RH = 75%.

Zenith Angle, θ	Water Vapor Scale-Height Parameter, λ					
	Clear Sky			Overcast Sky		
	2	3	4	2	3	4
0	1.0811	1.0768	1.0721	1.0417	1.0395	1.0350
15	1.0754	1.0714	1.0671	1.0388	1.0368	1.0327
30	1.0575	1.0546	1.0514	1.0297	1.0283	1.0253
45	1.0250	1.0238	1.0225	1.0129	1.0125	1.0113
60	0.9719	0.9731	0.9744	0.9854	0.9857	0.9868
70	0.9177	0.9212	0.9247	0.9578	0.9575	0.9601
80	0.8321	0.8382	0.8441	0.9176	0.9130	0.9153
G	0.2490	0.2386	0.2280	0.1241	0.1265	0.1197

Table B4.6 Variation of anisotropic function with surface emissivity for standard atmosphere; spectral range = 5-200 μ, Atm Top = 30 km, T_s = 288.15 K, λ = 3, = ε_c = 1.0, Z_c = 6 km, RH = 75%.

Zenith Angle, θ	Surface Emissivity, ε_s					
	Clear Sky			50% Cloud Cover		
	0.8	0.9	1.0	0.8	0.9	1.0
0	1.0647	1.0710	1.0768	1.0535	1.0572	1.0608
15	1.0602	1.0660	1.0714	1.0498	1.0532	1.0566
30	1.0460	1.0504	1.0546	1.0381	1.0408	1.0433
45	1.0200	1.0220	1.0238	1.0167	1.0178	1.0189
60	0.9775	0.9752	0.9731	0.9811	0.9798	0.9785
70	0.9347	0.9277	0.9212	0.9449	0.9407	0.9367
80	0.8681	0.8527	0.8382	0.8881	0.8790	0.8702
G	0.1966	0.2183	0.2386	0.1654	0.1782	0.1906

Table B4.7 Variation of anisotropic function high-cloud cover fraction for tropical atmosphere; spectral range = 5-200 μ, Atm Top = 30 km, T_s = 302.59 K, ε_s = 1.0, λ = 3, ε_c = 1.0, Z_c = 6 km, RH = 75%.

Zenith Angle, θ	Cloud Cover, %		
	0	50	100
0	1.0967	1.0810	1.0608
15	1.0900	1.0754	1.0567
30	1.0690	1.0579	1.0436
45	1.0303	1.0254	1.0192
60	0.9654	0. 709	0.9779
70	0.8976	0.9136	0.9342
80	0.7894	0.8225	0.8650
G	0.3073	0.2585	0.1958

Table B4.8 Variation of anisotropic function with cloud height for tropical atmosphere; spectral range = 5-200 μ, Atm Top = 30. km, T_s = 302.59, ε_s = 1.0, λ = 3, ε_c = 1.0, RH = 75%.

Zenith Angle, θ	Cloud Height (Z_c), km					
	50 Cloud Cover			100% Cloud Cover		
	2	6	10	2	6	10
0	1.0902	1.0810	1.0721	1.0833	1.0608	1.0308
15	1.0840	1.0754	1.0671	1.07761	1.0567	1.0287
30	1.0643	1.0579	1.0515	1.0594	1.0436	1.0222
45	1.0282	1.0254	1.0227	1.0260	1.0192	1.0099
60	0.9678	0.9709	0.9740	0.9704	0.9779	0.9884
70	0.9047	0.9136	0.9227	0.9124	0.9342	0.9650
80	0.8036	0.8225	0.8225	0.8403	0.8187	0.8560
G	0.2866	0.2585	0.2318	0.2646	0.9158	0.1050

Table B4.9 Variation of anisotropic function with high-cloud emissivity for tropical atmosphere; spectral range = 5-200 M, Atm Top = 30 km, T_s = 302.59 K, ε_s = 1.0, λ = 3, RH = 75%.

Zenith Angle, θ	High Cloud (Z_c = 10 km) Emissivity, ε_c			
	50% Cloud Cover		100% Cloud Cover	
	0.5	1.0	0.5	1.0
0	1.0858	1.0721	1.0721	1.0308
15	1.0799	1.0671	1.0671	1.0287
30	1.0612	1.0515	1.0515	1.0222
45	1.0269	1.0227	1.0227	1.0099
60	0.96921	0.9740	0.9740	0.9884
70	0.9087	0.9227	0.9227	0.9650
80	0.8120	0.8403	0.8403	0.9258
G	0.2738	0.2318	0.2318	0.1050

Table B4.10 Variation of anisotropic function with surface relative humidity for tropical atmosphere; special range = 5-200 μ, Atm Top = 30 km, T_s = 302.59 K, ε_s = 1.0, λ = 3, RH = 75%

Zenith Angle, θ	Surface Relative Humidity (RH), %					
	Clear Sky			Overcast Sky		
	50	75	100	50	75	100
0	1.0917	1.0967	1.1009	1.0588	1.0608	1.0621
15	1.0854	1.0900	1.0939	1.0548	1.0567	1.0579
30	1.0654	1.0690	1.0720	1.0423	1.0436	1.0445
45	1.0287	1.0303	1.0315	1.0187	1.0192	1.0196
60	0.9671	0.9654	0.9641	0.9784	0.9779	0.9776
70	0.9024	0.8976	0.8944	0.9354	0.9342	0.9336
80	0.7972	0.7894	0.7859	0.8660	0.8650	0.8645
G	0.2945	0.3073	0.3150	0.1958	0.1958	0.1976

Table B4.11 Variation of anisotropic function with water vapor scale height parameter for tropical atmosphere; spectral range = 5-200 μ, Atm Top = 30 km, T_s = 302.59 K, ε_s = 1.0, Z_c = 6 km, RH = 75%

Zenith Angle, θ	Water Vapor Scale-Height Parameter, λ					
	Clear Sky			Overcast Sky		
	2	3	4	2	3	4
0	1.1103	1.0967	1.0861	1.0671	1.0608	1.0522
15	1.1026	1.0900	1.0802	1.0624	1.0567	1.0488
30	1.0784	1.0690	1.0615	1.0476	1.0436	1.0377
45	1.0342	1.0303	1.0271	1.0207	1.0192	1.0167
60	0.9614	0.9654	0.9689	0.9768	0.9779	0.9805
70	0.8878	0.8976	0.9074	0.9332	0.9342	0.9410
80	0.7782	0.7894	0.8066	0.8702	0.8650	0.8747
G	0.3321	0.3073	0.2795	0.1969	0.1958	0.1775

Table B4.12 Variation of anisotropic function with surface emissivity for tropical atmosphere; spectral range = 5-200 μ, Atm Top = 30 km, T_s = 302.59 K, λ = 3, ε_c = 1.0, Z_c = 6 km, RH = 75%.

Zenith Angle, θ	Surface Emissivity, ε_c					
	Clear Sky			50% Cloud Cover		
	0.8	0.9	1.0	0.8	0.9	1.0
0	1.0787	1.0879	1.0967	1.0707	1.0759	1.0810
15	1.0732	1.0818	1.0900	0.0658	1.0707	1.0754
30	1.0561	1.0627	1.0690	1.0505	1.0542	1.0579
45	1.0246	1.0275	1.0303	1.0222	1.0238	1.0254
60	0.9717	0.9685	0.9654	0.9745	0.9727	0.9709
70	0.9154	0.9063	0.8976	0.9238	0.9187	0.9136
80	0.8197	0.8042	0.7894	0.8400	0.8311	0.8225
G	0.2590	0.2837	0.3073	0.2307	0.2448	0.2585

Table B4.13. Variation of anisotropic function with cloud cover fraction for subarctic-winter atmosphere; spectral range = 5-200 μ, Atm Top = 30 km, T_S = 257.28 K, ε_S = 1.0, λ = 3, ε_C = 1.0, Z_C = 6 km, RH = 75%.

Zenith Angle, θ	Cloud Cover, %		
	0	50	100
0	1.0493	1.0425	1.0225
15	1.0459	1.0396	1.0210
30	1.0354	1.0270	1.0163
45	1.0156	1.0120	1.0073
60	0.9819	0.9861	0.9914
70	0.9461	0.9582	0.9736
80	0.8871	0.9115	0.9423
G	0.1622	0.1310	0.0802

Table B4.14 Variation of anisotropic function with cloud height for subarctic winter atmosphere; spectral range = 5-200 μ, Atm Top = 30 km, T_s = 257.28 K, ε_s = 1.0, λ = 3, ε_c 1.0, RH = 75%.

Zenith Angle, θ	Cloud Height (Z_c), km					
	50% Cloud Cover			100% Cloud Cover		
	2	6	10	2	6	10
0	1.0485	1.0425	1.0309	1.0477	1.0225	1.0023
15	1.0452	1.0396	1.0288	1.0445	1.0210	1.0022
30	1.0348	1.0270	1.0222	1.0343	1.0163	1.0017
45	1.0154	1.0120	1.0098	1.0152	1.0073	1.0008
60	0.9822	0.9861	0.9887	0.9825	0.9914	0.9991
70	0.9468	0.9582	0.9661	0.9475	0.9736	0.9971
80	0.8884	0.9115	0.9288	0.8898	0.9423	0.9934
G	0.1601	0.1310	0.1021	0.1598	0.0802	0.0089

Table B4.15 Variation of anisotropic function with high-cloud emissivity for sub-arctic winter atmosphere; spectral range = 5-200 μ, Atm Top = 30 km, T_s = 257.28 K, ϵ_s = 1.0, λ = 3, RH = 75%.

Zenith Angle, θ	High Cloud (Z_c = 10 km) Emissivity, ϵ_c			
	50% Cloud Cover		100% Cloud Cover	
	0.5	1.0	0.5	1.0
0	1.0410	1.0309	1.0309	1.0023
15	1.0383	1.0288	1.0288	1.0022
30	1.0294	1.0222	1.0222	1.0017
40	1.0130	1.0098	1.0098	1.0008
60	0.9850	0.9887	0.9887	0.9991
70	0.9551	0.9661	0.9661	0.9971
80	0.9050	0.9288	0.9288	0.9934
G	0.1351	0.1021	0.1021	0.0089

Table B4.16 Variation of anisotropic function with surface emissivity for sub-arctic winter atmosphere; spectral range = 5-200 μ, Atm Top = 30 km, T_s = 257.28 K, λ = 3, ε_c 1.0 Z_c = 1.0 Z_c = 6 km, RH = 75%.

Zenith Angle, θ	Surface Emissivity, ε_s					
	Clear Sky			50% Cloud Cover		
	0.8	0.9	1.0	0.8	0.9	1.0
0	1.0359	1.0428	1.0493	1.0297	1.0337	1.0425
15	1.0336	1.0400	1.0459	1.0278	1.0314	1.0396
30	1.0261	1.0309	1.0354	1.0216	1.0243	1.0270
45	1.0118	1.0138	1.0156	1.0097	1.0109	1.0120
60	0.9860	0.9839	0.9819	0.9885	0.9873	0.9861
70	0.9569	0.9513	0.9461	0.9646	0.9614	0.9582
80	0.9066	0.8965	0.8871	0.9231	0.9172	0.9115
G	0.1293	0.1463	0.1622	0.1066	0.1165	0.1310

APPENDIX C1
SYMBOLS USED IN THE COMPUTER PROGRAM "FILAUFG"

APPENDIX C1

SYMBOLS USED IN THE COMPUTER PROGRAM "FILAUPG"

AISFUN	Anisotropic function
ALA	Altitude dependent average width of the lines of a molecule.
ALB	Altitude dependent individual width of the lines of a molecule.
AVSI	Average value of intensity for the lines in one decade in an interval.
AVS1 AVS2 AVS3 AVS4 AVS5	Average intensities of N_2O, CH_4, CO_2, H_2O and O_3
CC	Cloud cover
CEMI	Cloud emissivity
DEL	width of an interval
EMG	Surface emittance
FLUX	Upwelling flux at the top of the atmosphere, W/M^2
FRL	Lower frequency limit of the range.
IC	Integer which is equal to zero if effect of cloud is not considered and one if it is considered.
I1, I2 I3, I4 I5	Integer for each of the five gases considered is equal to 1. It is equal to zero if the effect of a gas is neglected.
JD	Number of adjacent intervals on both sides of an interval from which contribution is taken into account.
KR	Number of intervals in the band
LCB	Cloud height
LT	Height of the atmosphere

NL	Number of layers
NSI	Number of lines in a decade within an interval
NS1, NS2 NS3, NS4 NS5	Number of lines in an interval.
PL	Optical path length at the frequency under consideration.
PLG	Planck function of atmosphere evaluated at the average temperature of the layer.
PNTP	Pressure at NTP, bar.
PRG	Average pressure of a layer.
PSC	Planck function of the cloud evalulated at the average temperature of the cloud
PSG	Planck function of the surface evaluated at the surface temperature.
RADC1,RADC2 RADC3,RADC4 RADC5,RADC6	Radiances in each of the six spectral ranges considered. Watts M-2 Sr-1.
RDAG	Radiance emitted by the atmosphere, watts M-2 SR-1.
RDIG	Total Radiance at the top of the atmosphere, watts M-2 Sr-1.
RDSC	Radiance emitted by the cloud. Watts M-2 Sr-1.
RDSG	Radiance emitted by the surface, watts M-2 Sr-1.
TAG	Combined transmittance of all interfering gases.
TEG	Average temperature of a layer, K.
TEMPG	Surface temperature, K.
TEMR	Reference temperature for the line parameters, K.
TH	Thickness of a layer the atmospheric layer, km.
TNTP	Temperature of NTP, K.
TRAC	Cloud transmittance
VLIMDF	Limb darkening function

NL	Number of layers
NSI NS1, NS2 NS3, NS4 NS5	Number of lines in a decade within an interval Number of lines in an interval.
PL	Optical path length at the frequency under consideration.
PLG	Planck function of atmosphere evaluated at the average temperature of the layer.
PNTP	Pressure at NTP, bar.
PRG	Average pressure of a layer.
PSC	Planck function of the cloud evalulated at the average temperature of the cloud
PSG	Planck function of the surface evaluated at the surface temperature.
RADC1,RADC2 RADC3,RADC4 RADC5,RADC6	Radiances in each of the six spectral ranges considered. Watts M-2 Sr-1.
RDAG	Radiance emitted by the atmosphere, watts M-2 SR-1.
RDIG	Total Radiance at the top of the atmosphere, watts M-2 Sr-1.
RDSC	Radiance emitted by the cloud. Watts M-2 Sr-1.
RDSG	Radiance emitted by the surface, watts M-2 Sr-1.
TAG	Combined transmittance of all interfering gases.
TEG	Average temperature of a layer, K.
TEMPG	Surface temperature, K.
TEMR	Reference temperature for the line parameters, K.
TH	Thickness of a layer the atmospheric layer, km.
TNTP	Temperature of NTP, K.
TRAC	Cloud transmittance
VLIMDF	Limb darkening function

APPENDIX C2
LISTINGS OF COMPUTER PROGRAM "FILAUPG"

APPENDIX C2

LISTINGS OF COMPUTER PROGRAM "FILAUPG"

```
      PROGRAM FILAUPG (INPUT,OUTPUT,TAPE5=INPUT,TAPE6=OUTPUT,TAPE2)
C
C
C        THIS RADIATIVE TRANSFER PROGRAM USES QUASI-RANDOM BAND MODEL.
C     THE LONGWAVE REGION (50 - 2000CM-1) IS DIVIDED INTO 195 INTERVALS
C     OF 10CM-1 EACH.  THE ATMOSPHERE (30KM) IS DIVIDED INTO 15 LAYERS OF
C     THICKNESSES 1,1,1,1,1,1,1,1,1,1,1,4,5,5,5KM.  PURE RTATIONAL AND
C     6.3M(MICRON) BANDS AND CONTINUUM BAND OF WATER VAPOR IN 8-28.5M
C     REGION, 15M CARBON DIOXIDE BAND, 9.6M OZONE BAND, 7.8M NITRUS OXIDE
C     BAND AND 7.7M METHANE BAND ARE CONSIDERED.  SINCE NUMBER OF LINES
C     IN SOME BANDS IS VERY LARGE, PRECOMPUTED VALUES OF AVERAGED
C     INTENSITY AND NUMBER OF LINES FOR EVERY INTERVAL AND INTENSITY
C     DECADE ARE USED IN THIS PROGRAM.  TRANSMITTANCE COMPUTATION FOR
C     EACH BAND IS CARRIEDOUT IN SUBROUTINE TRANS WHICH USES A SIMPLE
C     INTEGRATION SCHEME EXPLAINED IN REPORT 75-T14.
C
C
      INTEGER X,TH
      DIMENSION PLG(195,15),RDSG(7),RDAG(7),RDSC(7)
      DIMENSION VLIMDF(7,4)
      DIMENSION SUG(5),SPUG(5),STUG(5),ULG(15,5),PULG(15,5),TULG(15,5)
      DIMENSION PR(30),TE(30),VMR(30,5),UG(15,5),PRG(15,5),TEG(15,5)
      DIMENSION PREG(15,5), TEMG(15,5),ALA(5),ALG(15,5),TH(15),ALT(30)
      DIMENSION AVS1(5,24),AVS2(5,29),AVS3(5,25),AVS4(5,195),AVS5(5,23)
      DIMENSION NS1(5,24),NS2(5,29),NS3(5,25),NS4(5,195),NS5(5,23)
      DIMENSION TRG(195,16),PPG(16),FAG(16)
      DIMENSION AG(90),ZX(7),ZEN(7),RADG(7),TAG(7,195,16)
      DIMENSION RDIG(7),RDG(195),FXG(195)
      DIMENSION PNUM(195),EEX(195),PSG(195),PSC(195)
      DIMENSION AISFUN(7,5,2),RADCC(7,5,2),FLUX(5,2),CC(5)
      DIMENSION TRAC(11),CEMI(11),RADNCL(195)
      DIMENSION RADC1(7,14),RADC2(7,14),RADC3(7,14),RADC4(7,14)
      DIMENSION RADC5(7,14),RADC6(7,14),RADZ(7,195)
      COMMON/TRANE/AVSI(5,195),NSI(5,195),FRC(195),TRA(195),
     1X1(26),T1(26),X2(21),T2(21),DELA,JD,PI
C
C     ZENITH ANGLE
C
      DATA ZEN/0.,15.,30.,45.,60.,70.,80./
C
```

```
C     CLOUD COVER FRACTION
C
      DATA CC/0.0,0.3,0.5,0.7,1.0/
      DATA  PNTP,TNTP,TEMR/1.00,273.15,296./
      DATA  ALA/0.079,0.054,0.066,0.063,0.110/
      DATA  UG/75*0./
      DATA  FRL1,FRL2,FRL3,FRL4,FRL5/1110.,1220.,550.,50.,950./
      DATA  DEL,DELA,JD,PI/10.,5.,4,3.1459/
      DATA  KR1,KR2,KR3,KR4,KR5,KRT/24,29,25,195,23,195/
      DATA  KB1,KB2,KB3,KB4,KB5/107,118,51,1,91/
      DATA  KE1,KE2,KE3,KE4,KE5/130,146,75,195,113/
      DATA  FRLC,KC,KBC,KEC/350.,90,31,120/
      DATA  A,B,BETA/1.25E-22,2.34E-19,8.30E-03/
      REWIND 2
C
C     VOLUME MIXING RATIOS N2O,CH4,CO2
C
      DO 4 L=1,30
      VMR(L,1)=0.28
      VMR(L,2)=1.6
      VMR(L,3)=330.
 4    CONTINUE
      DATA IC,RE/1,20./
C
C     ATMOSPHERE IS DIVIDED INTO 15 LAYERS
C
      DATA  TH/1,1,1,1,1,1,1,1,1,1,1,4,5,5,5/
C
C    PRESSURE AND TEMPERATURE PROFILE. VOLUME MIXING RATIOS
C    OF WATER VAPOR AND OZONE
C
      READ(5,*)(PR(L),TE(L),VMR(L,4),VMR(L,5),L=1,30)
C
C     FIVE GASES CONSIDERED ARE N2O,CH4,CO2,H2O,O3
C
       DATA I1,I2,I3,I4,I5/1,1,1,1,1/
C
C      NUMBER OF LAYERS CONSIDERED AND THE HEIGHT OF THE ATMOSPHERE
C
C      NL=10 IF ATMOSPHERE TOP IS AT 10KM
C      NL=13 IF ATMOSPHERE TOP IS AT 20KM
C
      DATA NL,LT/15,30/
      DATA X1/0.0,0.001,0.0015,0.002,0.003,0.004,0.005,0.006,
     10.008,0.01,0.015,0.02,0.03,0.04,0.05,0.06,0.08,0.10,
     20.15,0.20,0.30,0.40,0.50,0.60,0.80,1.00/
      DATA NL,LT/15,30/
      DATA T1/0.0006,0.0006,0.0006,0.0007,0.001,0.001,0.001,
     10.0015,0.002,0.003,0.005,0.008,0.01,0.01,0.01,0.015,
     20.02,0.03,0.05,0.08,0.1,0.1,0.1,0.15,0.2,0.1/
      DATA X2/-1.0,-0.9,-0.8,-0.7,-0.6,-0.5,-0.4,-0.3,-0.2,
     1-0.1,0.0,0.1,0.2,0.3,0.4,0.5,0.6,0.7,0.8,0.9,1.0/
      DATA T2/0.1,0.4,0.2,0.4,0.2,0.4,0.2,0.4,0.2,
     10.4,0.2,0.4,0.2,0.4,0.2,0.4,0.2,0.4,0.2,0.4,0.1/
C
C      AVERAGE LINE INTENSITIES AND NUMBER OF LINES IN EACH INTERVAL
```

```
C
      READ(2,*) ((AVS1(I,K),I=1,5),K=1,KR1)
      READ(2,*) ((NS1(I,K),I=1,5),K=1,KR1)
      READ(2,*) ((AVS2(I,K),I=1,5),K=1,KR2)
      READ(2,*) ((NS2(I,K),I=1,5),K=1,KR2)
      READ(2,*) ((AVS3(I,K),I=1,5),K=1,KR3)
      READ(2,*) ((NS3(I,K),I=1,5),K=1,KR3)
      READ(2,*) ((AVS4(I,K),I=1,5),K=1,KR4)
      READ(2,*) ((NS4(I,K),I=1,5),K=1,KR4)
      READ(2,*) ((AVS5(I,K),I=1,5),K=1,KR5)
      READ(2,*) ((NS5(I,K),I=1,5),K=1,KR5)
      DO 100 L=1,30
100   ALT(L) =L-0.5
      C=0.1*TNTP/PNTP
C
C      AVERAGE TEMPERATURE AND PRESSURE FOR ALL THE LAYERS OF
C      OF ATMOSPHERE ARE COMPUTED USING CURTIS_GODSON APPROXIMATION
C
      DO 101 N=1,5
      L2=LT
      SUG(N)=SPUG(N)=STUG(N)=0.
      DO 102 M=1,NL
      LA=NL+1-M


      ULG(LA,N)=PULG(LA,N)=TULG(LA,N)=0.
      L1=L2-TH(LA)+1
      DO 103 L=L1,L2
      DU=C*PR(L)*VMR(L,N)/TE(L)
      ULG(LA,N)=ULG(LA,N)+DU
      PULG(LA,N)=PULG(LA,N)+PR(L)*DU
      TULG(LA,N)=TULG(LA,N)+TE(L)*DU
      SUG(N)=SUG(N)+DU
      SPUG(N)=SPUG(N)+PR(L)*DU
103   STUG(N)=STUG(N)+TE(L)*DU
      UG(LA,N)=SUG(N)
      PRG(LA,N)=PULG(LA,N)/ULG(LA,N)
      TEG(LA,N)=TULG(LA,N)/ULG(LA,N)
      PREG(LA,N)=SPUG(N)/SUG(N)
      TEMG(LA,N)=STUG(N)/SUG(N)
      ALG(LA,N)=ALA(N)*(SQRT(TEMR/TEMG(LA,N)))*PREG(LA,N)/PNTP
102   L2=L1-1
101   CONTINUE
C
C     TRANSMITTANCE FOR THE N2O BAND IS COMPUTED FOR ALL THE 15
C     LAYERS. TRG IS THE FINAL TRANSMITTANCE, SO INDIVIDUAL
C     TRANSMITTANCES ARE MULTIPLIED INTO THIS ARRAY
C
      LD=NL+1
      DO 110 LA=1,LD
      DO 110 K=1,KRT
110   TRG(K,LA)=1.
      IF(I1.LT.1) GO TO 163
      DO 111 K=1,KR1
      DO 111 I=1,5
```

```
      FRC(K)=FRL1+(2*K-1)*DELA
      AVSI(I,K)=AVS1(I,K)
      NSI(I,K)=NS1(I,K)
111   CONTINUE
      DO 112 LA=1,NL
      CALL TRANS(ALG(LA,1),UG(LA,1),KR1)
      DO 113 K=KB1,KE1
113   TRG(K,LA)=TRG(K,LA)*TRA(K-KB1+1)
112   CONTINUE
C
C      TRANSMITTANCE FOR CH4 BAND
C
163   IF(I2.LT.1) GO TO164
      DO 116 K=1,KR2
      FRC(K)=FRL2+(2*K-1)*DELA
      DO 116 I=1,5
      AVSI(I,K)=AVS2(I,K)
      NSI(I,K)=NS2(I,K)
116   CONTINUE
      DO 117 LA=1,NL
      CALL TRANS(ALG(LA,2),UG(LA,2),KR2)
      DO 118 K=KB2,KE2
118   TRG(K,LA)=TRG(K,LA)*TRA(K-KB2+1)
117   CONTINUE
C
C      TRANSMITTANCE FOR CO2 BAND
C
164   IF(I3.LT.1) GO TO 165
      DO 121 K=1,KR3
      FRC(K)=FRL3+(2*K-1)*DELA


      DO 121 I=1,5
      AVSI(I,K)=AVS3(I,K)
      NSI(I,K)=NS3(I,K)
121   CONTINUE
      DO 122 LA=1,NL
      CALL TRANS (ALG(LA,3),UG(LA,3),KR3)
      DO 123 K=KB3,KE3
123   TRG(K,LA)=TRG(K,LA)*TRA(K-KB3+1)
122   CONTINUE
C
C      TRANSMITTANCE FOR WATER VAPOR FOR 6.3M AND PURE
C      ROTATIONAL BAND
C
165   IF (I4.LT.1) GO TO 166
      DO 126 K=1,KR4
      FRC(K)=FRL4+(2*K-1)*DELA
      DO 126 I=1,5
      AVSI(I,K)=AVS4(I,K)
      NSI(I,K)=NS4(I,K)
126   CONTINUE
      DO 127 LA=1,NL
      CALL TRANS(ALG(LA,4),UG(LA,4),KR4)
      DO 128 K=KB4,KE4
128   TRG(K,LA)=TRG(K,LA)*TRA(K-KB4+1)
127   CONTINUE
```

```
C
C       TRANSMITTANCE IS COMPTED CORRESPONDING TO WATER VAPOR
C       CONTINUUM ABSORPTION INTHE 350-1250CM_1
C
      DO 131 K=1,KC
131   FRC(K)=FRLC+(2*K-1)*DELA
      DO 132 LA=1,NL
      PPG(LA)=PREG(LA,4)*UG(LA,4)*VMR(1,3)*1.E-06/UG(LA,3)
132   FAG(LA)=(PPG(LA)*EXP(6.08*((TEMR/TEMG(LA,4))
     1-1.))+0.002*(PREG(LA,4)-PPG(LA)))
      DO 134 LA=1,NL
      DO 135 K=1,KC
135   AG(K)=2.69E+19*(A+B*EXP(-BETA*FRC(K)))*FAG(LA)
      DO 137 K=KBC,KEC
137   TRG(K,LA)=TRG(K,LA)*EXP(-UG(LA,4)*AG(K-KBC+1))
C
C       TRANSMITTANCE FOR O3 BAND
C
134   CONTINUE
136   IF (I5.LT.1) GO TO 167
      DO 142 K=1,KR5
      FRC(K)=FRL5+(2*K-1)*DELA
      DO 142 I=1,5
      AVSI(I,K)=AVS5(I,K)
      NSI(I,K)=NS5(I,K)
142   CONTINUE
      DO 143 LA=1,NL
      CALL TRANS(ALG(LA,5),UG(LA,5),KR5)
      DO 144 K=KB5,KE5
144   TRG(K,LA)=TRG(K,LA)*TRA(K-KB5+1)
143   CONTINUE
167   CONTINUE
      CONS=18.*6.625E-03
      CNST=6.625*0.3/1.38
      DO 147 M=1,7
      ZX(M)=1./COS(ZEN(M)/57.29578)
147   CONTINUE


C
C
C       PLANCK FUNCTIONS FOR EACH OF 195 INTERVALS AND THE 15
C       LAYERS OF ATMOSPERE ARE COMPUTED AND STORED
C
C
      DO 311 K=1,KRT
      FRC(K)=50.+(2*K-1)*DELA
      PNUM(K)=DEL*CONS*FRC(K)*FRC(K)*FRC(K)*1.E-07
      EEX(K)=CNST*FRC(K)
      DO 149 M=1,7
      DO 150 LA=1,NL
C
```

```
C     TRANSMITTANCES IN SOME OF THE INTERVALS ARE VERY LOW
C     BECAUSE OF STRONG ABSORPTION. TO AVIOD UNDERFLOW ERROR
C     THEY ARE EQUATED TO ZERO.
C
      IF(TRG(K,LA).LT.1.E-50) GO TO 200
      TAG(M,K,LA)=TRG(K,LA)**ZX(M)
      GO TO 150
 200  TAG(M,K,LA)=0.
 150  CONTINUE
      TAG(M,K,NL+1)=1.
 149  CONTINUE
      DO 152 LA=1,5
 152  PLG(K,LA)=PNUM(K)/(EXP(EEX(K)/TEG(LA,4))-1.)
      IF(NL.LE.5) GO TO 311
      DO 153 LA=6,NL
 153  PLG(K,LA)=PNUM(K)/(EXP(EEX(K)/TEG(LA,3))-1.)
 311  CONTINUE
C
C     SURFACE TEMPERATURE
C
      TEMPG=302.59
      DO 213 NTE=1,3
      TEMPG=TEMPG+5.
      DO 313 K=1,KRT
 313  PSG(K)=PNUM(K)/(EXP(EEX(K)/TEMPG)-1.)
C
C     HEIGHT OF THE CLOUD BASE CAN BE CHANGED BY CHANGING LCB HERE
C
      LCB=-2
      DO 212 NK=1,3
      LCB=LCB+4
      LCT=LCB+1
C
C     AVERAE CLOUD TEMPERATURE
C
      TEMPC=0.5*(TE(LCB)+TE(LCB+1))
      DO 312 K=1,KRT
 312  PSC(K)=PNUM(K)/(EXP(EEX(K)/TEMPC)-1.)
C
C            SURFACE EMISSIVITY
C
      EMG=0.70
      DO 211 NE=1,3
      EMG=EMG+0.1
 209  FORMAT("1SURFACE EMISSIVITY =",F6.2,//,"
     1SURFACE TEMPERATURE ="F6.2,//,"
     2HEIGHT OF THE ATMOSPHERE =",I2,"KM",//,"
     3CLOUD TOP HEIGHT=",I2,//,"
     4CLOUD EMISSIVITY =",F5.3,//)
```

```
      DO 214 M=1,7
      RADG(M)=0.
      DO 214 X=1,6
      RADC1(M,X)=RADC2(M,X)=RADC3(M,X)=RADC4(M,X)=RADC5(M,X)
     1=RADC6(M,X)=0.
 214  CONTINUE
      FLG=0.
C
C     CLEAR ATMOSPHERE UPWELLING RADINCES AND FLUXES FOR
C     ALL ZEITH ANGLES ARE COMPUTED
C
      DO 148 K=1,KRT
      DO 154 M=1,7
C
C     UPWELLING RADIANCE DUE TO SURFACE EMISSION
C
      RDSG(M)=EMG*PSG(K)*TAG(M,K,1)
      RDAG(M)=0.
      DO 155 LA=1,NL
C
C     UPWELLING RADIANCE DUE TO ATMOSPHERIC EMISSION
C
 155  RDAG(M)=RDAG(M)+PLG(K,LA)*(TAG(M,K,LA+1)-TAG(M,K,LA))
      RDIG(M)=RDSG(M)+RDAG(M)
      RADG(M)=RADG(M)+RDIG(M)
 154  CONTINUE
C
C     COMPUTES UPWELLING FLUX BY EXPONENTIATING TRANSMITTANCE
C     BY THE DIFFUSIVITY FACTOR 1.66 AND MULTIPLYING PLANCK
C     FUNCTION TIMES PI
C
      FLSG=EMG*PI*PSG(K)*(TRG(K,1)**1.66)
      FLAG=0.
      DO 157 LA=1,NL
 157  FLAG=FLAG+PI*PLG(K,LA)*((TRG(K,LA+1)**1.66)
     1-(TRG(K,LA)**1.66))
      FLXG=FLSG+FLAG
      FLG=FLG+FLXG
      RDG(K)=RDIG(1)
      FXG(K)=FLXG
 148  CONTINUE
      DO 159 X=1,2
C
C     ONLY TWO DIFFERENT CLOUD EMISSIVTIES ARE USED IN THIS
C     STUDY. DIMENSION OF X SHOULD BE CHANGED IF IT IS REQUIRED
C     TO VARY MORE THAN TWO
C
      FLC=0.
C
C     CLOUD EMISSIVITY
C     ONLY THE HIGH CLOUD HAS TWO DIFFERNT VALUES
C
```

```
      IF(LCB.LE.6.AND.X.EQ.2) GO TO 159
      IF(LCB.LE.6.AND.X.EQ.1) CEMI(X)=1.0
      IF(LCB.EQ.10.AND.X.EQ.1) CEMI(X)=0.5
      IF(LCB.EQ.10.AND.X.EQ.2) CEMI(X)=1.0


C
C     CLOUD TRANSMITTANCE IS EVALUATED
C
      TRAC(X)=1.-CEMI(X)
      DO 210 M=1,7
      DO 210 K=1,KRT
 210  RADZ(M,K)=0.
      IF(IC.EQ.0) GO TO 601
      DO 315 K=1,KRT
C
C     UPWELLING FLUX FROM CLOUD TOP
C
      FLSC=CEMI(X)*PI*PSC(K)*(TRG(K,LCT)**1.66)
      FLSG=EMG*PI*PSG(K)*(TRG(K,1)**1.66)
      FLAC=0.
C
C     UPWELLING FLUX FROM THE ATMSPHERIC LAYERS ABOVE THE CLOUD
C
      DO 222 LA=LCT,NL
 222  FLAC=FLAC+PI*PLG(K,LA)*((TRG(K,LA+1)**1.66)
     1-(TRG(K,LA)**1.66))
      FLXC=FLSC+FLAC
      FLC=FLC+FLXC
      IF(TRAC(X).EQ.0.0) GO TO 3909
      FLAT=0.
C
C     IF THE CLOUD EMISSIVITY IS LESS THAN 1, UPWELLING FLUX
C     COMPONENT BELOW THE CLOUD LAYER IS EVALUATED
C
      DO 223 LA=1,LCB
 223  FLAT=FLAT+PI*PLG(K,LA)*((TRG(K,LA+1)**1.66)
     1-(TRG(K,LA)**1.66))
      FLAB=(FLAT+FLSG)*TRAC(X)
      FLC=FLC+FLAB
3909  DO 158 M=1,7
C
C     UPWELLING RADIANCE FROM CLOUD TOP
C
      RDSC(M)=CEMI(X)*PSC(K)*TAG(M,K,LCT)
C
C     UPWELLING RADIANCE FROM THE SURFACE AND THE ATMOSPHERE
C     BELOW THE CLOUD
C
```

```
      RDSG(M)=EMG*PSG(K)*TAG(M,K,1)
      RADNCL(K)=0.
      DO 409 LA=1,LCB
      TERM2=PLG(K,LA)*(TAG(M,K,LA+1)-TAG(M,K,LA))
 409  RADNCL(K)=RADNCL(K)+TERM2
      RADNCL(K)=TRAC(X)*(RDSG(M)+RADNCL(K))
C      EMISSION FROM CLOUD
      RADNCL(K)=RADNCL(K)+RDSC(M)
C
C     UPWELLING RADIANCE FROM THE ATMOSPHERE ABOVE THE CLOUD
C
      DO 408 LA=LCT,NL
      TERM4=PLG(K,LA)*(TAG(M,K,LA+1)-TAG(M,K,LA))
 408  RADNCL(K)=RADNCL(K)+TERM4


C
C     UPWELLING RADIANCE AT THE TOP OF THE ATMOSPHERE FOR A
C     PARTICULAR ZENITH ANGLE AND A SUB-INTERVAL
C
      RADZ(M,K)=RADNCL(K)
158   CONTINUE
315   CONTINUE
601   CONTINUE
C
C
      DO 190 M=1,7
C
C     TOTAL UPWELLING RADIANCE IN THE SPECTRAL REGION 5-10M
C
      DO 180 K=96,195
      RADC1(M,X)=RADC1(M,X)+RADZ(M,K)
180   CONTINUE
C
C     TOTAL UPWELLING RADIANCE IN THE SPECTRAL REGION 10-20M
C
      DO 181 K=46,95
      RADC2(M,X)=RADC2(M,X)+RADZ(M,K)
181   CONTINUE
C
C     TOTAL UPWELLING RADIANCE IN THE SPECTRAL REGION 5-20M
C
      RADC3(M,X)=RADC1(M,X)+RADC2(M,X)
C
C     TOTAL UPWELLING RADIANCE IN THE WINDOW REGION 10.5-12.5
C
      DO 182 K=76,90
      RADC4(M,X)=RADC4(M,X)+RADZ(M,K)
182   CONTINUE
```

```
C
C      TOTAL UPWELLING RADIANCE IN THE SPECTRAL REGION 5-50M
C
       DO 183 K=16,45
       RADC5(M,X)=RADC5(M,X)+RADZ(M,K)
183    CONTINUE
       RADC5(M,X)=RADC5(M,X)+RADC3(M,X)
C
C      TOTAL UPWELLING RADIANCE IN THE SPECTRAL REGION 5-200M
C
       DO 184 K=1,195
       RADC6(M,X)=RADC6(M,X)+RADZ(M,K)
184    CONTINUE
190    CONTINUE
C
C      UPWELLING FLUXES AND RADIANCES ARE COMPUTED FOR PARTLY
C      CLOUDY CONDITIONS BY EVALUATING WEIGHED SUMS OF THE
C      CLEAR AND OVERCAST VALUES
C
       DO 414 NF=1,5
       FLUX(NF,X)=(1.-CC(NF))*FLG+CC(NF)*FLC
       DO 415 M=1,7
       RADCC(M,NF,X)=(1.-CC(NF))*RADG(M)+CC(NF)*RADC6(M,X)
C
C      ANISOTROPIC FUNCTIONS ARE CAUCULATED

415    AISFUN(M,NF.X)=PI*RADCC(M,NF,X)/FLUX(NF,X)
414    CONTINUE
159    CONTINUE
       RDG1=RDG2=RDG3=RDG4=RDG5=RDG6=RDG7=0.
       FXG1=FXG2=FXG3=FXG4=FXG5=FXG6=FXG7=0.


C
C
       DO 170 K=96,195
       RDG1=RDG1+RDG(K)
       FXG1=FXG1+FXG(K)
170    CONTINUE
C
C
       DO 171 K=46,95
       RDG2=RDG2+RDG(K)
       FXG2=FXG2+FXG(K)
171    CONTINUE
       RDG3=RDG1+RDG2
       FXG3=FXG1+FXG2
C
C
       DO 172 K=76,90
       RDG4=RDG4+RDG(K)
       FXG4=FXG4+FXG(K)
172    CONTINUE
C
C
```

```
      DO 173 K=16,45
      RDG5=RDG5+RDG(K)
      FXG5=FXG5+FXG(K)
173   CONTINUE
C
      RDG5=RDG5+RDG3
      FXG5=FXG5+FXG3
      DO 174 K=1,15
      RDG6=RDG6+RDG(K)
      FXG6=FXG6+FXG(K)
174   CONTINUE
      RDG7=RDG6+RDG5
      FXG7=FXG6+FXG5
C
C
      WRITE(6, 67)
67    FORMAT(1H1/19X21HMODEL ATMOSPHERE USED)
      WRITE(6, 68)
68    FORMAT(///7X3HALT,5X5HPRESS,6X4HTEMP,6X9HWATER VAP,8X5HOZONE)
      WRITE(6, 69)
69    FORMAT(6X4H(KM),5X5H(ATM),5X5H(KEL),9X6H(PPMV),7X6H(PPMV)//)
      WRITE(6, 70)(ALT(L),PR(L),TE(L),VMR(L,4),VMR(L,5),L=1,30)
70    FORMAT(F10.1,F10.5,F10.2,E15.4,E15.4)
      WRITE(6, 76)
76    FORMAT(1H1/25X29HCLEAR ATMOSPHERE PATH LENGTHS///)
      WRITE(6, 64)
64    FORMAT(6X2HTH,7X3HULG,8X3HPRG,7X3HTEG,8X2HUG,
     18X4HPREG,6X4HTEMG,6X3HALG)
      WRITE(6, 65)((TH(LA),ULG(LA,N),PRG(LA,N),TEG(LA,N),UG(LA,N),
     1PREG(LA,N),TEMG(LA,N),ALG(LA,N),LA=1,NL),N=1,5)
65    FORMAT(//5(16(I8,E12.3,F10.5,F10.2,E12.3,F10.5,F10.2,F8.3/)))
      WRITE(6, 71)
71    FORMAT(/40X30HINTEGRATED RADIANCE AND FLUXES)
      WRITE(6, 72)
72    FORMAT(/30X"VARIATION WITH NADIR ANGLE (THETA) AND ","CLOUD
     1COVER")


      WRITE(6,84)
84    FORMAT(/40X,"SPECTRAL RANGE =5 - 10 MU")
      WRITE(6, 73)
73    FORMAT(///18X,8HRADIANCE,4X8HRADIANCE,4X8HRADIANCE,
     14X8HRADIANCE,4X8HRADIANCE,4X8HRADIANCE,4X8HRADIANCE)
      WRITE(6, 74)
74    FORMAT(5X,"CLOUD COVER",2X,8HTHETA+00,4X8HTHETA=15,4X8HTHETA=30,
     14X8HTHETA=45,4X8HTHETA=60,4X8HTHETA=70,4X8HTHETA=80//)
      WRITE(6, 60)(CC(X),(RADC1(M,X),M=1,7),FLUX(X),X=1,2)
      WRITE(6,71)
      WRITE(6,72)
      WRITE(6,85)
85    FORMAT(/40X,"SPECTRAL RANGE = 10 - 20 MU")
      WRITE(6,73)
      WRITE(6,74)
      WRITE(6,60)(CC(X),(RADC2(M,X),M=1,7),FLUX(X),X=1,2)
```

```
      WRITE(6,71)
      WRITE(6,72)
      WRITE(6,86)
86    FORMAT(/40X,"SPECTRAL RANGE = 5 - 20 MU")
      WRITE(6,73)
      WRITE(6,74)
      WRITE(6,60)(CC(X),(RADC3(M,X),M=1,7),FLUX(X),X=1,2)


      WRITE(6,71)
      WRITE(6,72)
      WRITE(6,87)
87    FORMAT(/40X,"SPECTRAL RANGE = 5 - 30 MU")
      WRITE(6,73)
      WRITE(6,74)
      WRITE(6,60)(CC(X),(RADC4(M,X),M=1,7),FLUX(X),X=1,2)


      WRITE(6,71)
      WRITE(6,72)
      WRITE(6,88)
88    FORMAT(/40X,"SPECTRAL RANGE = 10.5 - 12.5 MU")
      WRITE(6,73)
      WRITE(6,74)
      WRITE(6,60)(CC(X),(RADC5(M,X),M=1,7),FLUX(X),X=1,2)


      WRITE(6,209) EMG,TEMPG,LT,LCB,CEMI(1)


      WRITE(6,71)
      WRITE(6,72)
      WRITE(6,89)
89    FORMAT(/40X,"SPECTRAL RANGE = 5 - 200 MU")
      WRITE(6,73)
      WRITE(6,74)
      WRITE(6,60)(CC(NF),(RADCC(M,NF,1),M=1,7),NF=1,5)
60    FORMAT(F12.2,2X,7E12.5/)
      WRITE(6,90)
90    FORMAT(/44X,"ANISOTROPIC  FUNCTIONS"/)
      WRITE(6,74)
      WRITE(6,60)(CC(NF),(AISFUN(M,NF,1),M=1,7),NF=1,5)
      IF(LCB.LE.6) GO TO 8585
      WRITE(6,209)EMG,TEMPG,LT,LCB,CEMI(2)
      WRITE(6,71)
      WRITE(6,72)
      WRITE(6,89)
      WRITE(6,73)
      WRITE(6,74)
```

ORIGINAL PAGE IS
OF POOR QUALITY

```
      WRITE(6,60)(CC(NF),(RADCC(M,NF,2),M=1,7),NF=1,5)
      WRITE(6,90)
      WRITE(6,74)
      WRITE(6,60)(CC(NF),(AISFUN(M,NF,2),M=1,7).NF=1,5)
8585  WRITE(6. 78)
78    FORMAT(1H1/17X64HCLEAR AND CLOUDY RADIANCES AND FLUXES IN THE
     1SPECTRAL RANGES///)
      WRITE(6, 79)
79    FORMAT(28X7HRANGE 1,8X7HRANGE 2,8X7HRANGE 3,
     18X7HRANGE 5,8X 15HRANGE 4(WINDOW),5X7HRANGE 6)
      WRITE(6, 80)
80    FORMAT(28X7H5_10 MU,7X8H10_20 MU,8X7H5_20 MU,8X7H5_50 MU,
     18X14H 10.5- 12.5 MU,5X8H5-200 MU//)
      WRITE(6,81)RDG1,RDG2,RDG3,RDG5,RDG4,RDG7
81    FORMAT(7X13HCLEAR ATM RAD,4E15.5,E20.5,E15.5)
82    FORMAT(8X12HOVERCAST RAD,4E15.5,E20.5/)
      WRITE(6,83)FXG1,FXG2,FXG3,FXG5,FXG4,FXG7
83     FORMAT(6X14HCLEAR ATM FLUX,4E15.5,E20.5,E15.5/)
      WRITE(6, 61)
61    FORMAT(1H1/25X45HSPECTRAL TRANSMITTANCES, RADIANCES AND FLUXES
      WRITE(6, 63)
63    FORMAT(///6X4HFREQ,7X8HTRANS TO,6X9HCLEAR ATM,6X9HCLEAR ATM,
     17X8HTRANS TO.6X9HCLOUD TOP,6X9HCLOUD TOP)
      WRITE(6, 75)
75    FORMAT(6X4HCM_1,8X7HSURFACE,7X8HRADIANCE,5X10HFLUX(W/M2),
     16X9HCLOUD TOP.7X8HRADIANCE,5X10HFLUX(W/M2)//)
      WRITE(6, 62)(FRC(K).TRG(K,1),RDG(K),FXG(K),TRC(K,LC),RDC(K),
     1FXC(K),K=1,KRT)
62    FORMAT(F10.0,F15.5,2E15.5,F15.5,2E15.5/)
211    CONTINUE
212    CONTINUE
213    CONTINUE
       STOP
       END


      SUBROUTINE TRANS(ALB,PL,KR)
      INTEGER W
      COMMON/TRANE/AVSI(5,195),NSI(5,195),FRC(195),TRA(195),
     1X1(26),T1(26),X2(21),T2(21),DELA,JD,PI
C
C     CALUCULATES TRANSMITTANCE IN EACH INTERVAL AT ALL
C     ALTITUDES CONSIDERING DIRECT AND WING CONTRIBUTIONS
C
```

```
      RHO=ALB/DELA
      DO 300 K=1,KR
      TRA(K)=1.
      DO 301 J=1,KR
      TRD=1.
      JA=IABS(J-K)
      IF(JA.GT.JD) GO TO 301
      ZI=FRC(K)-FRC(J)
      EPSI=ZI/DELA
      DO 302 I=1,5
      NSJ=NSI(I,J)
      PNUM=RHO*RHO*AVSI(I,J)*PL/(PI*ALB)
      RES=0.
      IF (J.NE.K) GO TO 303
      DO 304 W=1,26
      YY=PNUM/(X1(W)*X1(W)+RHO*RHO)
      IF (YY.GT.675.) GO TO 305
      Y=EXP(-YY)
      GO TO 304
305   Y=0.
304   RES=RES+Y*T1(W)
      GO TO 302
303   DO 306 W=1,21
      YY=PNUM/((EPSI-X2(W))*(EPSI-X2(W)))
      IF (YY.GT.675.) GO TO 307
      Y=EXP(-YY)
      GO TO 306
307   Y=0.
306   RES=RES+Y*T2(W)
      RES=RES/6.
302   TRD=TRD*RES**NSJ
301   TRA(K)=TRA(K)*TRD
300   CONTINUE
      RETURN
      END
```